BIOGEOCHEMICAL CYCLING OF CARBON DIOXIDE IN ESTUARIES AND THE CONTINENTAL SHELF OF THE SOUTHEASTERN UNITED STATES

by

LI-QING JIANG

(Under the Direction of Wei-Jun Cai)

ABSTRACT

In the first half of the dissertation, partial pressure of carbon dioxide ($p\mathrm{CO_2}$), dissolved inorganic carbon (DIC), and total alkalinity (TA) were measured at both high tide and low tide in the surface water of three Georgia estuaries from September 2002 to May 2004. Of the three estuaries, Sapelo and Doboy Sounds are marine-dominated estuaries, while Altamaha Sound is a river-dominated estuary. During all sampling months, the three estuaries were supersaturated in CO_2 with respect to the atmosphere (390 - 3380 μatm). The calculated annual air-water CO_2 flux in Altamaha Sound (69.3 mmol m^{-2} d^{-1}) is 2.4 times that of Sapelo and Doboy Sounds (28.7-29.4 mmol m^{-2} d^{-1}). The higher CO_2 degassing in the river-dominated estuary is largely fueled by CO_2 loading from the river. Due to the substantial differences between river- and marine-dominated estuaries, current estimates of air-water CO_2 fluxes in global estuaries (which are based almost entirely on river-dominated estuaries) could be overestimated.

In the second half of the dissertation, surface water $p\mathrm{CO_2}$, as well as vertical distributions of DIC, TA, dissolved oxygen (DO), dissolved organic carbon (DOC), pH, nitrate (NO_3^-) plus nitrite (NO_2^-), phosphate (PO_4^{3-}), silicic acid (H_4SiO_4), $\delta^{13}C$ and $\Delta^{14}C$ of DIC, and δD and $\delta^{18}O$ of H_2O, was measured over the entire continental shelf from North Carolina to Florida (also known as South Atlantic Bight, or SAB) during six months from January 2005 to May 2006. Results indicate that the SAB is a net sink of atmospheric $\mathrm{CO_2}$ on an annual and whole shelf basis (-0.48±0.21 mol $\mathrm{m^{-2}}$ $\mathrm{yr^{-1}}$). The inner shelf is a source of +1.20±0.24 mol $\mathrm{m^{-2}}$ $\mathrm{yr^{-1}}$, while the middle and outer shelves are sinks of -1.23±0.19 and -1.37±0.21 mol $\mathrm{m^{-2}}$ $\mathrm{yr^{-1}}$, respectively. After removing $p\mathrm{CO_2}$ variations due to the annual temperature cycle and air-sea gas exchange, residual $p\mathrm{CO_2}$ is calculated. Residual $p\mathrm{CO_2}$, along with salinity, DIC, DOC, is then used to evaluate mechanisms controlling $p\mathrm{CO_2}$ in this region. DIC results show that SAB is strongly controlled landside by carbon inputs and freshwater dilution from terrestrial sources, and seaside by biological activity on the middle and outer shelf.

INDEX WORDS: Carbon dioxide, Spatial and seasonal variability, Air-sea exchange, Fluxes, Controlling mechanisms, Dissolved inorganic carbon, Dissolved organic carbon, Dissolved oxygen, Alkalinity, Nitrate, Nitrite, Phosphate, Silicic acid, δ^{13}C-DIC, Δ^{14}C-DIC, δD-$\mathrm{H_2O}$, δ^{18}O-$\mathrm{H_2O}$, Estuary, River-dominated, Marine-dominated, Continental shelf, Southeastern United States, South Atlantic Bight

BIOGEOCHEMICAL CYCLING OF CARBON DIOXIDE IN ESTUARIES AND THE CONTINENTAL SHELF OF THE SOUTHEASTERN UNITED STATES

by

LI-QING JIANG

B.S., Ocean University of China, P. R. China, 2001

A Dissertation Submitted to the Graduate Faculty of The University of Georgia in Partial Fulfillment of the Requirements for the Degree

DOCTOR OF PHILOSOPHY

ATHENS, GEORGIA

2009

BIOGEOCHEMICAL CYCLING OF CARBON DIOXIDE IN ESTUARIES AND THE CONTINENTAL SHELF OF THE SOUTHEASTERN UNITED STATES

by

LI-QING JIANG

Major Professor:	Wei-Jun Cai
Committee:	James R. Nelson Lawrence R. Pomeroy Ming-Yi Sun Charles E. Tilburg

Electronic Version Approved:

Maureen Grasso
Dean of the Graduate School
The University of Georgia
May 2009

DEDICATION

To my parents—

MY FATHER, NENG-XI JIANG,

who has supported my education selflessly all over the years,

and

MY MOTHER, ZHEN-XIANG LI (1952-1998),

whose loving spirit has kept me moving forward.

ACKNOWLEDGEMENTS

First of all, I would like to thank my advisor, Dr. Wei-Jun Cai for the guidance all over the years. Without his generous financial and moral support, insightful advice, and endless patience, this dissertation would not have been possible. I appreciate the invaluable comments and suggestions from my committee members. Special thanks to Lawrence R. Pomeroy whose brilliant criticisms have helped to improve the dissertation significantly. The dissertation benefited greatly from the discussion with James E. Bauer, Rik Wanninkhof, Charles S. Hopkinson, Patricia L. Yager, and Eric M. Smith.

I can not thank more of the generous laboratory support from Yongchen Wang and Guirong Han. My gratitude also goes to all lab members: Xinping Hu, Feizhou Chen, Justin Hartmann, Xianghui Guo for help with data collection during some of the cruises. In addition, I received field help from Julia Diaz, Jennifer DeAlteris, Heike Lüger, Ed Sheppard, Matt Erickson, Longjun Zhang, Julie Amft, Ken Helm. I thank Wade Sheldon and Tim Hollibaugh for help with LTER data.

This dissertation was funded by National Science Foundation (OCE-0425153) and GCE-LTER (Georgia Coastal Ecosystems – Long Term Ecological Research) program (OCE-9982133). The cooperation of captains and crews of the R/V Cape Hatteras, R/V Savannah, and R/V F. G. Walton Smith is greatly acknowledged. Ship time from Dr. James R. Nelson and Jack Blanton helped to make this project possible. I also want to thank the Graduate School of the University of Georgia for the Dissertation Completion Award, which enabled me to focus on my

dissertation writing. Last but not the least, I would like to thank my wife, Shan Liu, for her continuous support of my research and most importantly, for cheering me up all over the years.

TABLE OF CONENTS

Page

LIST OF TABLES

Page

LIST OF FIGURES

CHAPTER 1

INTRODUCTION AND LITERATURE REVIEW

The burning of fossil fuel and deforestation release vast amounts of carbon dioxide (CO_2) into the atmosphere, about 50% of which remains there, while the rest is taken up by the oceans and land biosphere (Prentice et al., 2001; Sabine et al., 2004). The large uncertainties in the estimate of CO_2 fluxes between the atmosphere and the ocean limit our ability to predict future atmospheric CO_2 levels, and hence the ability to predict future climate change (Tans et al., 1990; Sarmiento and Quéré, 1996). The uncertainties also limit our ability to predict future ocean acidification (Feely et al. 2004). While the oceans and land biosphere have long been known to be important sinks of atmospheric CO_2, a major uncertainty has been the lack of knowledge of CO_2 fluxes in the land/sea margin (Chen et al., 2003; Ducklow and McCallister, 2004).

By linking the land, the ocean, and the atmosphere, land/sea margin (estuaries plus continental shelf) plays a key role in the global carbon cycle (Mackenzie 1991; Smith and Hollibaugh 1993). Despite its small surface area (7-8% of the global ocean surface area), land/sea margin sustains unusually high level of primary production, remineralization, and organic carbon burial (Walsh 1988; Wollast 1993; Gattuso et al. 1998; de Hass et al. 2002). It is thus expected to be a significant contributor to the global air-sea CO_2 exchange (Mackenzie 1991).

Smith and Mackenzie (1987) and Smith and Hollibaugh (1993) claimed that the coastal ocean is heterotrophic and a source of atmospheric CO_2 based on the imbalance between the land input of organic material and the organic carbon burial rate. However, recent studies have shown that the "coastal" net heterotrophy postulated by Smith and Mackenzie (1987) and Smith and Hollibaugh (1993) might be confined to the near shore ecosystem only (estuaries and proximal continental shelf), and the distal continental shelf might behave as a sink of atmospheric CO_2 (Rabouille et al. 2001; Chen and Borges 2009). Despite the progress, large uncertainties on the air-sea exchange of CO_2 in the land/sea margin remain, and more studies are needed to understand the biogeochemical cycling of carbon in this area.

Recent studies have shown that estuaries are significant sources of CO_2 to the atmosphere, with the partial pressure of CO_2 in sea water ($p\mathrm{CO_2}$) varying from ~400 to 9500 μatm (Frankignoulle et al. 1998; Borges 2005; Borges et al. 2005). Even though the surface area of global estuaries is only about 1/20th that of continental shelves (Woodwell et al. 1973), it is argued that CO_2 degassing by estuaries (Borges 2005; Borges et al. 2005; Chen and Borges 2009) could nearly counterbalance the continental shelf CO_2 sink (Tsunogai et al. 1999; Borges et al. 2005; Cai et al. 2006; Chen and Borges 2009), which is about 30-70% of the atmospheric CO_2 sink of the open ocean (1.2-1.6 Pg C yr^{-1}) (Takahashi et al. 2009).

The most frequently cited definition of an estuary is that of Cameron and Pritchard (1963): "a semi-enclosed coastal body of water, which has a free connection with the open sea, and within which seawater is measurably diluted with freshwater derived from land drainage." According to this definition, all river mouths as well as coastal brackish lagoons qualify as estuaries. Following Elliott and McLusky (2002), we have adopted the most widely held point of view that considers both river mouths and coastal brackish lagoons to be estuaries. The inclusion of coastal brackish lagoons as estuaries is also consistent with the fact that the most cited surface area of global estuaries was estimated "without differentiating mouths of rivers and coastal brackish lagoons" (Woodwell et al. 1973). For this dissertation, I refer to mouths of rivers which receive significant amounts of upland river inflow, as river-dominated estuaries; and coastal brackish lagoons which receive little freshwater besides precipitation and groundwater, as marine-dominated estuaries.

Unfortunately, most estuarine CO_2 studies have focused on river-dominated estuaries; little attention has been given to marine-dominated estuaries (Frankignoulle et al. 1998; Borges 2005; Borges et al. 2005). As a result, the estimated global air-water CO_2 fluxes in estuaries could be considerably biased towards river-dominated estuaries (Borges 2005; Borges et al. 2005; Chen and Wang 2009). To reduce the uncertainty of global air-water CO_2 fluxes in estuaries, a comparative study of air-water CO_2 fluxes in river- and marine-dominated estuaries is warranted. The first half of the dissertation reports a study of surface water CO_2 and its biogeochemical controlling mechanisms in these two types of estuaries around Sapelo Island, Georgia. The proximity of the studied estuaries and their similarities in physical conditions other than freshwater input provided a unique opportunity to compare the CO_2 fluxes in river- and marine-dominated estuaries.

The second half of the dissertation shows a new study of surface water pCO_2 and other inorganic carbon parameters in the continental shelf of the Southeastern United States. Continental shelves are another important site of air-sea CO_2 exchange in the land/sea margin. The concept of “continental shelf pump” was first coined out by Tsunogai et al. (1999), who estimated a global continental shelf sink of 1.0 Pg C yr^{-1} by assuming all continental shelves behave similarly as the East China Sea (ECS). Recent CO_2 flux measurements in several major continental shelves (the U.S. Middle Atlantic Bight, DeGrandpre et al., 2002; the U.S. Pacific coast off Oregon, Hales et al., 2005; and the West European Shelves, Bozec et al., 2005) all support the argument of a global continental shelves sink, although the sink might be much smaller than the estimate of Tsunogai et al. (1999). New synthesis efforts lean towards a smaller global “continental shelf pump” sink of 0.2-0.5 Gt C each year (Tsunogai et al., 1999; Borges et al., 2005; Cai et al., 2006; Chen and Borges 2009).

These early continental shelf studies all favor the importance of spring phytoplankton blooms (i.e., winter mixing brings nutrient into the surface, with the onset of stratification in the spring and increased solar radiation, phytoplankton blooms will occur, Sverdrup 1953) in the uptake of atmospheric CO_2. They concluded that the spatial decoupling of autotrophic processes in the surface layer and the subsequent remineralization and export in the deep layer is the key to the continental shelf pump (Borges et al. 2006).

Contrary to these conclusions, recent studies in the U.S. South Atlantic Bight (SAB) suggested that this continental shelf is a strong CO_2 source (Cai et al., 2003; Wang et al., 2005). The early surveys were launched on one onshore-offshore transect in the central part of the SAB during December 2000, April 2002, June 2002, October 2002, and December 2002 (Wang et al. 2005). Their results showed that sea surface CO_2 was undersaturated relative to the atmosphere in winter and supersaturated in all other seasons. They concluded that the SAB releases CO_2 to the atmosphere at an average rate of 30 g C m^{-2} yr^{-1} (2.5 mol C m^{-2} yr^{-1}) on an annual basis, which contrasts sharply to the ECS sink of -3.0 mol C m^{-2} yr^{-1}.

Since the study of Cai et al. (2003) and Wang et al. (2005), scientists have been wondering what makes the SAB so different from other continental shelves? The SAB differs from East China Sea, the North Sea and the Middle Atlantic Bight in that it does not have spring blooms (Yoder 1985). The shelf is very shallow, only about 50-75 m deep at the shelf break. Due to the shallow depth, euphotic zone extends all the way to the bottom. Consequently, the shelf water is nutrient poor throughout the water column. Thus, winter mixing and spring stratification does not trap nutrients. The lack of spring bloom, together with the warm water temperature (low latitude) and inputs of inorganic and organic carbon from salt marshes might be responsible for the large source of atmospheric CO_2 (Cai et al. 2003; Wang et al. 2005).

The above explanations will certainly contribute to the SAB trending toward a source of CO_2. However, the conclusion by Cai et al. (2003) and Wang et al. (2005) was based on a single cross-shelf transect in the central part of the SAB with limited seasonal coverage. Inference of the air-sea CO_2 fluxes over the entire SAB from one onshore-offshore transect may be biased due to the large latitudinal variability: 1) the climate varies from temperate in the northern part of the SAB to subtropical in the southern areas; 2) the continental shelf is narrow (5-30 km) in the northern and southern extremes and broadens to about 120 km in its central area off Georgia coast; 3) the influence of the Gulf Stream is greatest in the southern region and weakest in the middle SAB; 4) most of the river runoff is distributed in the central area of the SAB (between 31^{o} and 33^{o}N), with the southern portion of the SAB receiving the least water from rivers (Figure 3.1); 5) interaction with salt marshes is also strongest in the central SAB where most of the salt marshes are located and the tidal range is highest. It was recognized that more work was needed in order to better quantify the CO_2 flux over the whole SAB (Cai et al. 2003).

To better quantify the CO_2 flux in the SAB and examine the mechanisms controlling CO_2 in this area, an extensive field sampling campaign was conducted in this study. Surface water pCO_2, along with other biogeochemical parameters, including vertical distributions of dissolved inorganic carbon (DIC), dissolved organic carbon (DOC), total alkalinity (TA), pH, nutrients, dissolved oxygen (DO), pH, and $\delta^{13}C$ and $\Delta^{14}C$ of DIC were measured over the entire SAB in all seasons. Air-sea CO_2 fluxes are calculated, and the biogeochemical mechanisms underlying CO_2

exchange processes are discussed. The DIC cycling was also probed to help understand the continental shelf pump in the SAB.

CHAPTER 2

A COMPARATIVE STUDY OF CARBON DIOXIDE DEGASSING IN RIVER- AND MARINE-DOMINATED ESTUARIES[1]

---

[1] Jiang, L.-Q., W.-J. Cai, and Y. Wang. 2008. *Limnology and Oceanography*. 53(6):2603-2615. Reprinted here with permission of publisher.

Abstract

The partial pressure of carbon dioxide (pCO_2), concentration of total dissolved inorganic carbon (DIC) and total alkalinity (TA) were measured at both high tide and low tide in the surface water of three Georgia (United States of America) estuaries from September 2002 to May 2004. Of the three estuaries, Sapelo and Doboy Sounds are marine-dominated estuaries, while Altamaha Sound is a river-dominated estuary. During all sampling months, the three estuaries were supersaturated in CO_2 with respect to the atmosphere (39.5-342.5 Pa, or 390 - 3380 μatm) due to CO_2 inputs from the estuarine zone (mainly intertidal marshes) and the river. The calculated annual air-water CO_2 flux in Altamaha Sound (69.3 mmol m^{-2} d^{-1}) was 2.4 times that of Sapelo and Doboy Sounds (28.7-29.4 mmol m^{-2} d^{-1}). Findings show that the higher CO_2 degassing in the river-dominated estuary was largely fueled by CO_2 loading from the river. Due to the substantial differences between river- and marine-dominated estuaries, the current estimates of air-water CO_2 fluxes in global estuaries (which are based almost entirely on river-dominated estuaries) could be overestimated.

1. Introduction

Recent studies have shown that estuaries are significant sources of carbon dioxide (CO_2) to the atmosphere, with pCO_2 varying from about 40 to 960 Pa (or ~400-9500 μatm) (Frankignoulle et al. 1998; Borges 2005; Borges et al. 2005). Even though the surface area of global estuaries is only about 1/20th that of continental shelves (Woodwell et al. 1973), it is argued that CO_2 degassing by estuaries (Borges 2005; Borges et al. 2005) could nearly counterbalance the continental shelf CO_2 sink (Tsunogai et al. 1999; Borges et al. 2005; Cai et al. 2006), which is about 30-70% of the atmospheric CO_2 sink of the open ocean (1.2-1.6 Pg C yr^{-1}) (Takahashi et al. 2009). However, most estuarine CO_2 studies have focused on estuaries that receive substantial freshwater discharge; much less attention has been given to estuaries that receive little freshwater discharge besides precipitation and groundwater (Frankignoulle et al. 1998; Borges 2005; Borges et al. 2005).

Definitions of estuaries vary widely. Most definitions restrict an estuary to the mouth of a river or a body of seawater reaching inland, while others argue that an estuary extends to the continental shelf (Perillo 1995). The most frequently cited definition of an estuary is that of Cameron and Pritchard (1963): “a semi-enclosed coastal body of water, which has a free connection with the open sea, and within which seawater is measurably diluted with freshwater derived from land drainage.” According to this definition, all river mouths and coastal brackish lagoons qualify as estuaries, although the former have been the focus for most estuarine studies.

Following Elliott and McLusky (2002), we have adopted the most widely held point of view that considers both river mouths and coastal brackish lagoons to be estuaries. The inclusion of coastal brackish lagoons as estuaries is also consistent with the fact that the most cited surface area of global estuaries was estimated “without differentiating mouths of rivers and coastal brackish lagoons" (Woodwell et al. 1973). For this study, we refer to mouths of rivers which receive significant amounts of upland river inflow, as river-dominated estuaries; and coastal brackish lagoons which receive little freshwater besides precipitation and groundwater, as marine-dominated estuaries.

The saltmarsh-surrounded estuaries of the southeastern United States cover approximately 3×10^9 m^2 (Alexander et al. 1986). River- and marine-dominated estuaries are typical features of this region, with marine-dominated estuaries covering approximately 50% of the total estuarine area in this region (National Ocean Service 1985). In this paper we present a comparative study of CO_2 in river- and marine-dominated estuaries around Sapelo Island, Georgia (Figure 2.1). The proximity of these two types of estuaries and their similarities in physical conditions provide a unique opportunity to examine the CO_2 differences between these two types of estuaries. We also discuss this study's implications for air-water CO_2 fluxes of estuaries globally.

2. Materials and Methods

2.1. Study Site

Sampling was conducted in the GCE-LTER (Georgia Coastal Ecosystems – Long Term Ecological Research) study area, which is located on the central Georgia coast of the southeastern United States (Figure 2.1). This region is characterized by extensive areas of intertidal salt marshes (vegetated principally by cordgrass *Spartina alterniflora* and the rush *Juncus roemerianus*) and tidal creeks. Tides (as high as 2-3 m) flood and drain the intertidal salt marshes twice daily and transport materials back and forth into the estuaries. The Altamaha River, which is a piedmont river, is one of the largest rivers on the eastern coast of North America with a rainfall catchment area of 37,600 km^2 (Figure 2.1). Discharge of the Altamaha

River is usually greatest in February-April and may have a secondary peak in autumn of some years. The annual average discharge rate is 4.3-19.5 km^3 yr^{-1} (USGS, United States Geological Survey).

The study area in the vicinity of Sapelo Island comprises Sapelo Sound, Doboy Sound, and Altamaha River delta (Figure 2.1). The three estuaries, which have water depths of 5-15 m, experience similar physical conditions, i.e., tidal amplitude, wind forcing, solar radiation, precipitation etc. However, they show large differences in terms of riverine influence and variability in salinity. Sapelo Sound is a marine-dominated lagoonal estuary with a rainfall catchment area of approximately 150 km^2 on the lower coastal plain; Doboy Sound is also a marine-dominated coastal lagoon but receives some Altamaha River flow via the Darien River during high flow seasons; Altamaha Sound, however, is a river-dominated estuary that receives significant amounts of freshwater from the Altamaha River (Figure 2.1). Other differences among the three estuaries include: Altamaha Sound has a shorter water residence time than Sapelo and Doboy Sounds due to rapid freshwater flushing; and, Altamaha Sound has a smaller ratio of saltmarsh area to estuarine water volume than Sapelo and Doboy Sounds.

2.2. Sampling and Analytical Methods

Three transects in Sapelo, Doboy, and Altamaha Sounds, respectively, were surveyed during both low tide and high tide on five cruises: 16-20 September 2002, 15-21 June 2003, 01-05 December 2003, 10-16 March 2004, and 27-30 May 2004 (Figure 2.1). Surface water temperature and salinity were recorded continuously with an on-board SeaBird flow-through thermosalinograph (model: SBE 21) on the R/V Savannah. Surface water xCO_2 (mole fraction of CO_2 in the dried equilibrated carrier gas) was measured underway using a LI-COR 6252 infrared gas analyzer coupled to a gas-water equilibrator. The well mixed gas passes through an electric

Peltier cooler, which removes most of the water vapor, then a drying tube filled with magnesium perchlorate [$Mg(ClO_4)_2$] before entering LI-COR 6252. The LI-COR 6252 was calibrated every 6 hours using certified gas standards, which had xCO_2 values of 200, 500, and 1000 $\times 10^{-6}$ referenced against standards traceable to those of the National Institute of Standards and Technology (NIST). The temperature of equilibration was measured with a Yellow Spring Instrument (YSI) temperature sensor right before the equilibrator. Atmospheric xCO_2 was also measured during all cruises. Surface water and atmospheric pCO_2 were calculated by correcting the xCO_2 measurements to 100% saturation of water vapor pressure and the in situ surface water temperature (Jiang et al. 2008a).

Water samples for dissolved inorganic carbon (DIC) and total alkalinity (TA) were collected at each sampling station (Figure 2.1). River end-member samples were collected from JayCee Landing in Jesup, Georgia (Latitude: N31.67, Longitude: W81.85, about 60 km upstream Altamaha Sound) on the Altamaha River. The samples were preserved with $HgCl_2$ and stored in a refrigerator on the research vessel. After the cruise, they were measured in the laboratory within 24 hours. DIC concentration was determined using an automated DIC analyzer with a precision of 0.1 % (Wang and Cai 2004). A water sample of 0.5 mL was pumped into the reactor and acidified with 10% H_3PO_4. Then the extracted CO_2 gas was measured with a LI-COR 6252 infrared CO_2 detector (Wang and Cai 2004). TA was determined in a 12-mL water sample by Gran Titration to an end point pH of 3.0. The TA titration was carried out using a computer controlled Kloehn digital pump. The precision of the TA measurement was 0.1%. Both the DIC and TA analyzers were calibrated against certified reference materials (CRMs) supplied by A. G. Dickson from Scripps Institution of Oceanography.

2.3. Temperature Normalization of *p*CO$_2$

Temperature plays an important role in shaping the surface water *p*CO$_2$, by controlling the thermodynamic equilibrium of inorganic carbon system (Takahashi et al. 1993). To remove the temperature effect, *p*CO$_2$ needs to be normalized to a common temperature. Because the equation suggested by Takahashi et al. (1993) only works for open ocean water (when salinity is between 34 and 36), we used a different method to achieve temperature normalization. First, carbonate alkalinity (CA or $[HCO_3^-] + 2[CO_3^{2-}]$) was calculated from *p*CO$_2$ and DIC using the inorganic carbon dissociation constants suggested for estuaries (Cai and Wang 1998) at in situ temperature and salinity. Then temperature-normalized *p*CO$_2$ was calculated from the CA and DIC data using the dissociation constants at in situ salinity and the annual mean temperature of 22.63^{o}C. The values of $(\partial p\mathrm{CO}_2/\partial \mathrm{T})/p\mathrm{CO}_2$ (T is temperature) in these estuaries were about 0.027-0.042^{o}C^{-1}, which are less than the 0.0423 ^{o}C^{-1}, as derived by Takahashi et al. (1993) for open ocean water. The values of $(\partial p\mathrm{CO}_2/\partial \mathrm{T})/p\mathrm{CO}_2$ were lowest in river-dominated estuaries at low tide; and highest in marine-dominated estuaries at high tide.

2.4. Air-water CO$_2$ Flux Estimation

Air-water CO$_2$ flux (F, mmol m^{-2} d^{-1}) is calculated according to:

$$\mathrm{F} = \mathrm{k} \cdot \mathrm{K}_0 \cdot (p\mathrm{CO}_{2\mathrm{water}} - p\mathrm{CO}_{2\mathrm{air}}) \qquad (2.1)$$

where k (cm h^{-1}) is the gas transfer velocity (piston velocity) of CO$_2$; K$_0$ (mol m^{-3} Pa^{-1}) is the solubility coefficient of CO$_2$ at the in situ temperature and salinity; *p*CO$_{2water}$ and *p*CO$_{2air}$ (Pa) are the partial pressure of CO$_2$ in the water and the air, respectively. A positive F indicates a transfer of CO$_2$ from the water to the atmosphere.

While gas transfer velocities (k) in the open ocean are primarily dependent on wind regime, those in shallow estuaries are usually more complicated. Besides the wind regime, they are also influenced by tidal current and bottom stress (Raymond and Cole 2001; Zappa et al. 2007). Consequently, the relationships of gas transfer velocity with wind speed could be site and event specific (Kremer et al. 2003; Borges et al. 2004*a*). Unfortunately, gas transfer velocities have not been widely measured in estuaries, and researchers still have to rely on wind speed dependence to approximate gas exchange rates. For this purpose, a relationship of gas transfer velocity with wind speed was produced by regressing the literature data in coastal environments (Figure 2.2). The data used were mainly from the compilation by Raymond and Cole (2001), with newer measurements included (Table 2.1). The regressed equation is as below:

$$k_{600} = 0.314 \cdot U_{10}^{2} - 0.436 \cdot U_{10} + 3.990 \qquad (2.2)$$

where, k_{600} (cm h^{-1}) is the gas transfer velocity at the Schmidt number of 600; and U_{10} (m s^{-1}) is the wind speed referenced at 10 m above the water surface.

A comparison of Equation (2.2) with that of Raymond and Cole (2001) ($k_{600} = 1.91 \times e^{0.35 \cdot U_{10}}$) shows that when wind speeds are lower than 5 m s^{-1}, k_{600} estimated from Equation (2.2) is slightly higher than that of Raymond and Cole (2001) (Figure 2.2). However, when wind speeds are above 6 m s^{-1}, k_{600} from these two equations shows great differences: k_{600} calculated from Equation (2.2) tends to follow the trend in the open ocean (Wanninkhof 1992; Ho et al. 2006); while that from the exponential relationship of Raymond and Cole (2001) becomes considerably higher (Figure 2.2). The equation of Raymond and Cole (2001) was obtained by an exponential regressing of available literature data in rivers and estuaries from that time. Most of the data used were measured when wind speeds were lower than 7 m s^{-1}. While the equation reasonably estimates gas transfer velocities when wind speeds are low, it could substantially overestimate gas transfer velocities when extrapolated to high wind speeds (Figure 2.2). Since wind speeds during this study are up to 12 m s^{-1}, we used Equation (2.2), instead of Raymond and Cole's (2001), to estimate air-water CO_2 fluxes.

Wind speeds obtained at 10 m height from the Marsh Landing Climate Station located on Sapelo Island, Georgia (Figure 2.1) were used to calculate k_{600} from Equation (2.2). While the Marsh Landing Climate Station is very close to Doboy Sound, it is about 12-15 km from the sampling stations in Sapelo and Altamaha Sounds (Figure 2.1). After k_{600} was estimated from wind speeds, the gas transfer velocities at in situ temperature were calculated as:

$$k_{SST} = k_{600} \times \left(\frac{Sc_{SST}}{600}\right)^{-0.5} \qquad (2.3)$$

where, k_{SST} is the gas transfer velocity at the sea surface temperature and Sc_{SST} is the Schmidt number of CO_2 at the sea surface temperature (Wanninkhof 1992).

To estimate area-averaged CO_2 fluxes, the surveyed areas of the estuaries were divided into 5-8 segments, with each segment centered by one of the sampling stations (Figure 2.1). The area-averaged flux in each estuary was then calculated as:

$$F_{area-averaged} = \frac{\sum F_i \cdot S_i}{\sum S_i} \qquad (2.4)$$

where, $F_{area\text{-}averaged}$ is the area-averaged flux in the estuary; F_i is the average of all the fluxes within segment i; and S_i is the surface area of segment i. The fluxes in months when pCO_2 was not measured were approximated by assuming a linear seasonal change of pCO_2. Since wind speeds were fairly constant in all months, this is equivalent to a linear seasonal change of gas fluxes. The annual fluxes were calculated as the average of all of the monthly fluxes. Here one needs to keep in mind that the assumption of a linear seasonal change is not necessarily the case in the field, and thus could cause uncertainties.

3. Results

3.1. Hydrographic Data

Surface water temperature did not show noticeable differences between high tide and low tide and was very similar among the three estuaries in all sampling months. It was about 14-15^{o}C during the March 2004 and December 2003 cruises; and 27 – 29^{o}C during the May 2004, June 2003, and September 2002 cruises (Figure 2.3a).

The Altamaha River discharge was highest during the sampling months of March 2004 and June 2003 (high flow months), and the least during May 2004, September 2002, and December 2003 (low flow months) (Figure 2.3b). Of the two high flow months, June 2003 showed discharge rates that were significantly higher than the long-term average (Figure 2.3b).

The surface water salinity measurements confirm the various freshwater influences on the three estuaries (Figure 2.4). Sapelo and Doboy Sounds were rarely influenced by freshwater runoff, although Doboy Sound received slight freshwater input during the high flow months of March 2004 and June 2003 (Figure 2.4). On the contrary, Altamaha Sound showed surface water salinity that is typical of river-dominated estuaries (Figure 2.4).

3.2. Surface Water pCO$_2$

During all sampling months, the three estuaries were supersaturated in CO$_2$ with respect to the atmosphere (atmospheric xCO$_2$: 371-389×10^{-6}), with surface water pCO$_2$ ranging from 39.5 to 342.5 Pa (Figure 2.5). Some shared characteristics of the pCO$_2$ in the three estuaries include: surface water pCO$_2$ was lowest at the ocean end and increased towards the innermost area of the estuaries; and, surface water pCO$_2$ at low tide was always higher than at high tide for any given point in space, although the difference is barely noticeable for a given salinity value.

Surface water pCO_2 in the two marine-dominated estuaries (Sapelo and Doboy Sounds) showed similar seasonal variations as that in the Duplin River, a nearby blind tidal creek that receives no freshwater besides precipitation and groundwater (Wang and Cai 2004). pCO_2 in Sapelo and Doboy Sounds was lowest in the cold months of March 2004 and December 2003, and highest in the warm months of June 2003 and September 2002 (Figure 2.5). Spatially, pCO_2 showed the largest magnitude of seasonal change in the innermost area of Sapelo and Doboy Sounds (Figure 2.5).

Surface water pCO_2 in the river-dominated estuary of Altamaha Sound was always higher than that in the two marine-dominated estuaries during all sampling months (Figure 2.5). The highest pCO_2 in Altamaha Sound was 342.5 Pa compared to about 243.2 Pa in Sapelo and Doboy Sounds. Surface water pCO_2 in Altamaha Sound contrasted seasonally with that in the two marine-dominated estuaries. pCO_2 in Altamaha Sound peaked during the high flow months of March 2004 and June 2003; although in the low flow months, it showed seasonal variations similar to those in the two marine-dominated estuaries (Figure 2.5).

3.3. Air-water CO_2 Fluxes

The calculated air-water CO_2 fluxes in the three estuaries were always positive (releasing CO_2 to the air) during all sampling months (Table 2.2). Fluxes at low tide were always higher than those at high tide. Fluxes averaged over high- and low-tide in the three estuaries ranged from 9 to 128 mmol m^{-2} d^{-1}. The annual average air-water CO_2 flux of Altamaha Sound was 69.3 mmol m^{-2} d^{-1}, which is about 2.4 times that of the two marine-dominated estuaries (Sapelo and Doboy Sounds) where the fluxes were 28.7 and 29.4 mmol m^{-2} d^{-1}, respectively (Table 2.2).

One of the biggest uncertainties in the air-water CO_2 fluxes comes from the uncertainty in estimating gas transfer velocity. The monthly averaged gas transfer velocities based on field wind speeds during this study varied from 7.7 to 8.6 cm h^{-1} (Table 2.2). They are at the higher end of 3.0-7.0 cm h^{-1} as suggested for estuaries by Raymond and Cole (2001), and at the lower end of the 8.7 – 17.1 cm h^{-1} as estimated by Elsinger and Moore (1983) using the ^{222}Rn and ^{226}Ra disequilibria method in a nearby river — Pee Dee River, South Carolina. The generic relationship of gas transfer velocity as a function of wind speed in estuaries introduces large errors in gas transfer velocity (Borges et al. 2004*a*). Consequently, air-water CO_2 fluxes of this study might suffer from large uncertainties.

This uncertainty, however, should not affect the conclusion that CO_2 degassing in Altamaha Sound was much higher than that in Sapelo and Doboy Sounds. During the flux calculation, the same gas transfer velocity (k_{600}) was used for all three estuaries in the same sampling month (Table 2.2). In terms of key factors controlling gas transfer velocity in an estuary (wind speeds, tidal amplitude, bottom stress, and fetch; Borges et al. 2004*a*; Zappa et al. 2007), these three estuaries are similar. Gas transfer velocities in Altamaha Sound could be slightly higher than those in the two marine-dominated estuaries, due to added turbulence caused by discharge enhanced velocities in Altamaha Sound. This factor would strengthen the conclusion that Altamaha Sound has higher air-water CO_2 fluxes.

3.4. Dissolved Inorganic Carbon

DIC concentrations in the two marine-dominated estuaries (Sapelo and Doboy Sounds) ranged from 1500 to 2200 μmol kg^{-1} (Figure 2.6). Spatial patterns of DIC concentration in Sapelo and Doboy Sounds varied seasonally. DIC concentration was higher in the innermost area of the sounds than at the ocean end during the low flow months of May 2004, September 2002 and December 2003 (Figure 2.6). This trend was reversed during the high flow months of March 2004 and June 2003. The seasonal changes in spatial DIC distributions in the two marine-dominated estuaries are easier to observe in Doboy Sound, which receives more freshwater than Sapelo Sound during high flow months (Figure 2.6).

DIC concentrations in Altamaha Sound showed much larger spatial and seasonal variations (450 - 2100 μmol kg^{-1}) compared to the two marine-dominated estuaries (Figure 2.6). The DIC concentration always increased towards the ocean end. It increased almost linearly with salinity due to fast flushing of the estuary; although the external inputs of DIC during mixing can be seen from the upward curvature of the DIC vs. salinity plots (Figure 2.6). The non-conservative DIC inputs, however, are less noticeable than those observed in the Satilla River Estuary, which has a longer water residence time (Cai and Wang 1998). Seasonally, DIC concentrations in Altamaha Sound were mainly controlled by river discharge rates. They were lowest when river discharge rates were at their highest. Overall, DIC concentrations farthest upstream of Altamaha Sound showed the largest seasonal variations. Finally, a comparison of DIC at the river end-member (JayCee Landing in Jesup, Georgia) with the DIC at zero salinity within the estuary suggests that DIC sources in the 60-km freshwater stretch are also significant during low flow months (Figure 2.6).

4. Discussion

Estuarine $p\mathrm{CO}_2$ is controlled by seasonal changes of water temperature and net CO_2 inputs from: 1) the ocean; 2) the river; and 3) within the estuarine zone. Temperature is important in the thermodynamic equilibrium of inorganic carbon system: it increases $p\mathrm{CO}_2$ in summer and fall and decreases $p\mathrm{CO}_2$ in winter and spring in the northern hemisphere. CO_2 addition processes in the estuarine zone include: net ecosystem metabolism within the estuary, DIC transport between surrounding intertidal marshes and the estuary, groundwater input, air-water gas exchange, calcium carbonate formation or dissolution and all other processes within the estuarine zone that could contribute to the gain or loss of CO_2 except those of the river and the ocean. In the following sections, the different CO_2 controlling mechanisms in the three estuaries on the Georgia coast (marine- vs. river-dominated) are discussed.

4.1. CO_2 in Marine-dominated Estuaries

pCO_2 in the two marine-dominated estuaries (Sapelo and Doboy Sounds) is lowest in winter and spring, and highest in summer and fall. The seasonal changes of pCO_2 in these estuaries are mainly controlled by the annual cycle of water temperature and the seasonal net CO_2 inputs from within the estuarine zone.

After temperature normalization, pCO_2 of the two marine-dominated estuaries is still higher in the warm months of June and September than in other months (Figure 2.7). Comparisons of in situ pCO_2 with the corresponding temperature-normalized pCO_2 show that water temperature lowers or raises the pCO_2 value by 20-30% in winter and summer, respectively during the sampling months.

We estimated the net DIC input from within the estuarine zone by modifying the approach of Cai et al. (2003). At any sampling station, the DIC in excess of that from mixing of the river and ocean end-members (DIC_{excess}) can be expressed as:

$$\mathrm{DIC_{excess}} = \mathrm{DIC_i} - \mathrm{DIC_{mixing}} \qquad (2.5)$$

where, DIC_i is the DIC concentration of station i and DIC_{mixing} is the DIC concentration due to mixing of the ocean and freshwater end-members.

DIC_{mixing} can be estimated from the DIC mixing line using the end-member data (Figure 2.8a). When inputs of DIC from the river are negligible (e.g., during all sampling months in

Sapelo Sound, and low flow months in Doboy Sound), DIC_{mixing} can be calculated as (Figure 2.8a):

$$DIC_{mixing\ w/o} = \frac{S_i}{S_{ocean}} \cdot DIC_{ocean} \qquad (2.6)$$

where, $DIC_{mixing\ w/o}$ is the DIC concentration after the ocean end-member is only diluted by a zero DIC freshwater; S_i and S_{ocean} are the salinity of station i and the ocean end-member, respectively. When Equation (2.6) is used to calculate DIC_{mixing}, the estimated DIC_{excess} also includes any possible DIC input from the river river.

When inputs of DIC from the river are significant (e.g. during all months in Altamaha Sound, and the high flow months in Doboy Sound), DIC_{mixing} has a substantial contribution from freshwater, and can be calculated as (Figure 2.8a):

$$DIC_{mixing\ w/R} = \frac{S_i}{S_{ocean}} \cdot DIC_{ocean} + (1 - \frac{S_i}{S_{ocean}}) \cdot DIC_{river} \qquad (2.7)$$

where, $DIC_{mixing\ w/R}$ is the DIC concentration after mixing of the ocean and the river end-member; and DIC_{river} is the DIC concentration of the river end-member.

The excess DIC results show that during all sampling months in Sapelo Sound and the low flow months in Doboy Sound, excess DIC is lowest in winter and spring, and highest in summer and fall. Plots of temperature-normalized pCO$_2$ against excess DIC indicate that excess DIC is responsible for the spatial and seasonal variations of the temperature-normalized pCO$_2$ in the two marine-dominated estuaries (Figure 2.9). During the high flow months of March 2004 and June 2003 in Doboy Sound, excess DIC was lower than that of Sapelo Sound due to the shorter residence time of Doboy Sound caused by river flushing (Figure 2.9). Regulations of CO$_2$ in Doboy Sound during these high discharge months are more like those in river-dominated estuaries, which will be discussed later. Temperature-normalized pCO$_2$ in the river-dominated estuary (Altamaha Sound) is not correlated with excess DIC except for September 2002, when Altamaha Sound behaves similarly to a marine-dominated estuary due to the low river discharge and high water temperature (Figure 2.9).

Excess DIC in these estuaries is the sum of all DIC inputs from within the estuarine zone. Earlier studies argued that in these saltmarsh-surrounded estuaries, direct CO_2 input from the surrounding intertidal marshes is one of the most important excess DIC sources contributing to the high air-water CO_2 fluxes (Cai et al. 1999; Neubauer and Anderson 2003; Wang and Cai 2004).

The southeastern coast of the United States has large areas of intertidal salt marshes dominated by *Spartina alterniflora,* which has a high productivity of about 1100-2200 g C m^{-2} yr^{-1} (Dai and Wiegert 1996). After the *Spartina* dies, a large fraction of the organic matter decomposes in situ. Dissolved organic carbon exuded from the marsh grasses during growth also contributes to the decomposition. Some of the CO_2 produced in the intertidal marsh water and sediment (Middelburg et al. 1996) will be mixed into estuarine water via tidal oscillation (Neubauer and Anderson 2003) and drainage of marsh sediment interstitial water (Jahnke et al. 2003). This is the major mechanism fueling the high CO_2 degassing in these estuaries (Cai and Wang 1998; Cai et al. 1999; Wang and Cai 2004).

In summary, the seasonal changes of pCO_2 in these marine-dominated estuaries are mainly controlled by the annual cycle of water temperature as well as saltmarsh production and remineralization processes. In spring and early summer, organic carbon accumulates in the salt marshes due to high *Spartina* productivity (Dai and Wiegert 1996). In late summer and fall, the higher water temperature and greater availability of labile organic matter contribute to higher bacterial remineralization rates in the intertidal marshes (Middelburg et al. 1996; Cai et al. 1999;

Wang and Cai 2004). The transport of CO_2 released from intertidal marshes to the estuaries at this time of the year enhances temperature-normalized $p\mathrm{CO}_2$ (Figure 2.7). The annual temperature cycle further helps to shape the seasonal variations of in situ $p\mathrm{CO}_2$ in these estuaries.

4.2. CO_2 in River-dominated Estuaries

Temperature-normalized $p\mathrm{CO}_2$ in Altamaha Sound shows different seasonal trends compared to Sapelo and Doboy Sounds (Figure 2.7). Instead of peaking in the warmest months of June 2003 and September 2002, temperature-normalized $p\mathrm{CO}_2$ in Altamaha Sound reached maxima during March 2004 and June 2003 when river discharge rates were highest (Figure 2.7). The apparent seasonal covariation of temperature-normalized $p\mathrm{CO}_2$ (Figure 2.7) and river discharge rates (Figure 2.3b) in Altamaha Sound suggests the importance of freshwater runoff to CO_2 in this type of estuary.

Freshwater runoff from land is an important source of CO_2 to river-dominated estuaries (Raymond et al. 2000; Borges et al. 2006). River water entering estuaries is usually supersaturated with CO_2 (Abril and Borges 2004). Sources of CO_2 in the river include microbial decomposition of organic matter in soils, river waters, and sediments (Cole and Caraco 2001). High concentrations of humic substances also contribute to the high $p\mathrm{CO}_2$ in river water by increasing acidity of source waters (Cai and Wang 1998).

The relative contributions of CO_2 from within the estuarine zone and the river can be calculated. Specifically, CO_2 concentration that is due to inputs from within the estuarine zone ($\Delta[CO_2]_{estuarine}$) can be estimated by the difference between the in situ CO_2 concentration ($[CO_2]_i$) and the CO_2 concentration if only conservative mixing occurs between the ocean and river end-members ($[CO_2]_{mixing\ w/R}$) (Figure 2.8b). Similarly, CO_2 concentration that is due to input from the river ($\Delta[CO_2]_{river}$) can be estimated by the difference between $[CO_2]_{mixing\ w/R}$ and the CO_2

concentration if the ocean end-member is only diluted by a zero DIC freshwater ($[CO_2]_{\text{mixing w/o}}$) (Figure 2.8b).

As $[CO_2]$ change is not linear during mixing (Figure 2.8b), $[CO_2]_{\text{mixing w/o}}$ and $[CO_2]_{\text{mixing w/R}}$ can not be estimated from the CO_2 mixing line directly. However, they can be estimated indirectly based on the fact that: DIC and TA mix conservatively with salinity, and, $[CO_2]$ can be calculated from its corresponding DIC and TA values. Specifically, $[CO_2]_{\text{mixing w/o}}$ was calculated from $DIC_{\text{mixing w/o}}$ and $TA_{\text{mixing w/o}}$, the former of which was estimated according to Equation (2.6) (Figure 2.8a), and the latter of which was also estimated from Equation (2.6) simply by replacing DIC with TA. Similarly, $[CO_2]_{\text{mixing w/R}}$ was calculated from $DIC_{\text{mixing w/R}}$ and $TA_{\text{mixing w/R}}$, both of which were calculated from Equation (2.7) (Figure 2.8a). When CO_2 concentrations were calculated from DIC and TA, the annual average temperature of $22.63^{o}C$ was used; since the dissolved CO_2 concentration is subject to changes in water temperature.

The results show that CO_2 inputs from within the estuarine zone as well as the river jointly contribute to the CO_2 in river-dominated estuaries (Figure 2.10). Their relative importance is most likely a function of water residence time in the estuary (Borges et al. 2006). During high flow months (March 2004 and June 2003), CO_2 inputs from the river dominate, while inputs from the estuarine zone are less important due to the short water residence time (Figure 2.10). On the other hand, during low flow seasons (May 2004, September 2002 and December 2003), with diminished riverine influence, CO_2 inputs from within the estuarine zone become relatively more important (Figure 2.10). Overall, CO_2 inputs from the river are mainly dependent on river discharge rates; while CO_2 inputs from the estuarine zone depend mainly on the season and water residence time (Figure 2.10).

The contribution of river-borne CO_2 to overall CO_2 fluxes in river-dominated estuaries was first estimated by Borges et al. (2006) based on the concept of excess CO_2. Excess CO_2 was defined as the quantity of DIC that would transfer to the atmosphere as CO_2 after complete water-air equilibrium (Abril et al. 2000). Potential CO_2 fluxes from the upstream river were then calculated as the product of excess CO_2 and average river discharge rates divided by the estuarine surface area (Borges et al. 2006). However, this method assumed that excess CO_2 varies linearly during mixing, which may not be the case due to the thermodynamic equilibrium of the inorganic carbon system.

For this study, CO_2 fluxes contributed by the river at each sampling station (referred to as river-borne CO_2 fluxes hereafter) were estimated using a new method. Air-water CO_2 flux can be expressed as:

$$F = k([CO_{2w}] - [CO_{2a}]) \qquad (2.8)$$

where, k is the gas transfer velocity; $[CO_{2w}]$ and $[CO_{2a}]$ are the CO_2 concentration at the bottom and top of the aqueous mass boundary layer, respectively. Assuming $[CO_{2a}]$ is a constant, we differentiated both sides of Equation (8) to derive:

$$\Delta F = k \cdot \Delta[CO_{2w}] \qquad (2.9)$$

Equation (2.9) calculates the change in air-water CO_2 flux when a certain change in surface water CO_2 concentration ($\Delta[CO_{2w}]$) occurs. Since we had already calculated the dissolved CO_2 concentrations that are contributed by the river ($\Delta[CO_2]_{river}$), the corresponding fluxes contributed by the river (ΔF_{river}) can be easily estimated from Equation (2.9).

Air-water CO_2 fluxes in Altamaha Sound were plotted against the CO_2 fluxes that are contributed by the river (Figure 2.11). The positive correlation shows the importance of river-borne CO_2 to the air-water CO_2 fluxes in river-dominated estuaries. However, their poor linearity

(R^2=0.83) also suggests that CO_2 inputs from other sources (i.e., within the estuarine zone) contribute to the CO_2 fluxes in Altamaha Sound.

To determine whether CO_2 contributed by the river is responsible for the extra high CO_2 fluxes in the river-dominated estuary, we examined the flux differences in the two types of estuaries and plotted them against the calculated river-borne CO_2 fluxes. The flux differences were estimated as the air-water CO_2 fluxes in Altamaha Sound minus the average fluxes in Sapelo and Doboy Sounds (Table 2.2). The strong correlation between the flux differences and the CO_2 fluxes in Altamaha Sound that are contributed by the river (R^2 = 0.96) suggests that CO_2 inputs from the river are likely to be responsible for the extra higher CO_2 degassing in the river-dominated estuary relative to the two marine-dominated estuaries (Figure 2.11).

The data also show that the river-borne CO_2 fluxes are more than enough to account for the flux differences between these two types of estuaries (Figure 2.11), indicating that other processes must also contribute to the flux differences. Even though the river-dominated estuary gets extra CO_2 from freshwater runoff, it may receive relatively less CO_2 from within the estuarine zone due to its shorter residence time and smaller ratio of saltmarsh area to estuarine volume. Plus, estuarine net ecosystem metabolism may also be different between these two types of estuaries due to extra inputs of nutrients and organic matter from the river into the river-dominated estuaries.

4.3. Implications to the Estimation of Global CO_2 Fluxes from Estuaries

This study shows large differences in CO_2 degassing between river- and marine-dominated estuaries. Higher CO_2 degassing in estuaries that are more influenced by freshwater was also found in other regions of the world, e.g. the three estuaries in the Cantabrian Sea (north of Spain) (Ortega et al. 2005), and the estuaries in Kaneohe Bay, Oahu, Hawaii (Fagan and Mackenzie

2007). If the conclusions from the present study can be applied globally, one implication is that the current estimates of global air-water CO_2 fluxes from estuaries could be overestimated.

The global air-water CO_2 fluxes in estuaries based on the synthesis of Borges (2005) and Borges et al. (2005) is about +0.40 Pg C yr^{-1}. However, there might be problems associated with these pioneering global estimates. First, the air-water CO_2 fluxes used for the synthesis were mainly from river-dominated estuaries (of small and intermediate sized rivers) (Borges 2005; Borges et al. 2005). Second, the surface area of global estuaries used included both river- and marine-dominated estuaries (Woodwell et al. 1973). Since air-water CO_2 fluxes in marine-dominated estuaries could be considerably lower than those in river-dominated estuaries, the estimates of global CO_2 fluxes from estuaries by Borges (2005) and Borges et al. (2005) might be an overestimation.

Globally, estuaries are far more complicated than being simply classified as either river- or marine-dominated estuaries. Abril and Borges (2004) and Borges (2005) also demonstrated large CO_2 differences between macro-tidal and micro-tidal estuaries. In addition, there are estuaries that are dominated by large rivers, such as those of the Amazon River (Cooley et al. 2007), Mississippi River (Cai 2003; W.-J. Cai unpublished data, 2008), and Yangtze River (Zhai et al. 2007), where the estuaries are usually weaker CO_2 sources compared to most small and intermediate river-dominated estuaries that have been studied. There are also large estuarine systems such as Chesapeake Bay, Long Island Sound, Pamlico Sound and Puget Sound whose surface area covers a large proportion of the total surface area of global estuaries but have generally been under-studied in terms of CO_2. More work is clearly needed to better constrain the global air-water CO_2 fluxes from estuaries.

Table 2.1. Gas transfer velocities corrected to a Schmidt number of 600 (k_{600}) for rivers and estuaries. The measured gas transfer velocities were corrected to k_{600} using the equation provided by Wanninkhof (1992).

Study site	Method	Wind speed ($m\ s^{-1}$)	k_{600} ($cm\ h^{-1}$)	Reference
South San Francisco Bay	floating dome	1.8-5.3	0.8-23.3	Hartman and Hammond (1984)
Narragansett Bay	floating dome	1.8-3.3	4.4-11.9	Roques (1985)
Hudson River	floating dome	0.6-6.5	2.9-23.4	Marino and Howarth (1993)
Hudson River	purposeful gas tracer	2.5-4.9	1.5-9.0	Clark et al. (1994)
Parker River	purposeful gas tracer	0.3-2.1	0.8-3.5	Carini et al. (1996)
Two estuaries near Waquoit Bay, Massachusetts	floating dome	0.4-8.7	1.2-6.4	Kremer et al. (2003)
Randers Fjord, Scheldt and Thames Estuaries (Europe)	floating dome	0.5-11.1	2.1-51.0	Borges et al. (2004*a*)
Scheldt Estuary (Europe)	floating dome	1.8-10.5	7.7-30.5	Borges et al. (2004*b*)
Sinnamary River and Estuary (French Guiana)	floating dome	0.5-4.7	6.6-19.3	Guérin et al. (2007)*
Fukido River, Japan	floating dome	2.0-4.0	1.7-8.7	Tokoro et al. (2007)
Parker and Hudson River	gradient flux technique	3.0-8.7	4.4-25.7	Zappa et al. (2007)

*Averaged over wind speed bins of 1 ms^{-1}.

Table 2.2. Area-averaged air-water CO_2 fluxes (mmol m^{-2} d^{-1}) in Sapelo, Doboy, and Altamaha, sounds during all sampling months. "HT", "LT", and "Avg." are high tide, low tide, and the average of high tide and low tide, respectively. The bottom row of the table shows the gas transfer velocities (k_{600}) used to calculate the fluxes.

Estuaries	Tide	Mar 2004	May 2004	Jun 2003	Sep 2002	Dec 2003	Annual average
Sapelo Sound	HT	8.3	15.1	24.6	31.0	12.9	18.7
	LT	19.3	33.6	57.3	63.1	20.8	38.7
	Avg.	13.8	24.3	41.0	47.0	16.8	28.7
Doboy Sound	HT	4.2	12.2	23.9	29.1	12.8	16.8
	LT	14.0	30.4	71.2	72.7	21.0	42.0
	Avg.	9.1	21.3	47.5	50.9	16.9	29.4
Altamaha Sound	HT	43.5	16.8	86.8	51.7	19.2	43.4
	LT	112.4	58.2	169.0	107.9	37.5	95.2
	Avg.	78.0	37.5	127.9	79.8	28.4	69.3
K_{600} (cm h^{-1})	-	8.6	8.3	7.7	7.7	8.5	8.1

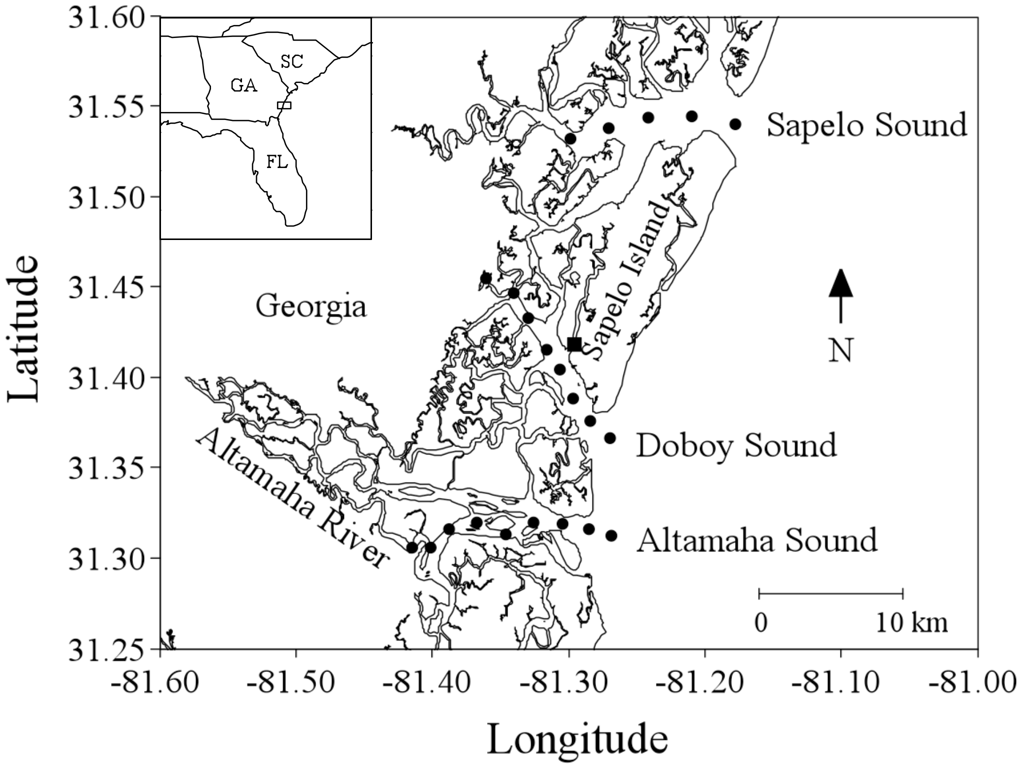

Figure 2.1. Map showing the three estuaries and the sampling stations. Filled circles show the sampling stations. The sampling stations are spaced at approximately 3 km intervals in Sapelo Sound and approximately 2 km intervals in Doboy and Altamaha Sounds. The filled square shows the location of Marsh Landing Climate Station.

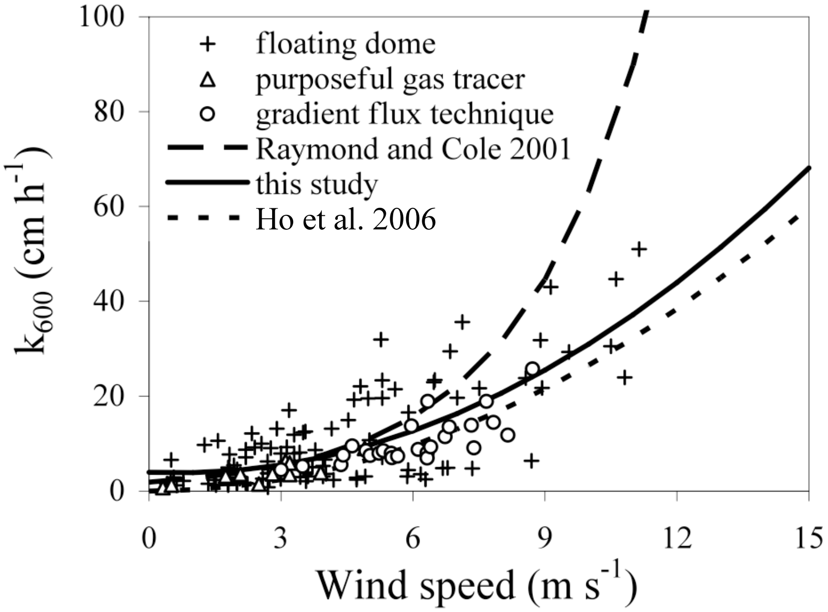

Figure 2.2. k_{600} as a function of wind speeds at 10 m above water surface (U_{10}). Pluses are the results from floating dome studies; open triangles are from purposeful gas tracer studies; and open circles are from gradient flux technique. The solid line is from regression of all the data. The dashed line and the dotted line are from the equations of Raymond and Cole (2001) ($k_{600} = 1.91\times e^{0.35\cdot U_{10}}$) and Ho et al. (2006) ($k_{600} = 0.266\times U_{10}^{2}$), respectively.

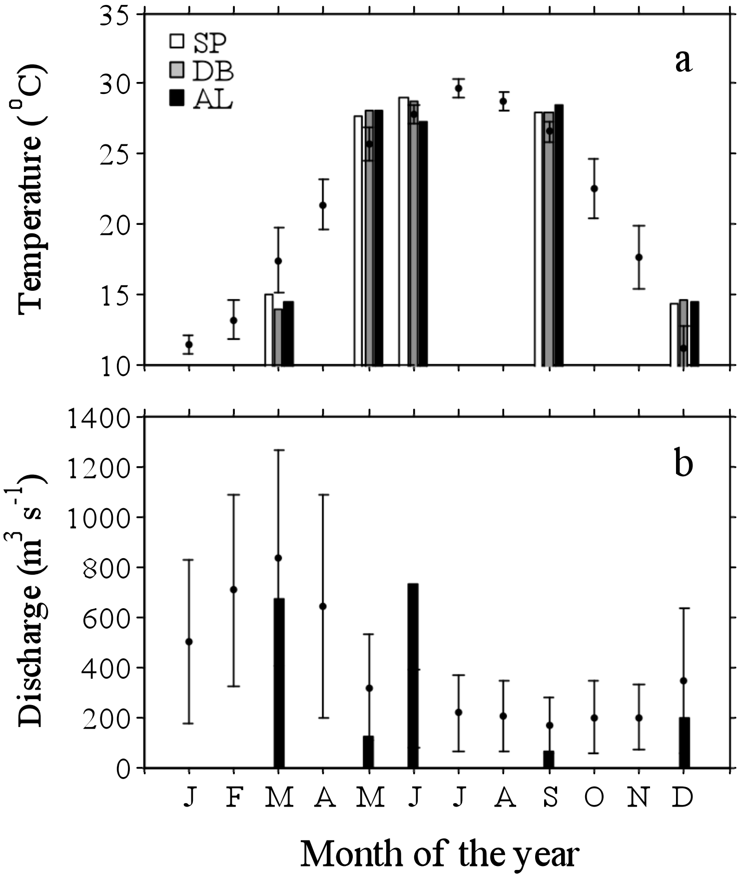

Figure 2.3. Surface water temperature and Altamaha River discharge rates. Columns in (a) show surface water temperature in the three estuaries during the sampling months of March 2004, May 2004, June 2003, September 2002, and December 2003. Open columns are for Sapelo Sound (SP), gray columns are for Doboy Sound (DB), and black columns are for Altamaha Sound (AL). Filled circles and dotted line in Panel (a) are the average water temperature from 2002 to 2005. Columns in (b) show Altamaha River discharge rates during all sampling months. Filled circles and dotted line in Panel (b) are the 30-year average discharge rates from 1976 to 2005.

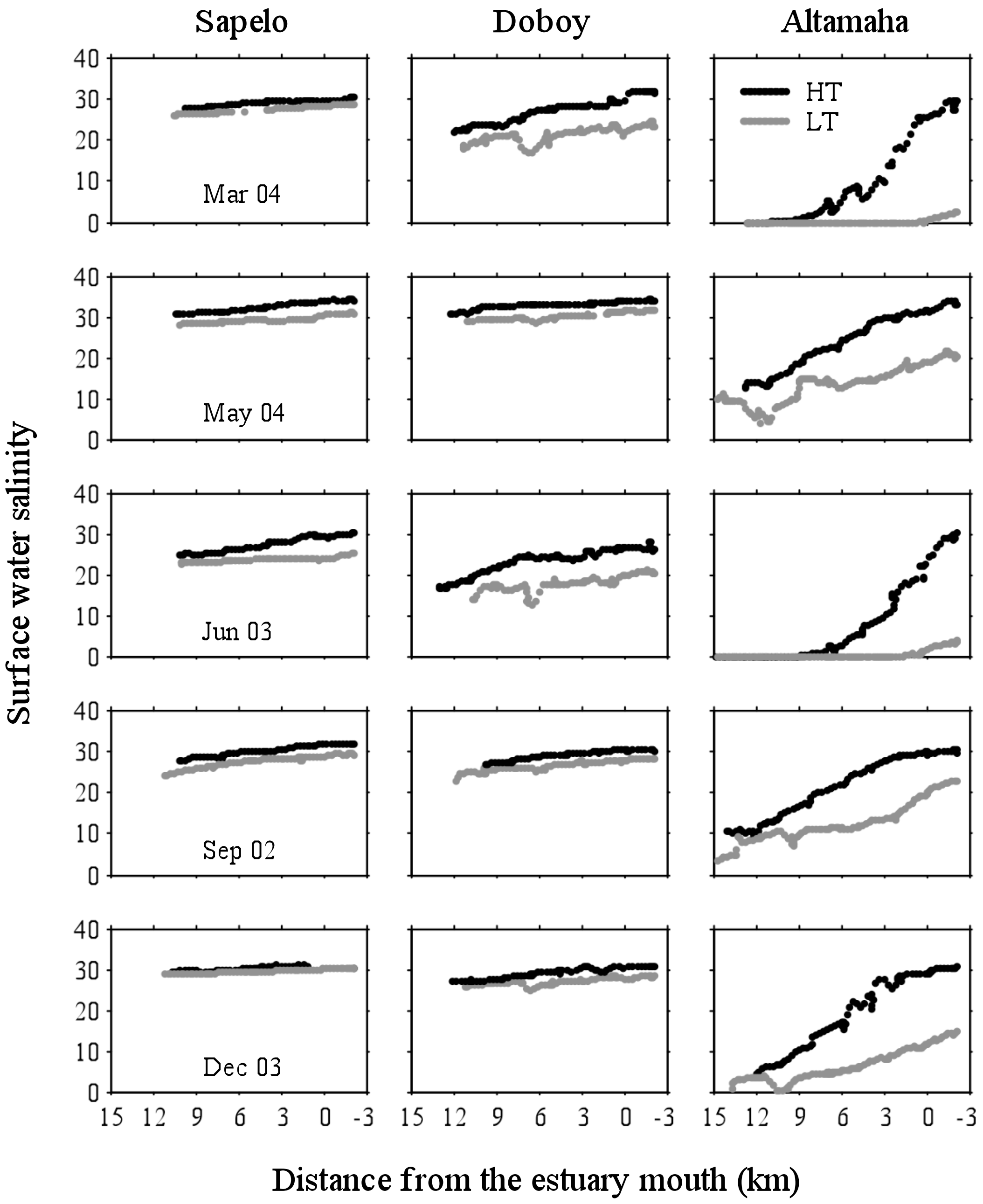

Figure 2.4. Spatial distributions of surface water salinity in the three estuaries during both high tide and low tide in all of the sampling months. Black dots are the salinity at high tide (HT), and gray dots are the salinity at low tide (LT). For the x-axis, positive values are inland and negative values are out to sea.

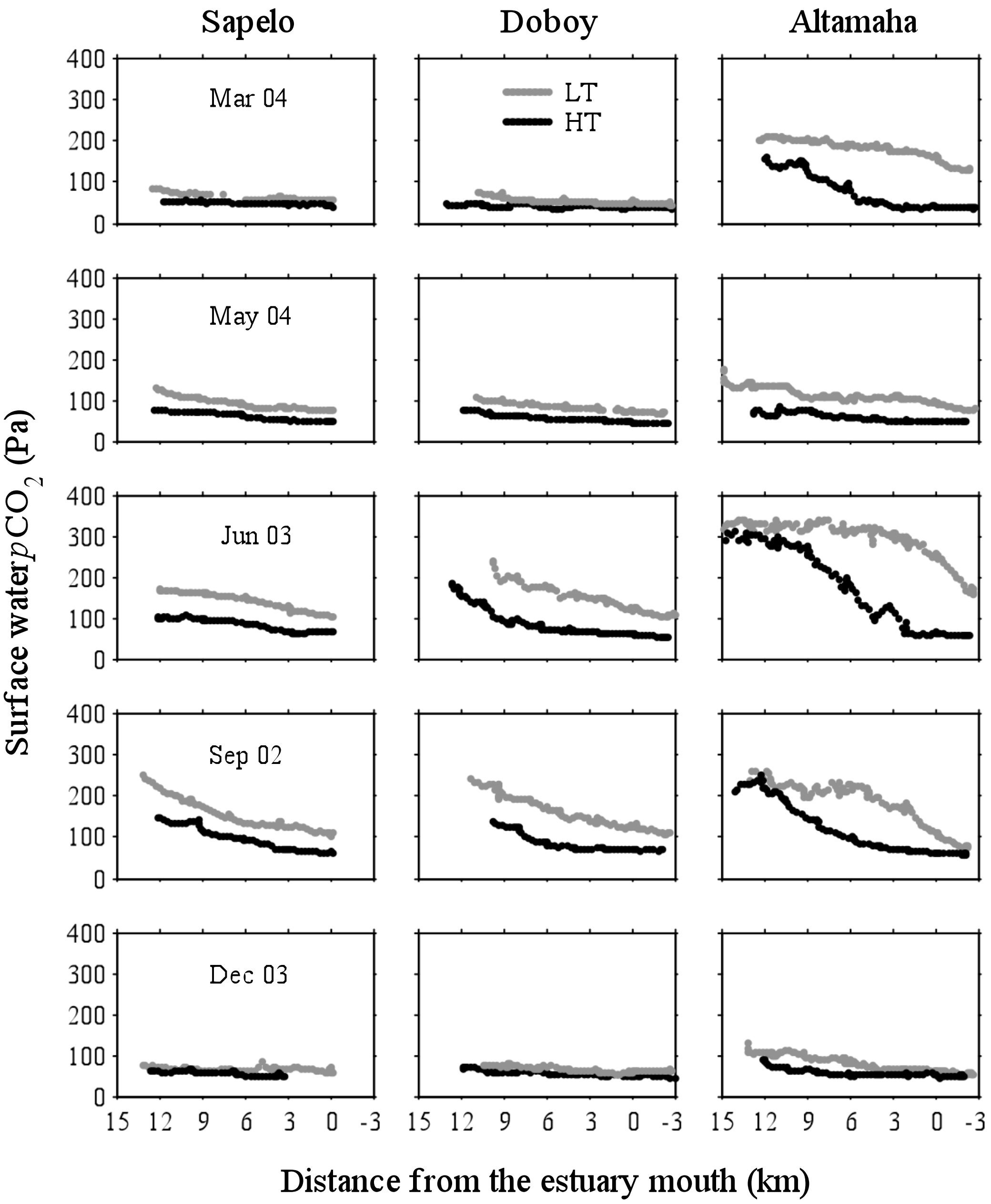

Figure 2.5. Spatial distributions of surface water pCO_2 in the three estuaries during both high tide and low tide in all of the sampling months. Gray dots are the pCO_2 at low tide (LT); and black dots are the pCO_2 at high tide (HT). For the x-axis, positive values are inland and negative values are out to sea.

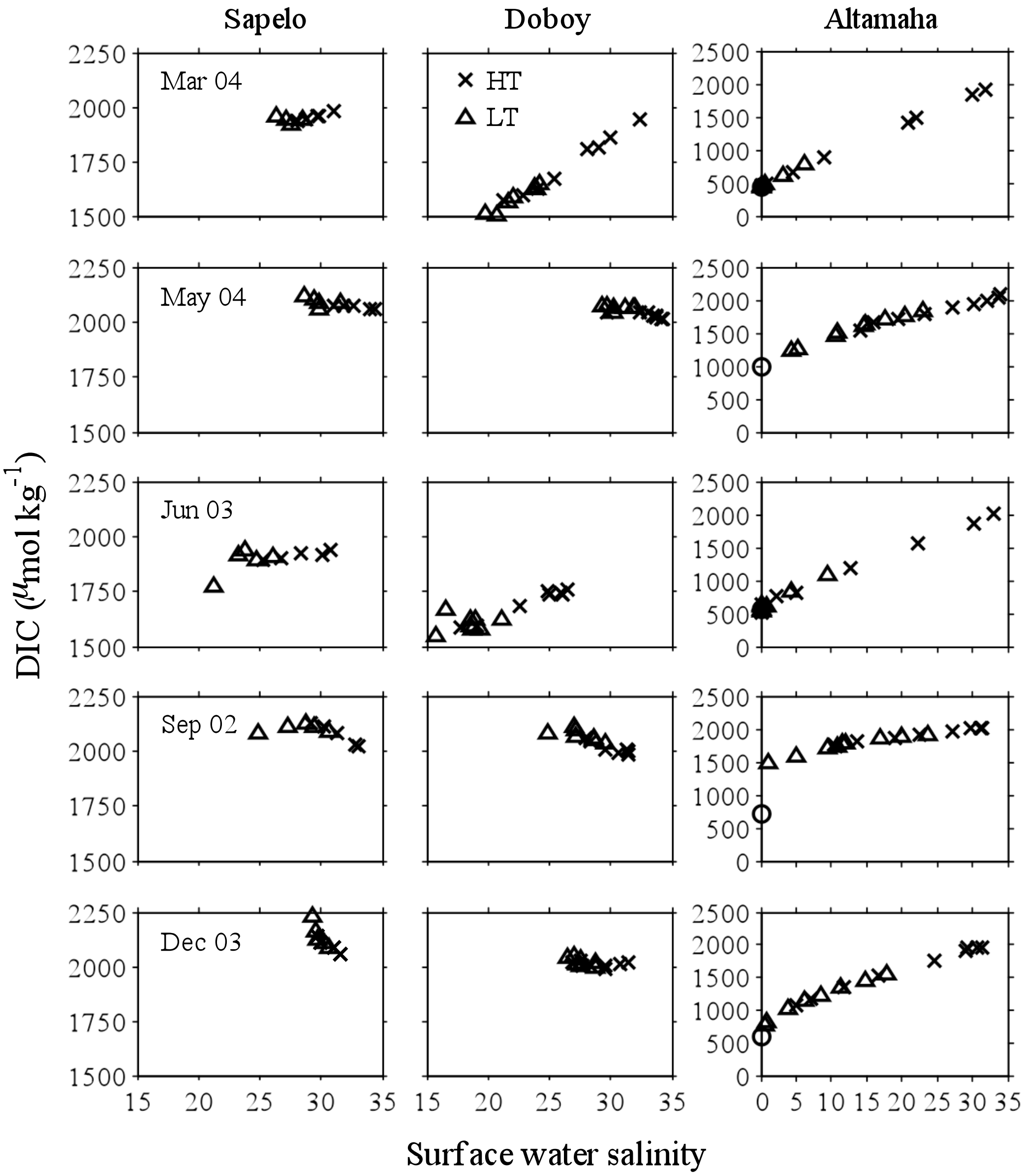

Figure 2.6. Dissolved inorganic carbon (DIC) vs. surface water salinity in the three estuaries during both high tide and low tide in all of the sampling months. Crosses are DIC at high tide (HT); and triangles are DIC at low tide (LT). Circles in the rightmost panels are DIC of the river end-member from JayCee Landing in Jesup, Georgia. During high flow months, e.g., March 2004 and June 2003, the end-member data may not be visible due to the fact that they are close to the value within the estuary at zero salinity.

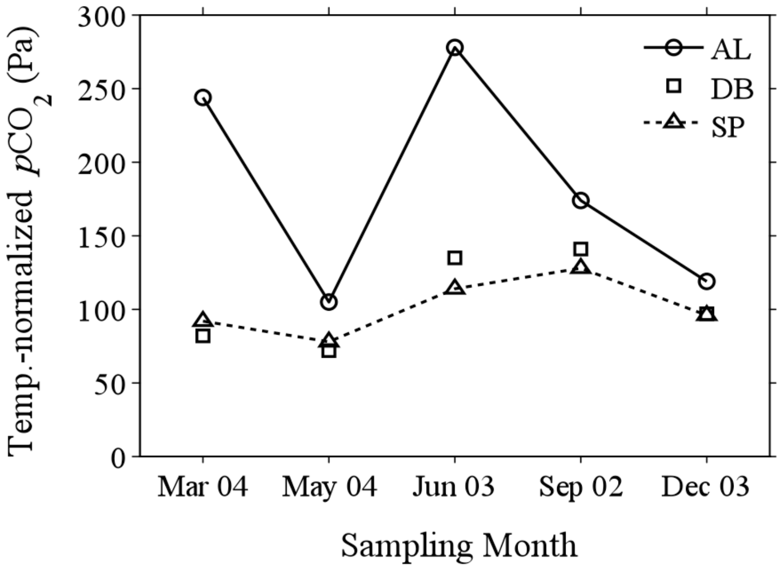

Figure 2.7. Temperature-normalized surface water pCO_2 (T=22.63 ^oC) in the three estuaries (area-averaged) at low tide in all of the sampling months. Circles and solid line are temperature-normalized pCO_2 in Altamaha Sound (AL), squares and dotted line are temperature-normalized pCO_2 in Doboy Sound (DB), and triangles and dashed line are temperature-normalized pCO_2 in Sapelo Sound (SP).

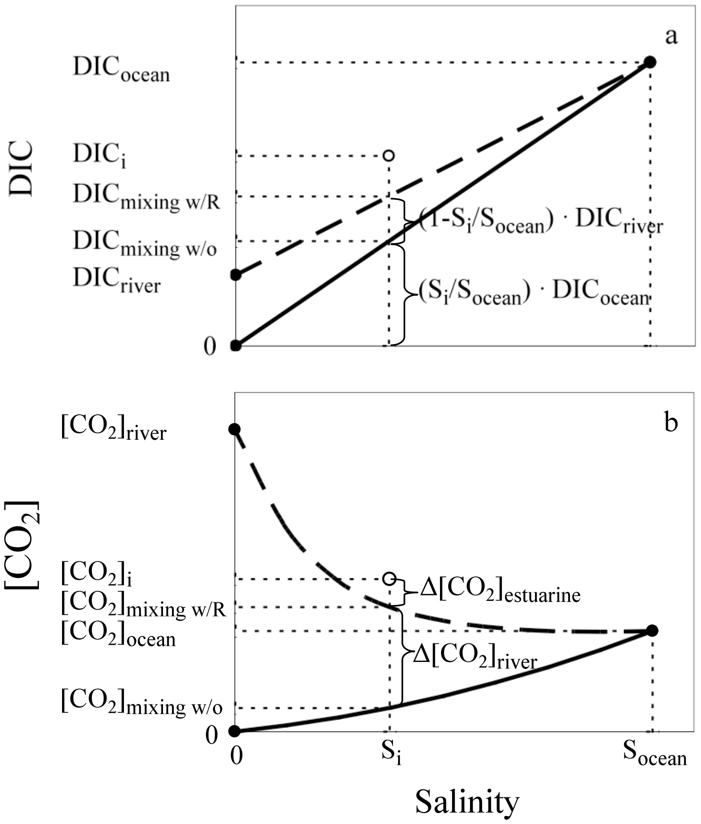

Figure 2.8. Diagrams showing DIC and dissolved CO_2 concentrations during estuarine mixing. (a) shows DIC concentrations during estuarine mixing. On the X-axis, S_i and S_{ocean} are salinity of station i and the ocean end-member, respectively. On the Y-axis, DIC_{ocean}, DIC_i, and DIC_{river} are DIC of the ocean end-member, station i, and the river end-member, respectively. $DIC_{mixing\ w/R}$ is DIC after conservative mixing of the ocean and river end-members; and $DIC_{mixing\ w/o}$ is DIC after the ocean end-member is only diluted by a zero DIC freshwater. (b) shows dissolved CO_2 concentrations during estuarine mixing. On the Y-axis, $[CO_2]_{river}$, $[CO_2]_i$, and $[CO_2]_{ocean}$ are dissolved CO_2 concentration of the river end-member, station i, and the ocean end-member, respectively. $[CO_2]_{mixing\ w/R}$ is CO_2 concentration after conservative mixing of the ocean and river end-members; and $[CO_2]_{mixing\ w/o}$ is CO_2 concentration after the ocean end-member is only diluted by a zero DIC freshwater.

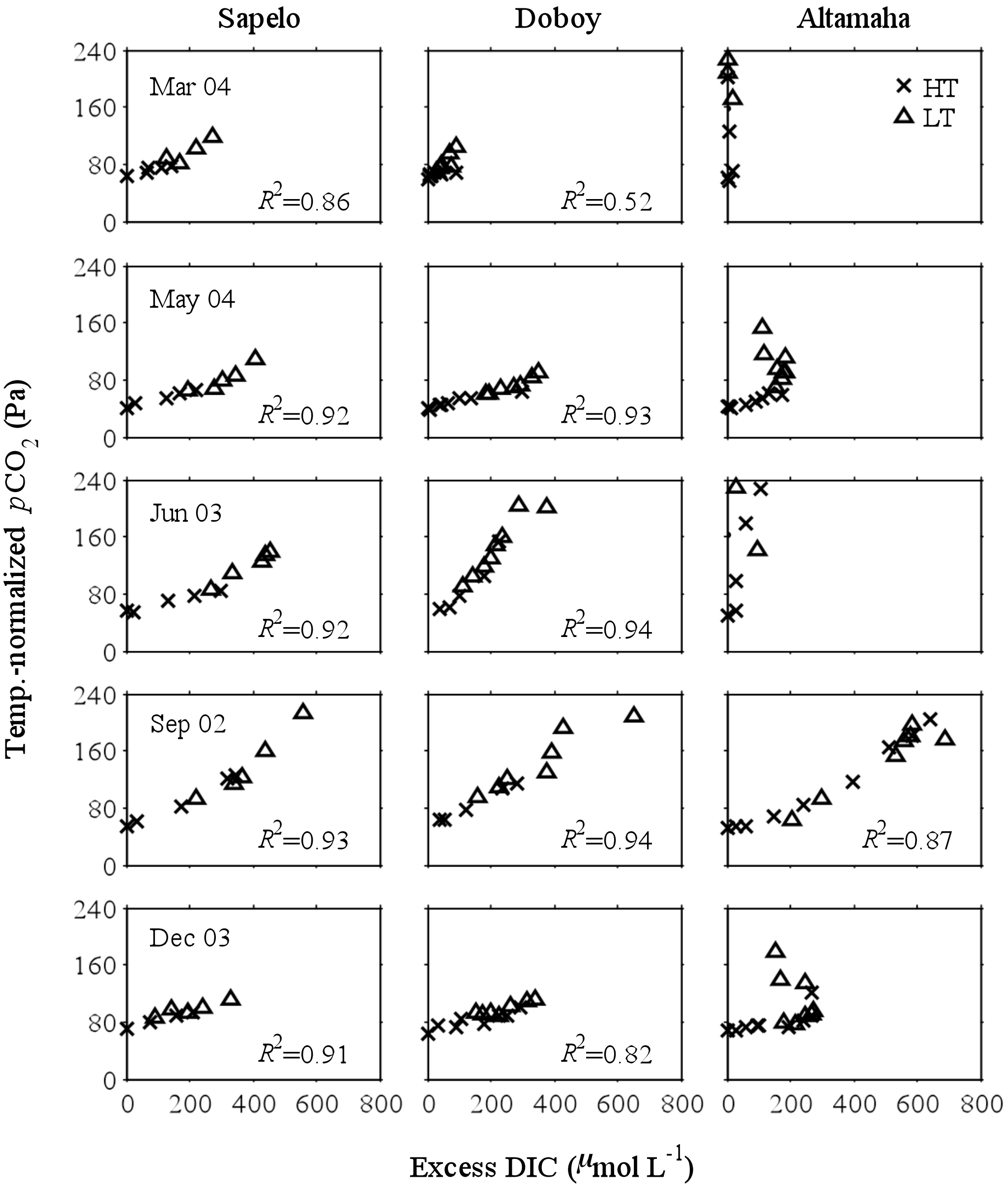

Figure 2.9. Temperature-normalized pCO_2 (T=22.63°C) plotted against excess DIC in Sapelo, Doboy and Altamaha, sounds. Crosses are data from high tide (HT) survey and triangles are data from low tide (LT) survey.

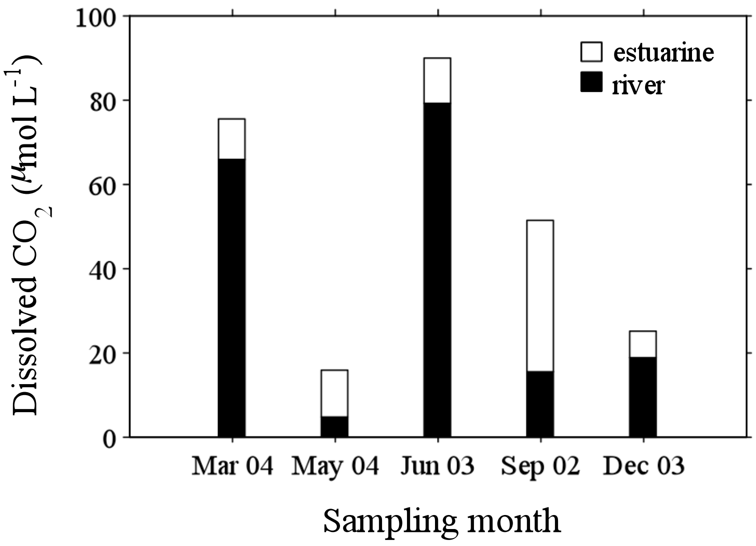

Figure 2.10. Dissolved CO_2 concentration (normalized to 22.63°C, area-averaged) that is due to inputs from the river and within the estuarine zone (intertidal marsh, net ecosystem metabolism, and all other sources except the ocean and river end-members) in Altamaha Sound at low tide. Open columns represent CO_2 from the estuarine zone; and filled columns represent CO_2 from the river.

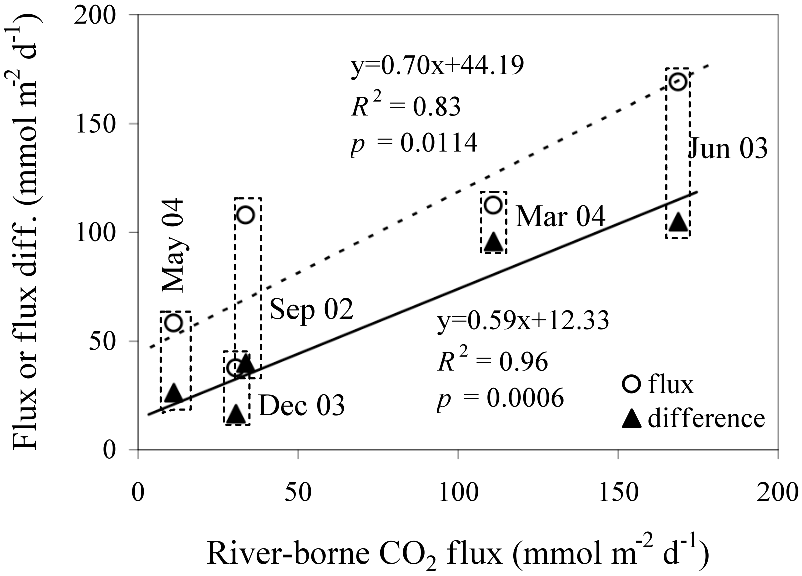

Figure 2.11. Air-water CO$_2$ fluxes in Altamaha Sound and the flux differences between the two types of estuaries against the river-borne CO$_2$ fluxes. Open circles are air-water CO$_2$ fluxes in Altamaha Sound at low tide, and filled triangles are the flux differences between the two types of estuaries at low tide. Dotted line is from a model II regression of air-water CO$_2$ fluxes against the river-borne CO$_2$ fluxes. Solid line is from a model II regression of the flux differences against the river-borne CO$_2$ fluxes.

CHAPTER 3

AIR-SEA CO_2 FLUXES ON THE CONTINENTAL SHELF OF THE SOUTHEASTERN UNITED STATES: SPATIAL AND SEASONAL VARIABILITY[1]

---

[1] Jiang, L.-Q., W.-J. Cai, R. Wanninkhof, Y. Wang, and Heike Lüger. 2008. *Journal of Geophysical Research*. 113: C07019, doi:10.1029/2007JC004366.
Reprinted here with permission of publisher.

Abstract

Partial pressure of carbon dioxide (pCO_2) in surface seawater on the US South Atlantic Bight (SAB) was measured during 6 cruises from January 2005 to May 2006. The high-resolution pCO_2 data allow us to create the first maps of sea surface pCO_2 over the SAB for all seasons. Contrary to an earlier study that was based on limited spatial and seasonal coverage, this study shows that the SAB is a net sink of atmospheric CO_2 on an annual and whole shelf basis (-0.48 ± 0.21 mol m^{-2} yr^{-1}). The inner shelf is a source of $+1.20 \pm 0.24$ mol m^{-2} yr^{-1}, while the middle and outer shelves are sinks of -1.23 ± 0.19 and -1.37 ± 0.21 mol m^{-2} yr^{-1}, respectively. Seasonally, the SAB shifts from a sink for atmospheric CO_2 in winter to a source in summer. The annual cycle of sea surface temperature plays a dominant role in controlling the seasonal variations of pCO_2. Wind speeds are highest when the shelf is taking up atmospheric CO_2, and lowest when the shelf is releasing CO_2 to the atmosphere. This seasonal anti-correlated of wind speeds with the direction of air-sea gas exchange is an important factor in contributing to the atmospheric CO_2 sink in the SAB. Factors related to the estimation of CO_2 fluxes in the coastal ocean, such as choice of wind speeds, correction of gas transfer equations with non-linearity coefficients, effect of diel variation of pCO_2, spatial extrapolation of pCO_2 to the nearshore area, and seasonal interpolation are also discussed.

1. Introduction

The burning of fossil fuel and deforestation release vast amounts of carbon dioxide (CO_2) into the atmosphere, about 50% of which remains there, while the rest is taken up by the oceans and land biosphere (Prentice et al. 2001; Sabine et al. 2004). The large uncertainties in the estimation of air-sea CO_2 fluxes limit our ability to predict future atmospheric CO_2 levels, and hence the ability to predict future climate change (Tans et al. 1990; Sarmiento and Le Quéré 1996). A major uncertainty has been the lack of knowledge of CO_2 fluxes in the ocean margins (Chen et al. 2003; Ducklow and McCallister 2004).

The ocean margin with its relatively small area but intense physical, chemical and biological processes is expected to be a significant contributor to the global air-sea CO_2 exchange (Mackenzie 1991). CO_2 studies in the East China Sea (ECS) (Tsunogai et al. 1999; Wang et al. 2000), the U.S. Middle Atlantic Bight (MAB) (Boehme et al. 1998; DeGrandpre et al. 2002), the U.S. Pacific coast off Oregon (Hales et al. 2005), and the West European Shelves (Frankignoulle and Borges 2001; Thomas et al. 2004a; Bozec et al. 2005) suggest that the ocean margin may act as an important sink for atmospheric CO_2. The “continental shelf pump”, which was originally proposed by Tsunogai et al. (1999), takes up CO_2 from the atmosphere at a rate of 0.2-1.0 Gt C each year (Tsunogai et al. 1999; Borges et al. 2005; Cai et al. 2006). Fluxes of this magnitude account for about 15-70% of the current estimate of the CO_2 uptake by the open ocean (1.2-1.6 Pg C yr^{-1}) (Takahashi et al. 2007), thus representing a significant portion of the oceanic uptake of CO_2.

Recent studies in the U.S. South Atlantic Bight (SAB), however, suggested that this continental shelf was a strong CO_2 source (Cai et al. 2003; Wang et al. 2005). The SAB is a low-latitude continental shelf bordered by abundant salt marshes on the land side and a western boundary current (i.e., the Gulf Stream) on the sea side (Figure 3.1). It was hypothesized that this type of continental shelves tends to behave as a source of atmospheric CO_2 (Cai et al. 2006). However, the conclusion by Cai et al. (2003) was based on the study of a single cross-shelf transect in the central part of the SAB.

Inference of the air-sea CO_2 fluxes of the whole SAB based on the study of one transect can be biased due to the large spatial variability. Several factors may contribute to the latitudinal heterogeneity in the SAB: 1) the climate varies from temperate in the northern part of the SAB to subtropical in the southern areas; 2) the continental shelf is narrow (5-30 km) in the northern and southern extremes and broadens to about 120 km in its central area off Georgia coast; 3) the influence of the Gulf Stream is greatest in the southern region and weakest in the middle SAB; 4) most of the river runoff is distributed in the central area of the SAB (between 31^{o} and 33^{o}N), with the southern portion of the SAB receiving the least water from rivers (Figure 3.1); 5) interaction with salt marshes is also strongest in the central SAB where most of the salt marshes are located and the tidal range is highest. It was recognized that more work was needed in order to better quantify the CO_2 flux over the whole SAB (Cai et al. 2003).

The purpose of this paper is to extend the sea surface $p\mathrm{CO}_2$ survey to the entire SAB with sufficient seasonal coverage. The results show that instead of being a source of CO_2 as concluded by Cai et al. (2003) and Wang et al. (2005), the SAB is a net sink on an annual basis, although the CO_2 sink is smaller compared to most other studied continental shelves. Possible reasons contributing to conclusions that contrast with those of the earlier study are discussed. The results from the SAB are compared to those from other continental shelves. Factors related to the estimation of the CO_2 fluxes in the coastal ocean are also discussed.

2. Study Site and Methods

2.1. Site Description

The U.S. South Atlantic Bight, also known as Southeastern United States Continental Shelf, extends along the eastern United States coast from Cape Hatteras, North Carolina to West Palm Beach, Florida (Figure 3.1). The shallow coastal water spreads out to the shelf break where the water depth is around 50-75 meters. For the purpose of discussion and conforming to traditional definitions, the SAB can be divided into three regimes: the inner shelf from the coastline to the 20m isobath; the middle shelf from the 20m to the 40m isobath; and the outer shelf from the 40m to the 100m isobath (Figure 3.1). The surface areas of the inner, middle, and outer shelves are 2.89, 4.53, and 1.64×10^4 km^2, respectively (Menzel 1993). The northward flowing Gulf Stream runs along the shelf break. The circulation of a semi-permanent gyre downstream of a bathymetric feature called the “Charleston Bump” off Long Bay, South Carolina brings nutrient-rich water from off the shelf edge and results in enhanced biological production (Bane and Dewar 1988; Lee et al. 1991).

A series of barrier islands lie off the coastline of Georgia and South Carolina. Between the barrier islands and the coastline there are extensive salt marshes (Menzel 1993). Tides, which can be as high as 2-3 m, flood and drain the inter-tidal salt marshes twice daily and transport materials back and forth onto the continental shelf. From north to south, eleven major rivers (the Cape Fear, Pee Dee, Santee, Cooper, Edisto, Savannah, Ogeechee, Altamaha, Satilla, St Mary’s, St Johns) input freshwater to the SAB (Figure 3.1). River discharge usually peaks in February-April and has minimum flow in September-November with a total annual discharge of about 66 km^3 (~2.7% of the SAB volume) (Menzel 1993). Release of groundwater, which can occur from salt marsh to the edge of the continental shelf, may also contribute to the freshwater supply

(Shaw et al. 1998). A Coastal Frontal Zone (CFZ) 10-30 km offshore, roughly the boundary of inner-mid shelf, can be formed by a pressure gradient induced by the freshwater discharge, and balanced by geostrophic forces (Blanton 1981). The CFZ presents a dynamic barrier to the seaward transport of dissolved and particulate materials (Blanton 1981; Blanton and Atkinson 1983).

2.2. Materials and Methods

2.2.1. Field Measurements

The survey was carried out on six cruises: 5-16 January 2005, 19-30 March 2005, 27 July - 5 August 2005, 7-17 October 2005, 16-21 December 2005, and 17-27 May 2006. In all of the sampling cruises except for the one in December 2005, the research vessel transected the whole SAB from coastline to about 500-m water depth. The survey focused on 5 onshore-offshore transects that are named E-, D-, C-, B-, and A-transects respectively from north to south (Figure 3.1). In December 2005, the ship transected the whole SAB, but did not cover D- and B-transects and did not go beyond the 200m isobath. Surface water and atmospheric xCO_2 (mole fraction of CO2 in the dried equilibrated carrier gas) were measured underway during all cruises. Sea surface temperature (SST) and salinity were recorded continuously with an on-board SeaBird® flow through thermosalinograph. Sea level pressure was recorded using an onboard R.M. Young® barometric pressure sensor.

Surface water xCO_2 was measured using a LI-COR 7000 infrared gas analyzer coupled to a gas-water equilibrator (referred to as UGA system hereafter). The equilibrator has a head-space volume of about 1 liter and is equipped with a specially designed water-drain system, which prevents direct contact of the gas in the head space with the outside air, and keeps pressure inside and outside the equilibrator balanced (see Figure A01 in Appendices for a diagram of the equilibrator). The well mixed gas first passes through an electric Peltier cooler, which removes most of the water vapor, and then a drying tube filled with Magnesium perchlorate [$Mg(ClO_4)_2$] before it gets to LI-COR 7000. The LI-COR 7000 was calibrated every 6 hours using certified gas standards, which had xCO_2 values of 201.51, 350.30, and 499.60 ppm referenced against standards traceable to those of the National Institute of Standards and Technology (NIST). The water temperature right before the equilibration chamber was recorded with a YSI® temperature sensor.

The partial pressure of CO_2 of the surface water at the temperature of equilibration [$p\mathrm{CO}_2$ (eq), units: μatm] was calculated as:

$$p\mathrm{CO}_2(\mathrm{eq}) = \mathrm{xCO}_2(\mathrm{water}) \times [\mathrm{P}_\mathrm{b}(\mathrm{eq}) - \mathrm{P}_\mathrm{w}(\mathrm{eq})] \tag{3.1}$$

where xCO_2(water) is the mole fraction concentration of seawater CO_2 in the dried sample gas flow (units: ppm). P_b(eq) is the barometric pressure of equilibration (atm). Since the pressure of equilibration was not measured in the UGA system during the survey, P_b(eq) is assumed to be the same as the barometric pressure at sea surface. Tests of the equilibrator in the lab show that the pressure inside and outside the equilibrator is the same. P_w(eq)is the water vapor pressure of equilibration (units: atm) that is calculated using salinity from the ship's thermosalinograph and temperature of equilibration (Weiss and Price 1980). For this study, the temperature of equilibration was assumed to be equal to the temperature from the YSI® sensor immediately before the equilibrator. The partial pressure of CO_2 at the in-situ temperature [$p\mathrm{CO}_2$(water), units: μatm] was then calculated according to Takahashi et al. (1993):

$$p\mathrm{CO}_2(\mathrm{water}) = p\mathrm{CO}_2(\mathrm{eq}) \times \exp[0.0423 \times (\mathrm{SST} - \mathrm{T}_\mathrm{eq})] \tag{3.2}$$

where SST is the in-situ sea surface temperature (units: $^\circ$C); and T_{eq} is the temperature of equilibration (units: $^\circ$C).

Atmospheric xCO_2 was measured 30-50 times in each cruise using the same CO_2 system. The inlet of the atmospheric CO_2 pipe, made of stainless steel, was set up on the highest platform in the front of the ship. In order to avoid possible contamination from the ship's stack gases, atmospheric xCO_2 was measured only when the ship was moving and the wind was blowing from the bow. The partial pressure of CO_2 in the air [pCO_2(air), units: μatm] was calculated as:

$$pCO_2\,(\text{air}) = xCO_2\,(\text{air}) \times [P_b\,(\text{sea surface}) - P_w\,(\text{sea surface})] \tag{3.3}$$

where xCO_2(air) is the mole fraction concentration of atmospheric CO_2 in the dried sample gas flow (units: ppm); P_b(sea surface) is the barometric pressure at sea surface (units: atm); and P_w(sea surface) is the water vapor pressure at sea surface (units: atm).

2.2.2. Comparison of the CO_2 Instrument

During the October 2005 and May 2006 cruises, a CO_2 system of Atlantic Oceanographic and Meteorological Laboratory (AOML, Miami, Florida) was deployed side-by-side with the UGA system. The system is described by Pierrot et al. (2007), and is referred to as AOML system hereafter. The AOML system was compared to a reference system in a comprehensive inter-comparison performed in Japan in 2003 and yielded values within 1 μatm of the reference system. Data from the AOML system are used to evaluate the UGA system, but only data from the UGA system are used for analysis in this study.

The pCO_2 measurements from the UGA and AOML systems during the October 2005 and May 2006 cruises showed similar variations with time. On average, the sea surface pCO_2 from the UGA system was about 3 μatm higher than that from the AOML system. The offsets were similar to that of the atmospheric pCO_2 measurements such that the ΔpCO_2 for the two systems was similar. However, occasional disagreements of up to 15 μatm between the two sets of CO_2 instrument were observed during the survey. The obvious pCO_2 reading differences were usually caused by events such as saturation of the $Mg(ClO_4)_2$ dryer, or malfunction of the equilibrator during bad weather. For the flux calculation, the questionable data (the data right after these events till the reading was back to normal) were not included.

2.2.3. Air-sea CO_2 Flux Calculation

The air-sea CO_2 flux on pixel i of a 0.1° longitude × 0.1° latitude grid on the SAB can be estimated as:

$$\mathrm{F_i} = \mathrm{k_i} \cdot \mathrm{K}_{0i} \cdot [p\mathrm{CO_2(water)_i} - p\mathrm{CO_2(air)_i}] \qquad (3.4)$$

where F_i is the air-sea CO_2 flux at pixel i (units: mmol m^{-2} d^{-1}). k_i is the gas transfer velocity (or piston velocity) of CO_2 (units: cm hr^{-1}); K_{0i} is the solubility coefficient of CO_2 (units: mol L^{-1} atm^{-1}) that is calculated from temperature and salinity (Weiss 1974); $pCO_2(water)_i$ is the partial pressure of CO_2 in seawater (units: μatm); and $pCO_2(air)_i$ is the partial pressure of CO_2 in the atmosphere (units: μatm). The mean value of the atmospheric xCO_2 during each cruise and the sea surface temperature, salinity and pressure is used to calculate the $pCO_2(air)_i$ from Equation (3.3). A positive F_i indicates a transfer of CO_2 from water to the atmosphere.

Gas transfer velocity was calculated from wind speeds. Relationships of gas transfer velocity with wind speed proposed by Wanninkhof (1992), Wanninkhof and McGillis, (1999), Nightingale et al. (2000), McGillis et al. (2001), McGillis et al. (2004), and Ho et al. (2006) were used to provide a range of the air-sea CO_2 fluxes. They are referred to as W92, WM99, N00, M01, M04, and H06 respectively hereafter.

Since the empirical relationships of gas transfer with wind speeds are non-linear, the temporal distribution of wind speeds will affect the gas transfer velocity as well when mean wind speeds are used. Wanninkhof (1992) addressed this issue by creating unique relationships for long-term and instantaneous winds respectively, assuming long-term winds followed a Raleigh

(Weibull) distribution. Here, the effect of wind speed variability over a month was determined in a more exact fashion by introducing an adjustment referred to as non-linearity coefficients of the wind speeds according to Wanninkhof et al. (2002):

$$C_2 = \left(\frac{1}{n}\sum_{j=1}^{n} U_j{}^2\right)/U_{mean}^2 \tag{3.5}$$

$$C_3 = \left(\frac{1}{n}\sum_{j=1}^{n} U_j{}^3\right)/U_{mean}^3 \tag{3.6}$$

where C_2 and C_3 are non-linearity coefficients for quadratic and cubic terms of the gas transfer relationships, respectively; U_j is the high frequency wind speed (units: m/s); U_{mean} is the monthly mean wind speed (units: m/s); and n is the number of available wind speeds in the month. After non-linearity coefficients were calculated for each month, the gas transfer relationships for steady winds were corrected by C_2 or C_3 to get the relationships of gas transfer velocity with wind speed specifically for the wind distribution in the month (Table 3.1).

Satellite-derived wind speeds (level 2B QuikSCAT) referenced at 10 m above the sea surface were used for the flux calculation. NASA’s Quick Scatterometer covers the region twice a day with a resolution of 25 km. Flagged scans, which are usually due to precipitation, were excluded from the analysis. Monthly mean wind speed for a specific pixel was calculated by averaging all available wind speeds in the month (usually 40-50 out of the 60 scans). The QuikSCAT signal within 25-km from the coast can be contaminated and are therefore masked. Wind speeds in the masked area were filled in using the average wind speeds outside this band on the inner shelf.

Wind speeds from two NOAA (National Oceanic & Atmospheric Administration) buoys were used to calculate non-linearity coefficients due to better temporal resolution of the buoy data (every 10 minutes compared to every 12 hours for the satellite data). Non-linearity coefficients of the inner shelf were calculated from winds of Buoy 41008 (Latitude: 31.402 N, Longitude: 80.871 W, water depth: 18m, distance from the coast: 36 km), and that of the middle and outer shelves were calculated from Buoy 41004 (Latitude: 32.501 N Longitude: 79.099 W, water depth: 33.5 m, distance from the coast: 68 km). During the calculation, wind speeds from the buoy were adjusted to 10 m by multiplying its original 5-m measurements with a factor of 1.06 (R. Wanninkhof, personal communication, 2008).

To estimate the monthly air-sea CO_2 fluxes on the shelf, sea surface pCO_2, temperature, salinity, wind speed, and sea level pressure were interpolated onto a $0.1^{o}\times 0.1^{o}$ grid. Flux F_i at each pixel of the grid was calculated using the interpolated data according to Equation (3.4). The area of each pixel was calculated as:

$$S_i = \frac{\Delta \mathrm{Lon}}{360} \times 2 \cdot \pi \cdot R^2 \cdot [\sin(\mathrm{Lat}_i + \frac{1}{2}\Delta \mathrm{Lat}) - \sin(\mathrm{Lat}_i - \frac{1}{2}\Delta \mathrm{Lat})] \qquad (3.7)$$

where S_i is the area surrounding pixel i; R is the radius of the earth; Lat_i is the latitude on pixel i (units: degree); ΔLon and ΔLat are the longitude and latitude intervals of the grid, respectively (units: degree). The area-averaged air-sea CO_2 flux was then calculated by the equation:

$$F_{\mathrm{area-averaged}} = \frac{1}{S_1 + S_2 + \ldots S_n} \times \sum_{i=1}^{n} F_i \cdot S_i \qquad (3.8)$$

where $F_{\mathrm{area\text{-}averaged}}$ is the area-averaged flux.

When fluxes on the inner shelf were calculated, pCO_2 values were first linearly interpolated along the coastline based on the available most close-to-shore data. Then the added values and the original data on the inner shelf were used for interpolation. When fluxes on the outer shelf were calculated, data were included up to the 100-m isobath (the depth at the shelf break is 50-75 m).

To calculate the annual fluxes, fluxes in months with no survey were also estimated. At each pixel on the grid, sea surface pCO_2, temperature, salinity, sea level pressure, and atmospheric

xCO_2 were estimated based on linear interpolation between the two adjacent months. Then these data, along with the in-situ wind speed data from QuikSCAT and the buoys were used to calculate the fluxes on the pixel. After the flux in every month was estimated, the annual fluxes were calculated by averaging the results in all months.

3. Results

3.1. Hydrographic Data

Sea surface temperature in the SAB showed large onshore-offshore gradients in winter and was relatively uniform over the whole shelf in summer. In cold months (January, March and December 2005), temperature was lowest on the inner shelf (10 - 14 ^{o}C) and increased towards the outer shelf (20 - 25 ^{o}C) (Figure 3.2). Smaller cross-shelf temperature gradients were seen on the southern part of the SAB where the SST was closer to the Gulf Stream. In May 2006, the SST on the inner shelf increased considerably compared to the winter conditions, although it only changed slightly on the outer shelf. In July 2005, SST across the whole continental shelf was between 28 and 31 ^{o}C without much spatial variation. In October 2005, SST on the inner shelf dropped slightly to around 26-28 ^{o}C. SST on the outer shelf was between 28 and 29 ^{o}C at this time.

Sea surface salinity measurements confirmed the existence of the Coastal Frontal Zone near shore (10 - 30 km offshore). In all sampling months, surface salinity was lowest close to the shore (30 - 33) and increased sharply towards the open ocean salinity (S = 36.5) at the CFZ (Figure 3.3). The extreme southern part of the shelf showed the smallest onshore-offshore salinity gradients with salinity close to that of the Gulf Stream. Seasonally, salinity on the inner shelf showed the largest variation. The lowest inner shelf salinity occurred during March and

October 2005, when sea surface salinity as low as 27 was seen at the innermost stations of C-transect. In July 2005, a body of low salinity water was found just south of E-transect on the middle and outer shelves. Occurrence of lower salinity shelf water in the offshore area around the "(Charleston) Bump" region between late June and early August has been reported by Singer et al. (1983), and they attribute this to the occurrence of sustained southerly to southwesterly winds.

3.2. Sea Surface pCO_2

Sea surface pCO_2 in the SAB showed strong seasonal and spatial variations (Figure 3.4, see also Figure A02 in Appendices for pCO_2 along the ship track). Seasonally, sea surface pCO_2 was undersaturated with respect to the atmosphere in cold months (January, March and December 2005) and supersaturated in warm months (July and October 2005). In May 2006, CO_2 in the water was almost in equilibrium with the atmosphere. Spatially, sea surface pCO_2 exhibited strong onshore-offshore gradients in both the cold and warm months: pCO_2 on the inner shelf was lower than that on the middle and outer shelves during cold months and this pattern was reversed during warm months (Figure 3.5). Onshore-offshore gradients of sea surface pCO_2 were not uniform from Cape Hatteras, NC to Cape Canaveral, FL. The largest onshore-offshore pCO_2 gradients occurred in the central part of the SAB, while the cross-shelf pCO_2 gradients in the extreme southern part of the shelf were smallest (Figures 3.4 and 3.5). Below is a detailed description of the sea surface pCO_2 on the inner, middle and outer shelves of the SAB.

3.2.1. Inner Shelf

Sea surface pCO_2 on the inner shelf showed the largest seasonal variation (Figures 4 and 5). In January 2005, the inner shelf was strongly undersaturated. The lowest sea surface pCO_2 was 260 μatm, which occurred on the inner shelf of E-transect. Inner shelf pCO_2 increased from north to south except for C-transect, where $p\mathrm{CO_2}$ was higher than both D and B transects. The innermost area of C-transect had the highest $p\mathrm{CO_2}$ of ~400 μatm. During March 2005, sea surface $p\mathrm{CO_2}$ on the inner shelf was also strongly undersaturated. Compared to January, $p\mathrm{CO_2}$ on central and southern part of the inner shelf increased noticeably (Figure 3.4). In May 2006, sea surface $p\mathrm{CO_2}$ on the inner shelf started to be slightly supersaturated. The central part of the SAB (C-transect) had the highest sea surface $p\mathrm{CO_2}$ of 460 μatm. $p\mathrm{CO_2}$ on the inner shelf peaked in July 2005. In the water just off Sapelo Island (C-transect), sea surface $p\mathrm{CO_2}$ reached as high as 1300 μatm. It was 400~500 μatm on the inner shelf of other transects based on our survey. In October 2005, sea surface $p\mathrm{CO_2}$ on the inner shelf was still highly supersaturated despite decreasing temperatures. $p\mathrm{CO_2}$ on the inner shelf of C-transect was around 800 μatm. It was 430-510 μatm on the inner shelf of other transects. From October 2005 to December 2005, inner shelf $p\mathrm{CO_2}$ dropped dramatically to an undersaturated state. It was around 275 μatm on the inner shelf of E-transect. The lowest $p\mathrm{CO_2}$ at this time was found on the inner shelf of D-transect, where it was 260 μatm. Toward south, sea surface $p\mathrm{CO_2}$ increased to 330, 340, 360 μatm on the inner shelves of C, B and A transects, respectively.

3.2.2. Middle and Outer Shelves

Sea surface $p\mathrm{CO_2}$ on the middle and outer shelves was also undersaturated in cold months (January, March and December 2005) and supersaturated in warm months (July and October 2005), although $p\mathrm{CO_2}$ here was generally closer to the atmospheric equilibrium compared to that on the inner shelf (Figures 4 and 5). The middle shelf was a $\mathrm{CO_2}$ transitional zone of the inner and the outer shelves, with $p\mathrm{CO_2}$ here closer to that of the outer shelf. Therefore, we focus on $p\mathrm{CO_2}$ levels on the outer shelf. In January 2005, the outer shelf $p\mathrm{CO_2}$ varied slightly from 330 μatm on E-transect to 360 μatm on A-transect. In March 2005, surface $p\mathrm{CO_2}$ on the outer shelf only increased slightly compared to that of January 2005. In May 2006, pCO$_2$ on the outer shelf was almost in equilibrium with the atmosphere. In July 2005, the outer shelf pCO$_2$ ranged from 390 to 440 μatm. A high pCO$_2$ zone located south of E-transect (Figure 3.4) was found where low salinity water occurred (Figure 3.3). In October 2005, pCO$_2$ on the outer shelf dropped slightly to 370~400 μatm. In December 2005, the outer shelf became undersaturated with respect to the atmosphere CO$_2$ again. The highest pCO$_2$ at this time was 370 μatm, which occurred on the outer shelf of A-transect. Towards north, the outer shelf pCO$_2$ decreased to around 350 μatm on the central part of the shelf, and continued to drop to around 330 μatm on the extreme northern part of the outer shelf.

3.3. Atmospheric xCO$_2$

The average atmospheric xCO$_2$ of each sampling month ranged from 387 to 396 ppm (Figure 3.6b) with standard deviations of ~1.5% for all months. Atmospheric xCO$_2$ was highest in March and relatively low in summer. The atmospheric xCO$_2$ measurement during our cruises was on average 10 ppm higher than the observations from the flask network of the NOAA Environmental Science Research Laboratory (ESRL) at Bermuda, which range from 374 ppm to 385 ppm in 2005 (Figure 3.6b). During the flux calculation, mean values of the atmospheric xCO$_2$ from each cruise were used.

Continental sources have been found to influence the atmospheric CO$_2$ results over the continental shelf, making atmospheric xCO$_2$ here more variable and relatively higher than that of the open-ocean. To improve the estimate of the air-sea CO$_2$ fluxes in the coastal ocean, further research is needed to study the atmospheric xCO$_2$ variability in this region.

3.4. Wind Speeds

Wind speeds showed opposite seasonal trends compared to the sea surface $p\mathrm{CO_2}$. They were highest in winter and lowest in summer (Figure 3.6e). The monthly area-averaged wind speeds over the whole shelf from January to March 2005 were very high and relatively constant at 7.7-8.6 m/s. From March to August, wind speeds dropped continuously from 8.6 m/s to about 5.3 m/s (Figure 3.6e). In fall, the wind speeds increased sharply to the wintertime conditions again. From September to December, area-averaged wind speeds were 7.6-8.5 m/s. Spatially, wind speeds decreased from north to south and from outer to inner shelf in all months (Figure 3.7). This is true especially during winter when the wind speeds were high. The average standard deviations of the wind speeds on all pixels of the grid in all months were around 50%.

3.5. Air-sea CO_2 Fluxes

Air-sea CO_2 fluxes calculated in this study were based on $p\mathrm{CO_2}$ data from Cape Hatteras, NC to Cape Canaveral, Florida (Figure 3.4). For the purpose of easy comparison with other studies, the fluxes are reported using different gas transfer relationships (Table 3.2). The calculated monthly air-sea CO_2 fluxes for all parts of the SAB in all months ranged from -20.8 to 28.5 mmol m^{-2} d^{-1} (Table 3.2). The SAB showed a strong seasonal pattern, shifting from a sink for atmospheric CO_2 from January to April, to a source from June to October, then back to a sink again after November (Figure 3.6f).

Hereafter, the fluxes are presented as the values calculated from gas transfer relationship of Wannnikhof (1992). On an annual basis, the SAB was a net sink of atmospheric CO_2 (-0.48 mol m^{-2} yr^{-1}). The inner shelf was a source of +1.20 mol m^{-2} yr^{-1}, while the middle and outer shelves were sinks of -1.23 and -1.37 mol m^{-2} yr^{-1} respectively (Table 3.2).

3.6. Factors Related to the Flux Estimate

Several factors can bias the estimation of the air-sea CO_2 fluxes in the coastal ocean. These include choice of wind speeds; non-linearity of the relationships of gas transfer velocities with wind speeds; diel variations of sea surface pCO_2; cool skin effect; spatial extrapolation of pCO_2 to the nearshore area; and seasonal interpolation to estimate the annual fluxes. These effects are not well constrained and still under debate. Below we evaluate the magnitudes of these effects on the estimation of air-sea CO_2 fluxes in the SAB.

3.6.1. Choice of Wind Speeds

Since gas transfer velocities have to be estimated from wind speeds, air-sea CO_2 fluxes are subject to the use of different sources of wind speeds. Wind speeds usually show large spatial and temporal variability (e.g., Figure 3.7). Ideally, they should be measured with sufficient spatial and temporal coverage in order to better constrain the gas transfer velocities over the whole shelf for a long period. Wind speed data are usually available from two sources: buoys and satellites. Buoy-derived wind speeds usually have high temporal coverage (e.g. every 10 minutes); however, their spatial coverage is very limited. On the other hand, satellite-derived wind speeds have very good spatial coverage but with a poor temporal resolution (e.g. every 12 hours).

For the purpose of comparison, the annual CO_2 fluxes were also calculated using wind speeds from two NOAA buoys: Buoy 41004 and Buoy 41008 (Figure 3.1). Wind speeds from these two buoys have very different seasonal variation (Figure 3.8). The calculated results show that except for the inner shelf, air-sea CO_2 fluxes based on wind speeds of Buoy 41004 are very close to those based on wind speeds of the satellite (Table 3.3). Fluxes calculated from wind speeds of Buoy 41008, however, show a much smaller sink of atmospheric CO_2 (Table 3.3) due to the smaller seasonal variation of wind speeds (Figure 3.8) (DeGrandpre et al. 2002).

It appears that satellite-derived wind speeds are the best choice for the calculation of air-sea CO_2 fluxes over a large area. If wind speeds from buoys are the only choice, caution must be applied for the selection of a representative buoy. For the flux calculation of this study, temporally-averaged wind speeds from the satellite are used to calculate the fluxes; and wind speeds from the buoys were used to calculate the non-linearity coefficients. In this way, the advantages of satellite-derived winds (better spatial coverage) and those of buoy-derived winds (better temporal coverage) are combined.

3.6.2. Non-linearity of Gas Transfer Relationships

When using long-term averaged wind speeds to calculate fluxes, omission of the non-linearity correction will underestimate the magnitude of air-sea CO_2 fluxes. The average non-linearity coefficients for quadratic terms of the gas transfer velocity (C_2) in this study ranged from 1.13-1.26 with an average of 1.18, which was slightly smaller than that of 1.26 by Wanninkhof (1992) when Rayleigh distribution of wind speed was assumed. The average non-linearity coefficients for cubic terms (C_3) ranged from 1.39 to 1.79 with an average of 1.54. Therefore, when mean wind speeds are used to calculate gas transfer velocities, if the non-linearity correction is ignored, the calculated gas transfer velocities will be underestimated. For the flux calculation of this study, non-linearity correction was applied to all gas transfer relationships (Table 3.1).

After non-linearity correction, air-sea CO_2 fluxes (on any part of the shelf in any months) calculated from different gas transfer relationships are closer to each other, with an average standard deviation of 14% compared to 25% before the correction. The smaller standard deviations after non-linearity correction are due to the fact that when non-linearity correction is not applied, the long-term gas transfer equation of Wanninkhof (1992) assumes Rayleigh distribution of wind speeds, while the other equations do not taken into account of temporal variations of wind speeds.

3.6.3. Diel Variation of *p*CO_2

The onshore-offshore surveys usually started on the inner shelf in the morning and ended on the outer shelf in the night. Consequently, air-sea CO_2 fluxes could be biased due to diel variations of sea surface *p*CO_2. Time series results at a station in the center of C-transect (middle shelf) in May 2006 showed large diel variations (Figure 3.9). *p*CO_2 was lowest at around 6 AM (local time) and highest at around 6 PM (local time) (Figure 3.9a). Correlation shows that SST was mainly responsible for the diel changes of *p*CO_2 (Figure 3.9b). Accordingly, diel cycles of *p*CO_2 can be simulated from the observed *p*CO_2 and diel variations of temperature. Assuming temperature differences between any point of the ship track and the nearby NOAA buoys are constant over the day, diel cycles of SST for any point of the ship track can be assessed by comparing the measured SST at that point with the SST recorded on the NOAA buoys in the same day. Then sea surface *p*CO_2 at any time of the day can be simulated. To examine the effect of diel variation on air-sea CO_2 fluxes, the simulated diel cycles of sea surface *p*CO_2 were also used to calculate air-sea CO_2 fluxes. Comparative calculations show that accounting for diel variation of *p*CO_2 can change air-sea CO_2 fluxes by up to 0.80 mmol m^{-2} d^{-1}, with an average of 0.17 mmol m^{-2} d^{-1}. However, this effect is largely cancelled out (<0.07 mmol m^{-2} d^{-1}) when calculating the annual mean flux. Moreover, the simulated *p*CO_2 probably shows the maximum diel changes, since photosynthesis often counteracts *p*CO_2 excursions caused by temperature. Therefore, the flux results presented in this study were not corrected for possible diel variations.

3.6.4. Cool Skin Effect

Robertson and Watson (1992) argued that cool skin effect could enhance oceanic uptake of CO_2 considerably, by lowering pCO_2 at the surface compared to the pCO_2 in the bulk layer, i.e., the measured pCO_2. However, recent studies show that such effect could have been overestimated as the mass diffusive layer is significantly thinner than the thermal diffusive layer (McGillis and Wanninkhof 2006). Zhang and Cai (2007) further pointed out that this small cool skin effect is counteracted by the salty skin effect, which is caused by sea surface evaporation. Tentative calculation shows that omission of cool skin effect will cause an error usually less than 1% of the air-sea CO_2 fluxes. Thus, for this study the cool skin effect was not taken into account.

3.6.5. Spatial Extrapolation to the Nearshore Area

Triangle-based linear interpolation (Matlab® function ‘griddata’) was used to interpolate the data in this study (Watson and Philip 1984). The method was good on the middle and outer shelves where spatial gradients of the pCO_2 were small and the spatial sampling coverage was relatively complete. However, for the inner shelf, interpolation can not reach all areas close to the coastline due to limited spatial coverage and the curved shape of the coastline (Figure 3.1). Thus, extrapolation becomes necessary in order to approximate the real fluxes.

Several methods were tried to constrain air-sea CO_2 fluxes on the inner shelf. Method one is to calculate the fluxes using triangle-based linear interpolation only. No extrapolation is attempted. This method is expected to underestimate the overall fluxes. It misses the most close-to-shore areas, where sea surface pCO_2 is extremely high in summer, although the pCO_2 in winter is not lower than the areas further offshore on the inner shelf. Method two is to first interpolate the data over the shelf; then the pixels close to the coast where interpolated values are not available are filled in using the available most close-to-shore interpolated values. Method two also underestimates the inner shelf fluxes due to the quick shoreward increase of pCO_2 in summer.

Since pCO_2 gradients alongshore are generally much smaller than those across-shelf, it appears reasonable to first fill in data along the coastline based on linear interpolation. Therefore, method three first generates values along the coastline using the available most close-to-shore measurements; then the added values together with all of the original data are interpolated. Method four is similar to method three. The only difference is that instead of interpolating the added values together with all of the original data, it interpolates the added values with the data on the inner shelf only. The results from all four methods are listed in Table 3.4. For this study, method four was chosen to estimate the fluxes on the inner shelf due to the less interpolation interferences on the across-shelf direction (i.e. between the inner shelf and the middle and outer shelves).

It seems that to derive accurate fluxes in the nearshore area, the cruise track design is very critical. For example, for the three non-wintertime surveys (May, July, October 2005), flux deviations among the four extrapolation methods are largest in July 2005 when the nearshore coverage was poor and smallest in May 2006 when the nearhsore coverage was best (Table 3.4). Nevertheless, this may be less of a concern when the spatial variability of pCO_2 is small such as in the three wintertime cruises.

3.6.6. Seasonal Interpolation

Air-sea CO_2 fluxes during the six sampling months were estimated from spatially interpolated pCO_2 and observed wind speeds for the particular month. The fluxes in months with no surveys were also approximated to determine the annual air-sea CO_2 flux in the SAB. In order to do so, surface water pCO_2 on each pixel of the $0.1^o \times 0.1^o$ grid was estimated by linear interpolation between the adjacent sampling months using the gridded value. The data was then combined with the real QuikSCAT wind speeds for the particular month to estimate the flux using Equation (3.4). The annual flux on the SAB estimated by this approach is -0.48 mol m^{-2} yr^{-1}, with fluxes on the inner, middle and outer shelf being 1.20, -1.23, and -1.37 mmol m^{-2} d^{-1} , respectively (Table 3.2).

For comparison, annual air-sea CO_2 fluxes in the SAB were also determined by direct linear interpolation of fluxes during the 6 sampling months. This approach yielded an annual average uptake of -0.78 mol m^{-2} yr^{-1}. The calculated fluxes for the inner, middle and outer shelf are 0.97, -1.54, and -1.65 mmol m^{-2} d^{-1}, respectively. This method assumes that both gas transfer velocity and sea surface pCO_2 vary in a systematic fashion from month to month. However, as shown in Table 3.2 and Figure 3.8, winds over the SAB show significant month to month variability. Since air-sea CO_2 flux is proportional to the second or third order of wind speeds (Table 3.1) times air-sea pCO_2 gradient, this method could cause large errors.

3.7. Uncertainties of Air-sea CO_2 Fluxes

One of the large uncertainties of air-sea CO_2 fluxes comes from the estimation of gas transfer velocity. In this study, gas transfer velocities had to be approximated based on their relationships with wind speeds. However, gas transfer velocities show considerable scatter when they are correlated with wind speeds due to their dependence on other factors besides wind speeds, such as fetch (Woolf 2005), the presence of surface–active organic matter (Frew 1997), and chemical enhancement (Wanninkhof and Knox 1996). Even after non-linearity correction, the flux standard deviations based on different relationships of gas transfer velocity are up to 19% (with an average of 14%). The sign and magnitude of the flux differences between various calculations depend on the wind speeds in different seasons (Table 3.2). This error from gas transfer velocity probably includes a systematic and a random component reflecting our lack of full understanding of gas transfer processes. For this study, we treat the uncertainties of gas transfer velocities purely as random.

Uncertainties of air-sea CO_2 fluxes also arise from the estimation of air-sea pCO_2 gradients. For coastal waters, a large part of the pCO_2 gradient uncertainties is from the measurements of atmospheric xCO_2. The results of this study show that atmospheric xCO_2 can be highly variable on the continental shelf. The standard deviations of atmospheric xCO_2 in this study were as high as ±6 ppm, which will generate an air-sea CO_2 flux uncertainty of about ±0.8 mmol m^{-2} d^{-1}. This is about ±5-12% of the fluxes, when the magnitude of air-sea pCO_2 gradients are large, as in January, March, July, October, and December 2005; and could be greater than ±100%, when the magnitude of air-sea pCO_2 gradients are very small, as in May 2006.

Assuming an average error of 14% for different gas transfer equations and an error of 6 μatm from measurements of air-sea pCO_2 gradient, the error for fluxes on part n of the shelf (n could be i, m, or o, for inner, middle, or outer shelf, respectively) in a particular month $(F_{error})_n$ will be (Taylor 1997):

$$(F_{error})_n = F_n \times \sqrt{0.14^2 + \left(\frac{6}{pCO_{2w} - pCO_{2a}}\right)^2} \qquad (3.9)$$

where F_n is the air-sea CO_2 fluxes on part n in a certain month; and pCO_{2w} and pCO_{2a} are the partial pressure of the sea surface and atmospheric CO_2, respectively. The results show that the errors of fluxes on part n of the shelf for a particular month ranged from ±0.1 to ±3.8 mmol m^{-2} d^{-1} with an average of ±1.5 mmol m^{-2} d^{-1} (or ±0.5 mol m^{-2} yr^{-1}).

Since the flux error in a particular month could happen to cancel out some of the error in another month; the error of annual fluxes will be less than the mean of the errors in all months

(Taylor 1997). The error of annual fluxes on part n of the shelf $(F_{error})_n$ (yr) can then be calculated as:

$$(F_{error})_n(\text{yr}) = \frac{1}{12} \times \sqrt{[(F_{error})_n \text{ of Jan}]^2 + [(F_{error})_n \text{ of Feb}]^2 \ldots + [(F_{error})_n \text{ of Dec}]^2} \qquad (3.10)$$

The calculated errors of the annual fluxes for the inner, middle, and outer shelves are ±0.24, ±0.19, and ±0.21 mol m^{-2} yr^{-1}, respectively.

Because the same atmospheric xCO_2 in a particular month were used to calculate air-sea CO_2 fluxes on the inner, middle, and outer shelves; the errors of annual fluxes on the inner, middle, and outer shelves are not random to each other. Thus, the error of annual flux over the whole shelf [$(F_{error})_{SAB}$ (yr)] was calculated as:

$$(F_{error})_{SAB}(\text{yr}) = (F_{error})_i(\text{yr}) \cdot \frac{S_i}{S_{SAB}} + (F_{error})_m(\text{yr}) \cdot \frac{S_m}{S_{SAB}} + (F_{error})_o(\text{yr}) \cdot \frac{S_o}{S_{SAB}} \qquad (3.11)$$

where S_i, S_m, S_o, and S_{SAB} are the surface area of the inner shelf, middle shelf, outer shelf, and the whole SAB, respectively. Overall, the error of annual flux on the whole SAB is ±0.21 mol m^{-2} yr^{-1}.

Uncertainties of air-sea CO_2 fluxes also come from the spatial and seasonal interpolation of sea surface pCO_2. Even though the spatial coverage of pCO_2 during this study is much greater compared to the earlier work and is one of the most comprehensive CO_2 surveys in the ocean margin to date, the interpolation of sea surface pCO_2 on the inner shelf may cause large uncertainties due to the great spatial gradients of sea surface pCO_2 in that area (Figure 3.4). In addition, the temporal interpolation of fluxes may also cause large uncertainties due to limited seasonal sampling.

4. Discussion

4.1. Comparison with Earlier Studies in the SAB

The calculated air-sea CO_2 fluxes based on this study show that the SAB is a net sink of atmospheric CO_2 of -0.48 ± 0.21 mol m^{-2} yr^{-1}. This contrasts with the earlier studies, which concluded that the SAB was a strong atmospheric CO_2 source of 2.5 mol m^{-2} yr^{-1} (Cai et al. 2003, Wang et al. 2005). Besides the inter-annual variations, other factors such as the data reduction procedure, atmospheric xCO_2 and wind speeds used for the calculation of fluxes, and the spatial and seasonal sampling coverage all contribute to the difference.

First, the earlier studies did not correct the sea surface pCO_2 for temperature differences between the water inlet and the equilibrator. Omission of this correction (temperature is usually about 0.2-0.4 ^{o}C higher in the equilibrator than in the water inlet) will bias the sea surface pCO_2. As an example, if the sea surface pCO_2 is 400 μatm, a 0.4 ^{o}C temperature difference between water inlet and equilibrator will increase the sea surface pCO_2 in the equilibrator by ~7 μatm, and make the SAB towards a source by 0.40 mol m^{-2} yr^{-1}.

Second, the atmospheric xCO_2 used by earlier studies contributes to the overestimation of air-sea CO_2 fluxes. Atmospheric xCO_2 of 370 ppm from the open ocean was used by Cai et al. (2003) and Wang et al. (2005) to calculate the fluxes. This study shows that the average atmospheric xCO_2 in the SAB is almost 10 ppm higher than that measured in the open ocean (Figure 3.6b), although the minimum measurements are close to that of the open ocean. Calculation shows that an atmospheric CO_2 decrease of 10 ppm would make the SAB towards a source by 0.56 mol m^{-2} yr^{-1}.

Third, the wind speeds used to calculate gas transfer velocity also contribute to the difference. In the earlier studies, wind speeds from a NOAA Buoy (#41008) were used to calculate the air-sea CO_2 fluxes (Wang et al. 2005). Comparison with the QuikSCAT wind speeds shows that the wind speeds recorded on Buoy #41008 do not represent the wind speeds over the whole SAB well (Figure 3.8). They are up to 2 m/s lower than the average satellite-derived wind speeds and show much smaller seasonal variation (Figure 3.8). Consequently, the seasonal anti-correlation of wind speeds with sea surface $p\mathrm{CO}_2$ levels, which is the key for the net uptake of atmospheric CO_2 (to be discussed in section 4.3), is partially cancelled out.

Fourth, the earlier studies measured sea surface $p\mathrm{CO}_2$ at much smaller spatial coverage. It was based on a single cross-shelf transect located in the central part of the SAB. The central part of the continental shelf usually has the highest sea surface $p\mathrm{CO}_2$ due to greater influences from salt marshes and freshwater discharge. Therefore, extrapolation from one transect in the central part of the shelf to the whole SAB overestimates sea surface $p\mathrm{CO}_2$. In addition, the earlier study included part of the Wassaw Sound, GA, where the surface water $p\mathrm{CO}_2$ was particularly high.

Last but not the least, the earlier studies had limited seasonal sampling coverage. There were no cruises from January to March, sea surface $p\mathrm{CO}_2$ at this time of the year had to be extrapolated based on the data of December and April. In this study, we find that sea surface $p\mathrm{CO}_2$ from January to March is lowest of the whole year. Thus, the seasonal extrapolation by Cai et al. (2003) and Wang et al. (2005) overestimated the sea surface $p\mathrm{CO}_2$ from January to March.

4.2. Temperature as the Primary Factor Controlling Sea Surface $p\mathrm{CO}_2$

Sea surface temperature (Figure 3.6c) is one of the most important factors controlling the seasonal changes of sea surface $p\mathrm{CO}_2$ (Figure 3.6a) in the SAB. Regressions of area-averaged sea surface $p\mathrm{CO}_2$ with their corresponding SST in different months show that temperature explains most of the seasonal variations of sea surface $p\mathrm{CO}_2$ on all parts of the SAB (Figure 3.10). The slopes of natural logarithms of $p\mathrm{CO}_2$ vs. SST are 0.034, 0.029, and 0.026 for the inner, middle, and outer shelf respectively, which are smaller than the isochemical factor of 0.042, which is applicable when only temperature is varied, but DIC, alkalinity, and salinity in the water are invariant (Takahashi et al. 1993). The smaller slopes on the middle and outer shelves compared to that on the inner shelf (Figure 3.10) are caused by the higher autotrophic status on the middle and outer shelves during summer and fall (Jiang et al., in preparation).

Spatially, sea surface $p\mathrm{CO}_2$ also showed similar trends with SST in cold months (January, March and December 2005) when cross-shelf temperature gradients were large; however this was not the case in warm months (July and October 2005) (Figure 3.5). As solar radiation decreases in fall, water temperature on the inner shelf drops more quickly than on the middle and outer shelf due to the shallower inner shelf and the input of colder river discharge. This inner shelf cooling, together with the influence of warmer Gulf Stream on the outer shelf, results in the strong onshore-offshore temperature gradient observed during cold months (Figure 3.5). Sea surface $p\mathrm{CO}_2$ in these months was low on the inner shelf and increased towards the outer shelf (Figure 3.5). However, during the warm months (July and October 2005) when SST was almost uniform over the whole shelf (Figure 3.5), sea surface $p\mathrm{CO}_2$ was much higher on the inner shelf than that on the middle and outer shelves (Figure 3.5), illustrating the importance of other processes. More discussion about the other controls (e.g. biological activity, mixing, and air-sea exchange etc) on the sea surface CO_2 of the SAB will be presented in Chapter 4.

4.3. Wind Distribution Contributes to the Net Annual CO_2 Sink

Wind speeds in the SAB (Figure 3.6e) were highest in cold months when sea surface $p\mathrm{CO}_2$ was undersaturated (Figure 3.6a); and lowest in warm months when sea surface $p\mathrm{CO}_2$ was supersaturated. This, together with the positive relationship of gas transfer velocity with wind speed, suggests that gas transfer velocity was highest when the shelf was taking up atmospheric

CO_2, and lowest when the shelf was releasing CO_2. Over an annual cycle, this will favor the uptake of atmospheric CO_2 (DeGrandpre et al. 2002). Spatially, winds speeds were usually greatest in the northern part of the SAB where $p$$CO_2$ was more undersaturated, and weakest in the southern part where the $p$$CO_2$ was more supersaturated (Figure 3.7). Such spatial distribution pattern of the wind speeds also contributes to the overall CO_2 uptake in the SAB.

4.4. SAB as a Weak Continental Shelf Pump

The CO_2 sink in the SAB is -0.48 ± 0.21 mol m^{-2} yr^{-1}, which is smaller than the Middle Atlantic Bight (-1.33 mol m^{-2} yr^{-1}, using an atmospheric xCO_2 of 365 ppm) (DeGrandpre et al. 2002), the North Sea (-1.38 mol m^{-2} yr^{-1}) (Thomas et al. 2004b), and the East China Sea (-2.92 mol m^{-2} yr^{-1}) (Tsunogai et al. 1999). Possible reasons for the smaller sink in the SAB include: higher sea surface temperature, larger influences from salt marshes, and less efficient biological uptake.

First, the higher annual temperature due to the low latitude in the SAB contributes to the smaller CO_2 sink (Cai et al. 2006). For example, the temperature on the inner shelf of the SAB ranged from 10 to 31 ^{o}C compared to only 4-25 ^{o}C in the MAB. The temperature increase of around 6 ^{o}C could increase sea surface $p$$CO_2$ by ~30% (Takahashi et al. 1993). Second, the inputs of carbon from salt marshes contribute to the SAB being a smaller sink of atmospheric CO_2. About 80% of the salt marshes on the eastern United States coast are located in the SAB (Reimold 1977). The inputs of DIC and DOC from salt marshes help increase the nearshore $p$$CO_2$ in the SAB (Wang and Cai 2004; DeAlteris 2007). Third, the well-mixed shelf water makes biological activity less efficient in the uptake of CO_2 in the SAB. The SAB is very shallow, only about 50-75 m at the shelf break. The shallow water depth together with the strong wind and tidal amplitude are sufficient to make the shelf well-mixed during most of the year

(Menzel 1993). The well-mixed shelf water makes it easier for the produced organic matter to be remineralized back into CO_2 in the mixed layer before it is buried in the shelf sediments or exported to the deep waters (Verity et al. 2002; Jahnke et al. 2005). This makes biological activity less efficient in the uptake of atmospheric CO_2. In comparison, the CO_2 sinks in the ECS and the northern North Sea are enhanced by the seasonal stratification (Tsunogai et al. 1999; Bozec et al. 2005). For example, in the ECS, the shelf water is strongly stratified due to warming and addition of freshwater during summer (Tsunogai et al. 1999). In the upper layer, high primary production causes the surface mixed layer to be severely undersaturated (Tsunogai et al. 1999). In the deeper layer, organic carbon that sinks from above is decomposed, and the produced DIC is transported into the deeper layer of the Kuroshio Current via isopycnal mixing (Tsunogai 2002). The spatial decoupling of primary production and remineralization makes it possible for the surface mixed layer to be strongly autotrophic, which is vital for the biological uptake of atmospheric CO_2 (Borges et al. 2006).

5. Summary

High-resolution pCO_2 surveys in the SAB show that this area is a net atmospheric CO_2 sink of -0.48 ± 0.21 mol m^{-2} yr^{-1}. The SAB shows a strong seasonal pattern, shifting from a sink of atmospheric CO_2 in winter to a source of CO_2 in summer. It also shows a strong cross-shelf pCO_2 gradient, increasing seaward in wintertime and decreasing seaward in summertime. The annual temperature cycle is largely responsible for the seasonal variations of sea surface pCO_2. The seasonal anti-correlation of the wind speeds with sea surface pCO_2 levels contributes to the SAB being a net sink of atmospheric CO_2. The large flux differences between this work and earlier studies suggest that due to the large spatial and seasonal variations of sea surface pCO_2 in the coastal ocean, sea surface pCO_2 must be surveyed with sufficient spatial and seasonal coverage in order to get an accurate flux estimate.

Table 3.1. Non-linearity corrected equations for gas transfer velocities at pixel i of the 0.1° × 0.1° grid. C_2 and C_3 are the non-linearity coefficients for the quadratic and cubic terms, respectively. U_i is the monthly mean wind speeds on pixel i of the grid. Sc_i is the Schmidt number, which can be calculated from the in-situ sea surface temperature (Wanninkhof 1992).

Gas transfer velocity (k_i)	**Reference**
$(0.31 \cdot C_2 \cdot U_i^2) \times (\frac{Sc_i}{660})^{-0.5}$	Wanninkhof (1992)
$(0.0283 \cdot C_3 \cdot U_i^3) \times (\frac{Sc_i}{660})^{-0.5}$	Wanninkhof and McGillis (1999)
$(0.222 \cdot C_2 \cdot U_i^2 + 0.333 \cdot U_i) \times (\frac{Sc_i}{600})^{-0.5}$	Nightingale et al. (2000)
$(0.026 \cdot C_3 \cdot U_i^3 + 3.3) \times (\frac{Sc_i}{660})^{-0.5}$	McGillis et al. (2001)
$(0.014 \cdot C_3 \cdot U_i^3 + 8.2) \times (\frac{Sc_i}{660})^{-0.5}$	McGillis et al. (2004)
$(0.266 \cdot C_2 \cdot U_i^2) \times (\frac{Sc_i}{600})^{-0.5}$	Ho et al. (2006)

Table 3.2. Air-sea CO_2 fluxes in all months of the sampling year on the U.S. South Atlantic Bight. Relationships of gas transfer with wind speed proposed by Wanninkhof (1992), Wanninkhof and McGillis (1999), Nightingale et al. (2000), McGillis et al. (2001), McGillis et al. (2004), and Ho et al. (2006) are referred to as W92, WM99, N00, M01, M04, and H06, respectively in the table. The fluxes shown are the area-averaged with non-linearity correction applied. The italic fonts in the first row of the table show the months when no surveys are available. The 'pCO$_2$' and 'Wind' in the first column of the table represent area-averaged sea surface pCO$_2$ and wind speed on that part of the shelf, respectively. These are listed for illustrative purposes. The units for air-sea CO_2 fluxes of each month are mmol m^{-2} d^{-1}; the units for the annual air-sea CO_2 fluxes are mol m^{-2} yr^{-1}; the units for pCO$_2$ are μatm, and the units for wind speed are m/s.

Area	**Jan 05**	***Feb 05***	**Mar 05**	***Apr 05***	**May 06**	***Jun 05***	**Jul. 05**	***Aug 05***	***Sep 05***	**Oct 05**	***Nov 05***	**Dec 05**	**Annual flux**	**Reference**
Inner	-16.9	-10.6	-11.1	-2.0	2.9	10.0	16.5	14.7	25.7	22.2	3.5	-15.4	**1.20**	W 92
	-20.1	-10.6	-11.5	-1.9	2.1	7.4	11.1	10.0	26.9	21.9	3.7	-14.8	0.74	WM99
	-13.1	-8.4	-8.6	-1.6	2.4	8.2	13.8	12.2	20.2	17.4	2.8	-12.1	1.01	N 00
	-20.8	-11.7	-12.0	-2.1	2.6	9.5	15.0	13.7	28.5	23.4	3.9	-15.8	1.05	M 01
	-15.7	-10.0	-9.3	-1.8	2.8	10.4	17.5	16.0	22.8	19.0	3.2	-12.8	1.28	M 04
	-13.8	-8.6	-9.1	-1.7	2.4	8.2	13.5	12.0	21.1	18.1	2.9	-12.6	0.99	H 06
pCO$_2$	300	317	335	371	407	482	557	544	523	501	403	304	-	-
Wind	7.6	7.1	8.0	7.4	6.2	5.7	5.6	5.4	7.8	7.9	7.2	8.0	-	-
Middle	-13.7	-10.8	-15.5	-5.2	0.4	3.5	5.9	4.8	7.2	3.5	-4.9	-15.6	**-1.23**	W 92
	-14.3	-10.2	-16.8	-5.0	0.2	2.7	3.8	3.7	8.7	3.2	-5.0	-15.1	-1.35	WM99
	-10.7	-8.7	-12.0	-4.1	0.3	2.9	5.0	4.0	5.6	2.8	-3.8	-12.2	-0.94	N 00
	-15.0	-11.1	-17.2	-5.5	0.3	3.4	5.3	4.8	9.0	3.5	-5.3	-15.9	-1.33	M 01
	-11.7	-9.5	-12.7	-4.6	0.3	3.6	6.3	5.3	6.7	3.0	-4.3	-12.5	-0.91	M 04
	-11.2	-8.9	-12.7	-4.2	0.3	2.8	4.9	4.0	5.9	2.9	-4.0	-12.7	-1.00	H 06
pCO$_2$	312	316	320	352	384	413	443	428	413	399	353	308	-	-
Wind	8.0	7.7	8.7	7.4	6.3	5.8	5.5	5.3	8.0	8.0	7.7	8.5	-	-
Outer	-11.0	-10.5	-16.2	-5.6	-0.1	2.3	3.8	2.7	4.3	1.4	-4.2	-12.0	**-1.37**	W 92
	-12.2	-10.6	-18.7	-5.6	-0.1	1.9	2.3	2.0	5.5	1.3	-4.5	-12.5	-1.56	WM99
	-8.5	-8.3	-12.5	-4.4	-0.1	1.9	3.2	2.3	3.3	1.1	-3.3	-9.3	-1.05	N 00
	-12.5	-11.2	-18.9	-6.0	-0.1	2.3	3.3	2.7	5.6	1.4	-4.7	-12.9	-1.55	M 01
	-9.3	-8.9	-13.3	-4.8	-0.1	2.3	4.1	3.1	4.0	1.2	-3.6	-9.6	-1.06	M 04
	-9.0	-8.6	-13.3	-4.6	-0.1	1.9	3.1	2.2	3.5	1.2	-3.4	-9.8	-1.12	H 06
pCO$_2$	332	327	322	350	379	399	420	408	396	385	358	331	-	-
Wind	8.7	8.5	9.3	8.0	6.6	6.2	5.4	5.1	8.1	7.9	8.1	9.1	-	-
SAB	-14.2	-10.7	-14.2	-4.3	1.1	5.3	8.9	7.6	12.6	9.1	-2.1	-14.9	**-0.48**	W 92
	-15.8	-10.4	-15.5	-4.1	0.8	4.0	5.8	5.4	13.9	8.8	-2.2	-14.5	-0.72	WM99
	-11.0	-8.5	-11.0	-3.4	0.9	4.4	7.4	6.3	9.8	7.1	-1.6	-11.6	-0.34	N 00
	-16.4	-11.3	-15.8	-4.5	1.0	5.1	8.0	7.2	14.6	9.5	-2.3	-15.3	-0.61	M 01
	-12.5	-9.6	-11.7	-3.7	1.1	5.6	9.5	8.3	11.4	7.8	-1.8	-12.1	-0.24	M 04
	-11.7	-8.7	-11.6	-3.5	0.9	4.4	7.3	6.2	10.3	7.4	-1.7	-12.2	-0.39	H 06
pCO$_2$	312	319	325	358	390	433	475	461	445	429	370	311	-	-
Wind	8.0	7.7	8.6	7.5	6.3	5.9	5.5	5.3	7.9	7.9	7.6	8.5	-	-

Table 3.3. Comparison of the annual air-water CO_2 fluxes calculated using different wind speeds. The results are calculated using gas transfer with wind speed relationships proposed by Wanninkhof (1992), with non-linearity correction applied. The units for the annual air-sea CO_2 fluxes are mol m^{-2} yr^{-1}.

Wind speeds source	**Study area**			
	Inner shelf	**Middle shelf**	**Outer shelf**	**Whole SAB**
Buoy 41008	1.08	-0.54	-0.55	-0.03
Buoy 41004	0.65	-1.29	-1.18	-0.65
QuikSCAT	**1.20**	**-1.23**	**-1.37**	**-0.48**

Table 3.4. Air-water CO_2 fluxes on the inner shelf calculated using different methods. Shown results are calculated using gas transfer with wind speed relationships proposed by Wanninkhof (1992), with non-linearity correction applied. The units for the air-sea CO_2 fluxes of each sampling month are mmol m^{-2} d^{-1}; and the units for the annual air-sea CO_2 fluxes are mol m^{-2} yr^{-1}.

Jan. 2005	**Mar. 2005**	**May 2006**	**Jul. 2005**	**Oct. 2005**	**Dec. 2005**	**Annual Flux**	**Extrapolation Method**
-14.5	-11.3	2.2	9.7	20.29	-16.89	**0.42**	Method one [a]
-14.6	-10.6	2.3	10.8	25.1	-12.0	**0.93**	Method two [b]
-16.3	-11.0	3.0	18.0	23.3	-14.5	**1.50**	Method three [c]
-16.9	-11.1	2.9	16.5	22.2	-15.4	**1.20**	Method four [d]

[a] Method one is to interpolate the data based on triangle-based interpolation only. No extrapolation is attempted.

[b] Method two is to first interpolate the data over the whole shelf. Then $p\text{CO}_2$ in areas close to shore where no interpolated values are available are filled in using the most close-to-shore interpolated value.

[c] Method three is to first generate values along the coastline using the most near-shore data based on linear interpolation, then interpolate the added values together with all of the original data.

[d] Method four is similar to method three. The only difference is that instead of interpolating the added values together with all of the original data, it interpolates the added values with the data on the inner shelf only.

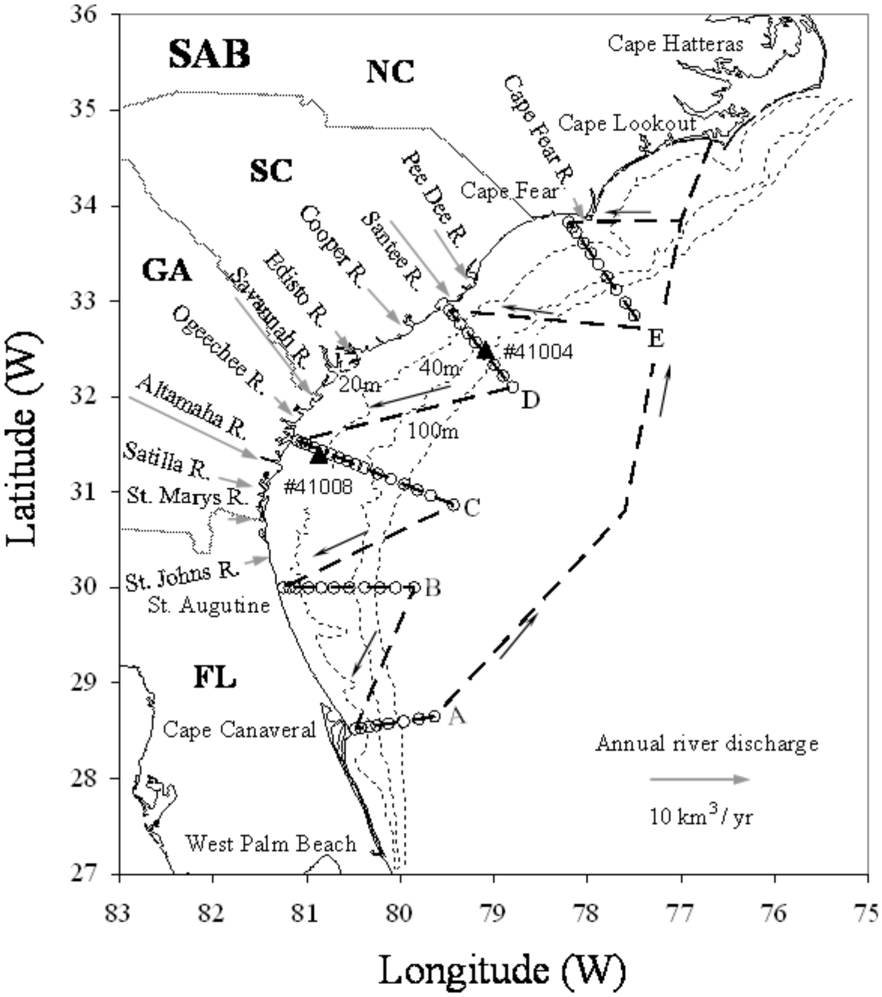

Figure 3.1. Study area is the U.S. South Atlantic Bight from Cape Lookout, North Carolina to Cape Canaveral, Florida. The thin dotted lines on the continental shelf are the depth contours at 20, 40, and 100m, delineating the inner, middle and outer shelf. The lengths of the gray arrows on the land indicate the annual river discharge rates. The dashed lines on the continental shelf are the typical ship track during each cruise. The dark arrows close to the ship track show the direction of the ship movement. The circles are the sampling stations, which start from the shoreline and extend to about ~500 m water depth. The two filled black triangles show the position of two NOAA Buoys (#41004 and #41008).

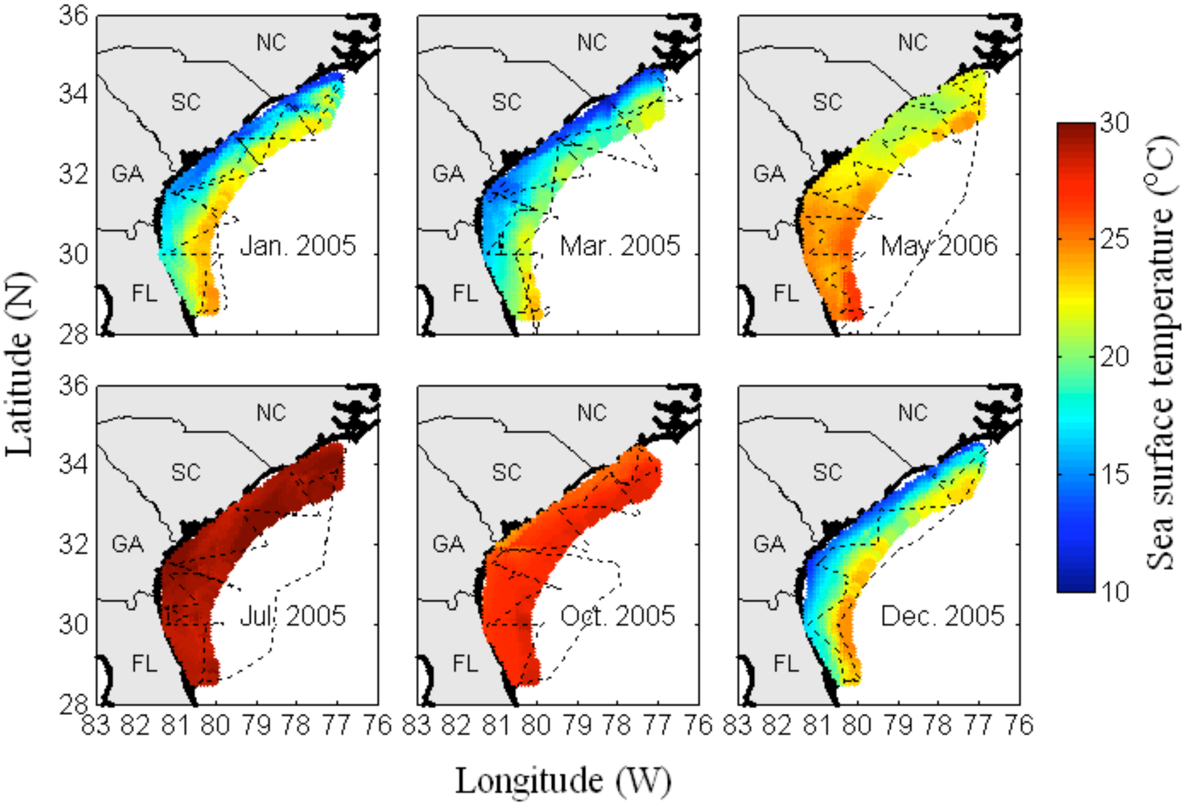

Figure 3.2. Spatial distributions of sea surface temperature on the U.S. South Atlantic Bight during all sampling months. The colored contour is from triangle-based liner interpolation. The dashed lines show the ship track on which the temperature data are based.

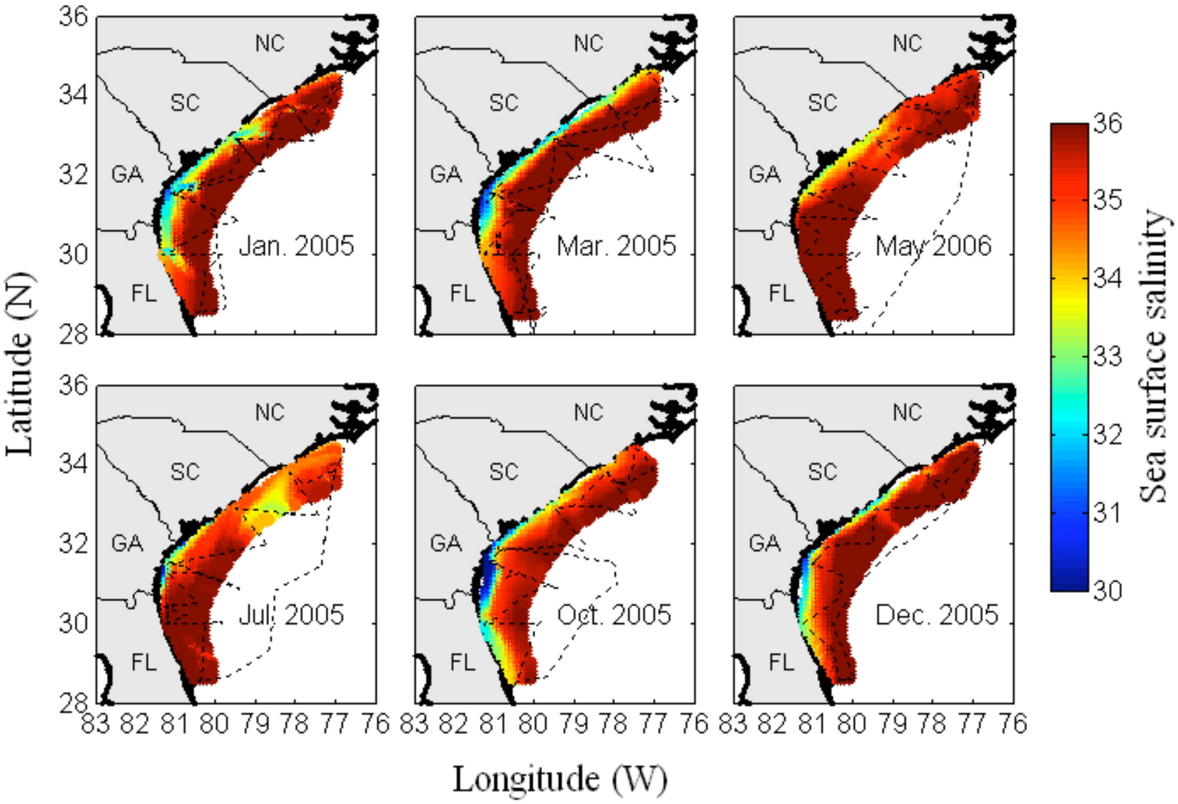

Figure 3.3. Spatial distributions of sea surface salinity on the U.S. South Atlantic Bight during all sampling months. The colored contour is from triangle-based liner interpolation. The dashed lines show the ship track on which the salinity data are based.

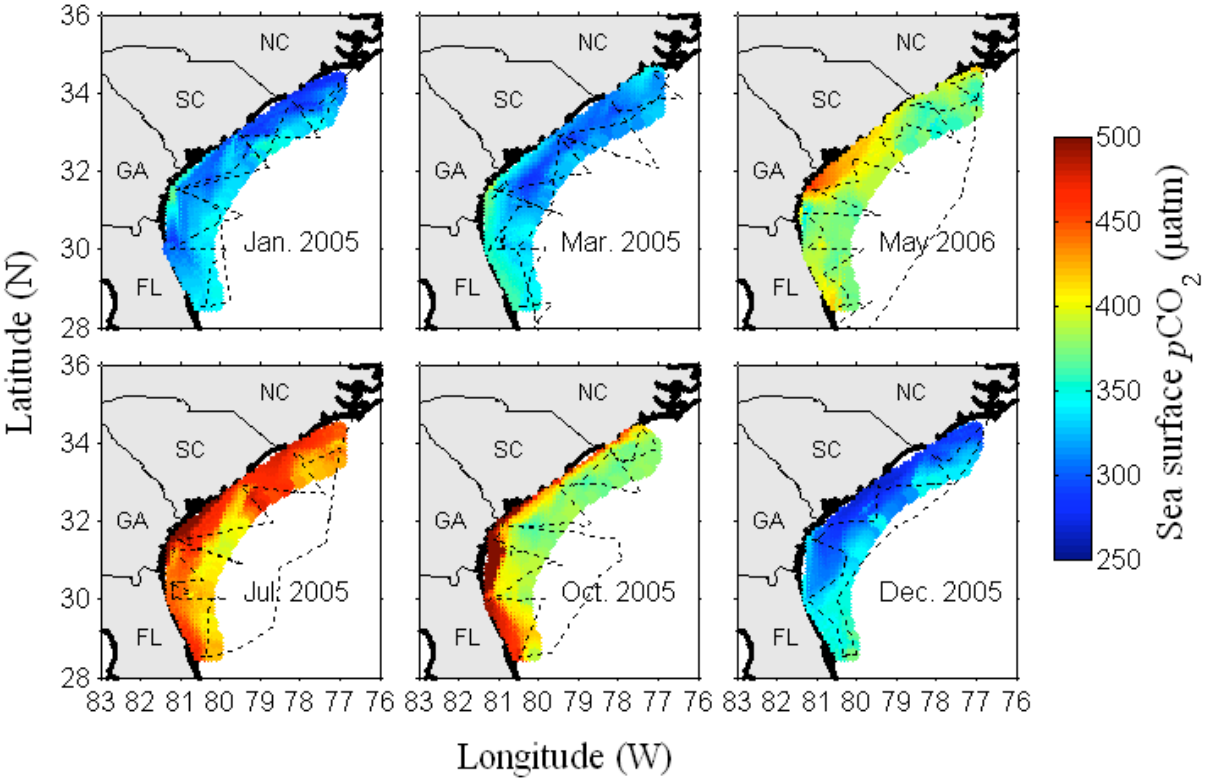

Figure 3.4. Spatial distributions of sea surface $p\mathrm{CO}_2$ on the U.S. South Atlantic Bight in all of the sampling months. The colored contour is from triangle-based liner interpolation. The dashed lines show the ship track on which the $p\mathrm{CO}_2$ data are based.

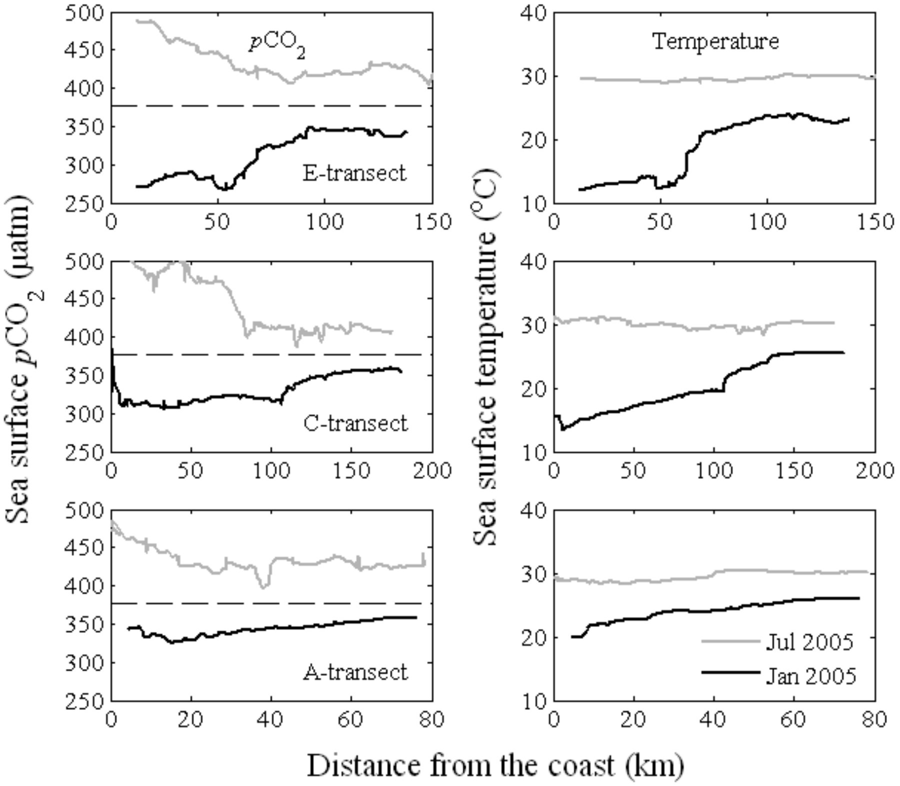

Figure 3.5. Onshore-offshore distributions of sea surface pCO_2 (panels on the left) and sea surface temperature (panels on the right) on E-, C-, and A-transects during January 2005 and July 2005. The black lines are the results from the January 2005 cruise, and the gray lines are from the July 2005 cruise. The dashed lines in the three panels on the left side show the average atmospheric pCO_2 of the two months. X-axis is distance from the coast in kilometers.

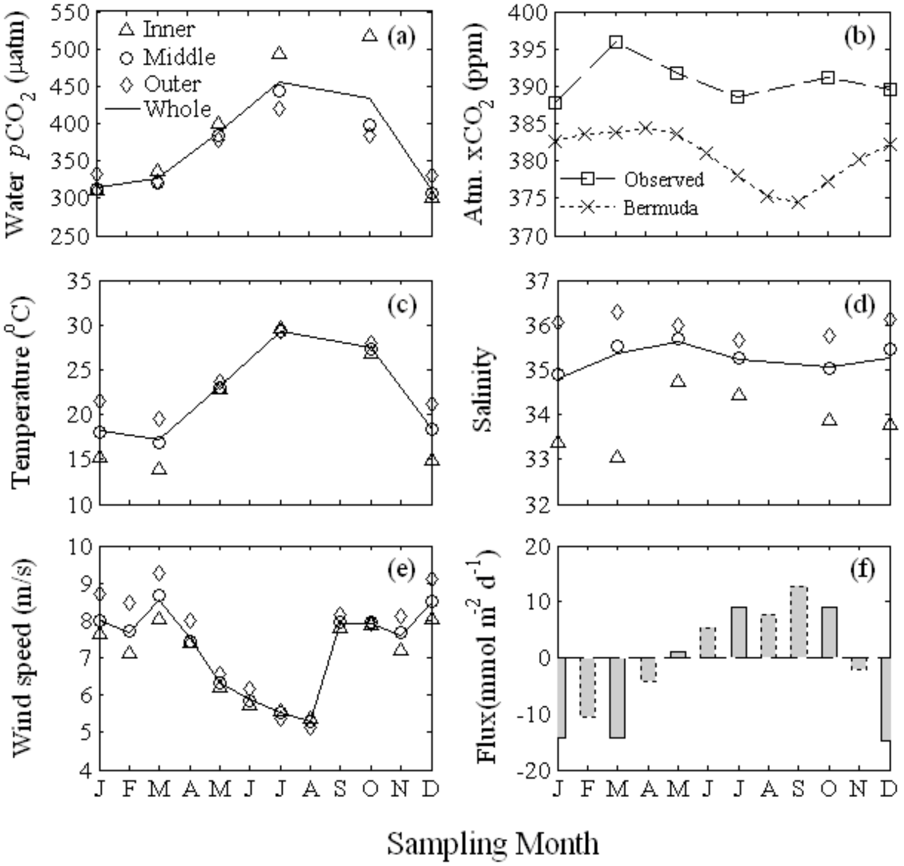

Figure 3.6. Seasonal variations of area-averaged sea surface pCO_2 (a), average atmospheric xCO_2 (b), area-averaged sea surface temperature (c), area-averaged sea surface salinity (d), area-averaged wind speeds (e), and area-averaged air-sea CO_2 fluxes (f) in the SAB. In panel (b), the crosses and dotted line are the atmospheric xCO_2 observations from the flask network of the NOAA ESRL at Bermuda (ftp://ftp.cmdl.noaa.gov/ccg/co2/flask/month/bme_01D0_mm.co2). In panel (f), the bars with solid lines show the air-sea CO_2 fluxes over the whole SAB during the sampling month, and bars with dotted line shows the fluxes during the months with no surveys. The dashed line in panel (f) shows zero flux.

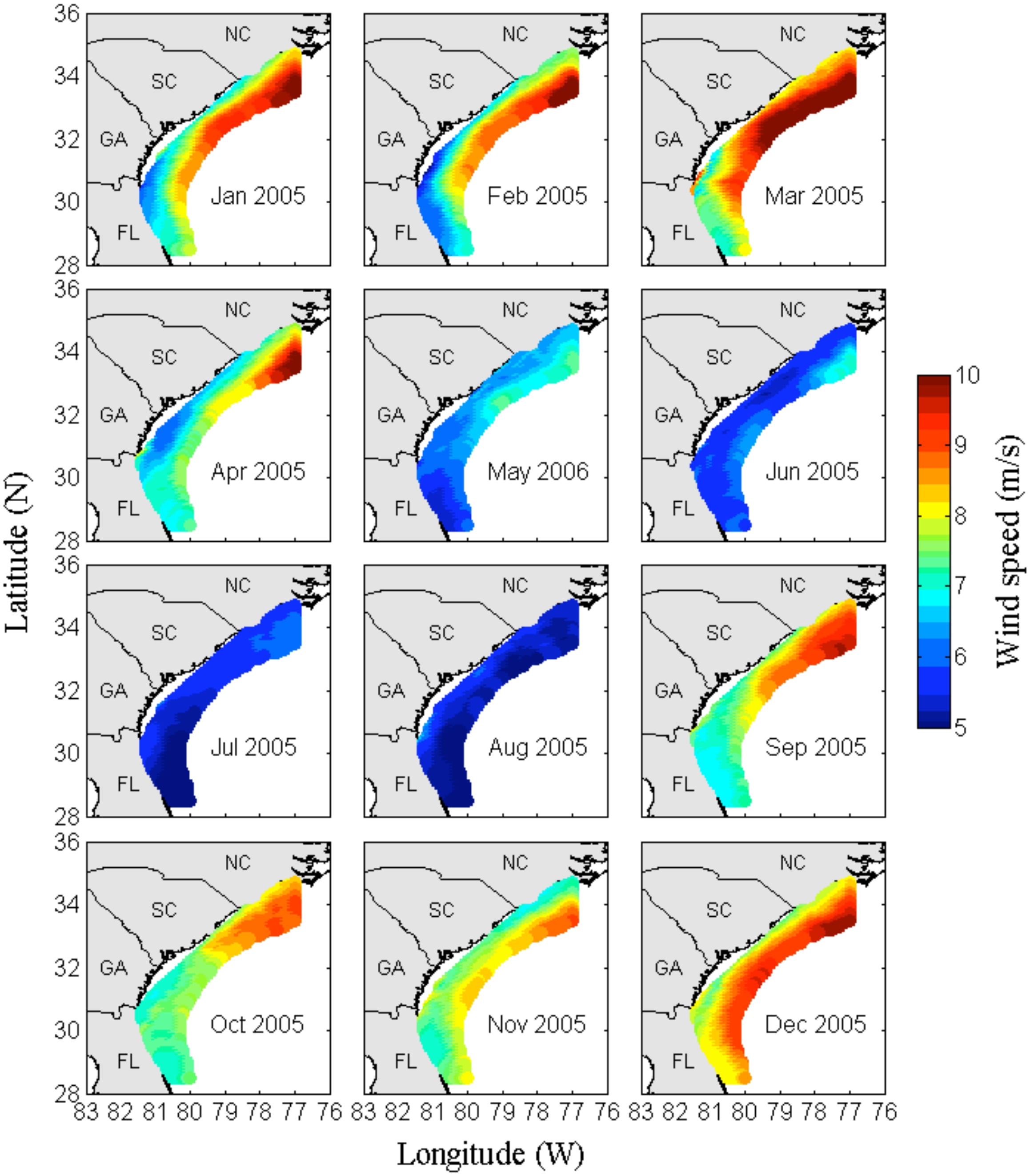

Figure 3.7. Spatial distributions of wind speeds at 10 m above the sea surface in the SAB. The wind speeds are obtained from the PO.DAAC (Physical Oceanography Distributed Active Archive Center) at the NASA (National Aeronautics and Space Administration) Jet Propulsion Laboratory, Pasadena, California, United States (http://podaac.jpl.nasa.gov/).

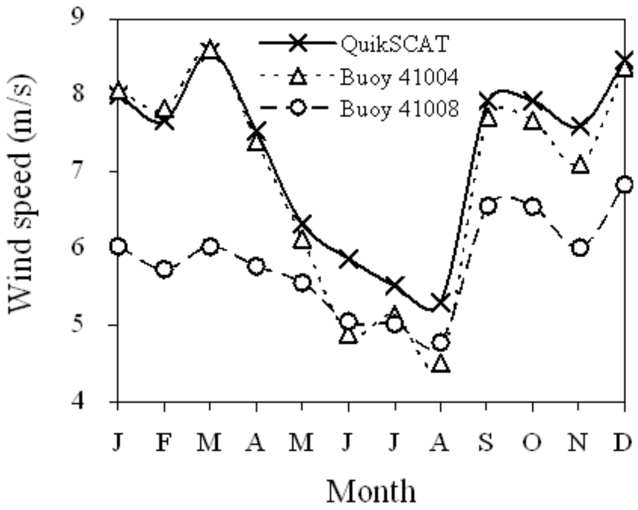

Figure 3.8. Wind speeds from different sources: satellite and buoys during all months of the sampling year. The crosses and solid line are the area-averaged wind speeds over the whole shelf from the QuikSCAT; the triangles and dotted line are the wind speeds from NOAA Buoy 41004; and the circles and dashed line show the wind speeds from NOAA Buoy 41008.

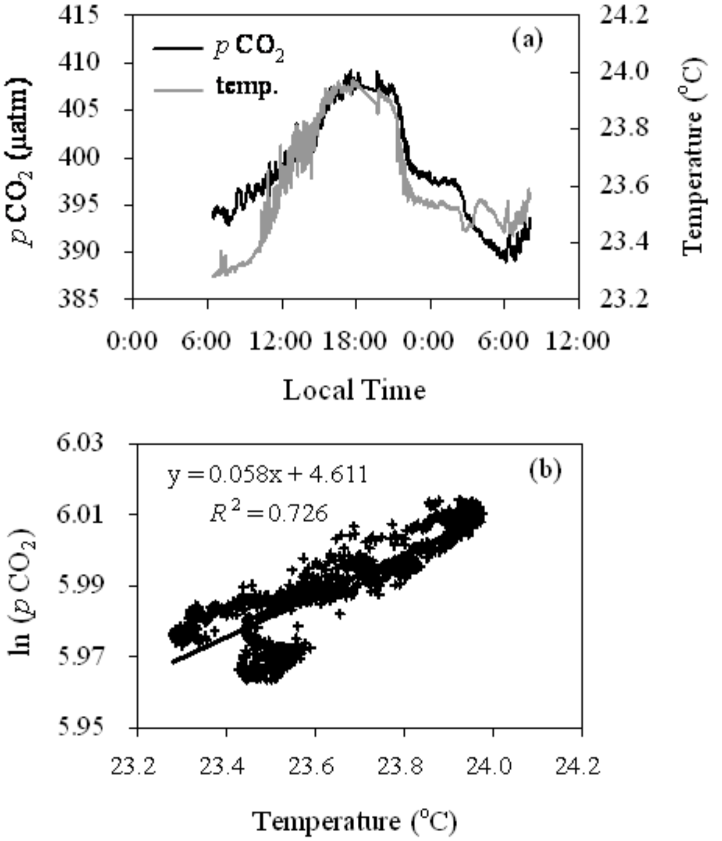

Figure 3.9. Time-series $p\mathrm{CO}_2$ measurements at a station in the center of C-transect (middle shelf) in May 2006. Panel (a) shows the diel variations of sea surface $p\mathrm{CO}_2$ (black line) and sea surface temperature (gray line). Panel (b) shows the relationship between natural logarithms of $p\mathrm{CO}_2$ and sea surface temperature (Takahashi et al. 1993). The solid line is from linear regression.

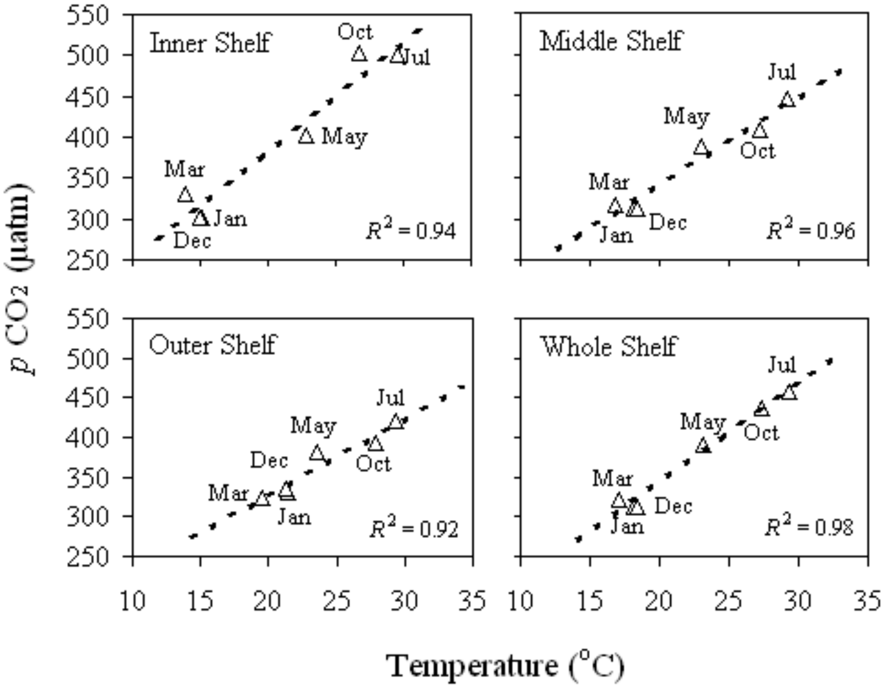

Figure 3.10. Area-averaged sea surface pCO_2 in different months vs. their corresponding sea surface temperature for different part (inner-, middle-, outer-shelf, and the whole shelf) of the SAB.

CHAPTER 4

CONTROLLING MECHANISMS OF SEA SURFACE CARBON DIOXIDE ON THE CONTINENTAL SHELF OF THE SOUTHEASTERN UNITED STATES[1]

---

[1] Jiang, L.-Q., W.-J. Cai, Y. Wang, and J.E. Bauer. Submitted to *Journal of Geophysical Research-Ocean*, 9/24/2008.

Abstract

Seasonal and spatial variations of sea surface pCO_2 (partial pressure of carbon dioxide) have recently been reported for the U.S. South Atlantic Bight (SAB), a low-latitude shallow continental shelf bordered landward by abundant salt marshes and freshwater discharge and seaward by a western boundary current (i.e., the Gulf Stream). In the current study, the mechanisms controlling sea surface pCO_2 in the SAB are examined. After removing pCO_2 variations due to the annual temperature cycle and air-sea gas exchange from the in situ pCO_2, residual pCO_2 is estimated. Residual pCO_2, along with other parameters, e.g., dissolved inorganic carbon (DIC) and dissolved organic carbon (DOC), is then used to assess the mechanisms controlling sea surface pCO_2 in the SAB. Findings suggest that temperature plays a key role in the seasonal variation of pCO_2 over the entire SAB. Air-sea gas exchange helps to modulate pCO_2 on the inner shelf due to the shallow water depth. In addition, CO_2 shoreward of the Coastal Frontal Zone (a dynamic barrier along the shelf at about 10-30 km offshore) is controlled by terrestrial inputs of inorganic and organic carbon from rivers and salt marshes, as well as net heterotrophy on the inner shelf. In contrast, CO_2 seaward of the Coastal Frontal Zone is mainly controlled by primary production that is itself strongly dependent on Gulf Stream-induced nutrient intrusions. These findings help to establish the physical and biogeochemical processes controlling the temporally and spatially variable fluxes of CO_2 in a major subtropical continental shelf system.

1. Introduction

Surface seawater $p\mathrm{CO_2}$ is controlled primarily by temperature, biological activity, and mixing of the upper ocean (Takahashi et al. 2002). $p\mathrm{CO_2}$ in seawater changes with temperature as $\partial(\ln p\mathrm{CO_2})/\partial T = 0.0423\ ^{o}\mathrm{C}^{-1}$, assuming the chemical composition of seawater (dissolved inorganic carbon, alkalinity, salinity) remains constant (Takahashi et al. 1993). For example, over the global range of surface water temperature (-2 to 30 ^{o}C), $p\mathrm{CO_2}$ in a body of seawater could change from 200 to 770 μatm due to temperature increase alone. Biological activity will alter sea surface $p\mathrm{CO_2}$ depending on the magnitude of net ecosystem metabolism in the surface mixed layer (Borges et al. 2006). Mixing can also change sea surface $p\mathrm{CO_2}$ by direct physical and chemical processes (Shim et al. 2007). While $p\mathrm{CO_2}$ on continental shelves is also controlled by these processes, it is further impacted by features unique to shelf environments such as shallow water depth, influences from land, and interactions with the open ocean.

The generally shallow depths of continental shelves (typically < ~200 m) make them more sensitive to annual changes in insolation and consequently cause them to have a larger annual temperature range. Shallow depth and the correspondingly small dissolved inorganic carbon (DIC) inventory per unit area suggest that air-sea gas exchange could play an important role in controlling DIC and hence sea surface $p\mathrm{CO_2}$ on shelves (Boehme et al. 1998). Interactions between the shallow water column and sediments may be an additional important source of carbon and nutrients to shelf waters, which may eventually affect its $p\mathrm{CO_2}$ (Jahnke et al. 2005).

At the land-ocean interface, continental shelves are impacted by nutrients and inorganic and organic carbon inputs from land (Thomas et al. 2004). Due to nutrient inputs, shelves sustain a relatively high level of biological productivity (Walsh 1988; Wollast 1993), which could potentially draw down $\mathrm{CO_2}$. However, this effect is often counteracted by enhanced heterotrophic activity supported by organic carbon inputs from land (Smith and Hollibaugh 1993). In addition, direct CO_2 inputs from land sources may play an important role in enhancing pCO_2 of shelf waters. Rivers usually discharge water with supersaturated CO_2 to continental shelves (Raymond et al. 2000; Borges et al. 2006; Jiang et al. 2008b). Tidal exchanges with salt marsh (Wang and Cai 2004) and mangrove (Borges et al. 2003) systems may also increase pCO_2 in continental shelf waters.

Near the shelf break, continental shelves are strongly influenced by interactions with the open ocean, usually via upwelling. Typically, upwelled waters have supersaturated levels of CO_2, and are therefore a natural source of CO_2 to shelves (Friederich et al. 2002). However, upwelling concomitantly introduces nutrients to shelf surface waters, which stimulate photosynthesis and draw down CO_2 there (Borges and Frankignoulle 2002; Hales et al. 2005).

The heterogeneous nature of continental shelves globally with respect to their physical, chemical, and biological processes suggests that the mechanisms controlling pCO_2 on different continental shelves may vary substantially, and as a whole, these mechanisms have thus far been poorly constrained (Cai and Dai 2004; Borges et al. 2005; Cai et al. 2006). The U.S. South Atlantic Bight (SAB) is a low-latitude shallow continental shelf bordered landward by extensive salt marshes and rivers, and seaward by a western boundary current (the Gulf Stream). Freshwater is discharged to the coast by a distributed set of rivers. A recent study has shown that the SAB as a whole is a net sink of the atmospheric CO_2 on an annual and whole shelf basis, although regional (i.e., within the SAB) and seasonal variability is large (Jiang et al. 2008a). The aim of the current study is to examine the specific biogeochemical mechanisms controlling sea surface pCO_2 in the SAB.

2. Study Site and Methods

2.1. Site Description

The South Atlantic Bight (SAB) is shallow, about 10-15 m deep inshore and 50-75 m deep at the shelf break (Figure 4.1). The SAB has traditionally been divided into three regimes: the inner shelf (coastline to 20-m isobath), the middle shelf (20- to 40-m isobath), and the outer shelf (40-m isobath to the shelf break). The Gulf Stream flows northward along the shelf break.

The shorelines of Georgia and South Carolina contain extensive salt marshes (3000 km^2, Alexander et al. 1986). Tidal currents flood and drain intertidal salt marshes twice daily and transport materials between salt marshes and the SAB (Hopkinson 1985). River discharge usually peaks in February-April and a secondary peak may occur in fall, with a total annual discharge of about 66 km^3 (~2.7% of the SAB volume) (Menzel 1993). Groundwater may also be an important source of freshwater to the shelf (Shaw et al. 1998; Moore 2007).

A Coastal Frontal Zone (CFZ) formed by a pressure gradient induced by freshwater discharge frequently occurs ~10-30km offshore in the SAB (Blanton 1981). The CFZ presents a dynamic barrier to the seaward transport of materials (Blanton and Atkinson 1983). Shelf water shoreward of the CFZ is turbid as a result of particulates contained in river runoff and from water exchanged with intertidal salt marshes and strong tidal mixing (Pomeroy et al. 2000). Primary production on the inner shelf is mainly driven by recycled nutrients in the water column (Dunstan and Atkinson 1976; Hanson et al. 1990) and from sediments (Jahnke et al. 2005). Seaward of the CFZ, water clarity increases dramatically, and the euphotic zone extends all the way to the seafloor (Nelson et al. 1999). Primary and secondary production on the middle and outer shelf is strongly influenced by upwelling associated with Gulf Stream frontal eddies (Atkinson et al. 1984; Lee et al. 1991).

2.2. Sampling

A survey of the SAB shelf consisting of five onshore-offshore transects (designated E-, D-, C-, B- and A-transects from north to south) was carried out during six cruises: 05-16 January 2005 19-30 March 2005, 27 July - 05 August 2005, 07-17 October 2005, 16-21 December 2005, and 17-27 May 2006. Surface water $p\mathrm{CO}_2$, temperature, salinity, and sea level pressure were measured while underway during all cruises. A detailed description of the sampling techniques for $p\mathrm{CO}_2$ can be found in Jiang et al. (2008a). Surface water DIC was sampled on all five transects except for December 2005, when only E-, C-, and A-transects were covered (Figure 4.1). Dissolved organic carbon (DOC) samples were collected in the surface water on D-, C-, and B-transects during January, March, and October 2005, and on all 5 transects during May 2006.

2.3. Sample Analysis

DIC concentration was measured using an automated DIC analyzer with a precision of 0.1% (Wang and Cai 2004). DOC samples collected during the cruises of March, July, and October 2005 were measured at the Virginia Institute of Marine Science Radiocarbon Laboratory using a Shimadzu TOC-5000A high-temperature Pt-catalyzed analyzer with a mean analytical error of 1.4 $\mu\mathrm{mol\ L^{-1}}$ (DeAlteris 2007). The DOC samples from May 2006 were analyzed in W. L. Miller's lab (University of Georgia) using a Shimadzu TOC-VCPN analyzer. Reference standards (deep Sargasso Sea seawater from D. A. Hansell's group at the University of Miami) and blanks (Milli-Q water) were analyzed every five samples to check accuracy and baseline stability.

2.4. Calculation of Residual $p\mathrm{CO_2}$

A method commonly used to assess processes controlling CO_2 in natural waters is to examine the $p\mathrm{CO_2}$ changes between two consecutive sampling surveys. The overall $p\mathrm{CO_2}$ change between the two surveys ($\Delta p\mathrm{CO_2}$) can be split into several components:

$$\Delta p\mathrm{CO_2} = \Delta p\mathrm{CO_2}(\mathrm{t}) + \Delta p\mathrm{CO_2}(\mathrm{a\text{ - }s}) + \Delta p\mathrm{CO_2}(\mathrm{m}) + \Delta p\mathrm{CO_2}(\mathrm{b}) + \Delta p\mathrm{CO_2}(\mathrm{other}) \quad (4.1)$$

in μatm, where $\Delta p\mathrm{CO_2}$(t), $\Delta p\mathrm{CO_2}$(a-s), $\Delta p\mathrm{CO_2}$(m), $\Delta p\mathrm{CO_2}$(b) and $\Delta p\mathrm{CO_2}$(other) are the $p\mathrm{CO_2}$ changes occurring between the two surveys as a result of temperature, air-sea gas exchange, mixing, biological activity, and other processes, respectively. This approach works best for relatively isolated systems, such as, lakes or open oceanic water masses. If applied to a system where water is replaced periodically, this approach requires the sampling interval to be much smaller than the water residence time (Boehme et al. 1998). Sinces the residence time of the whole SAB is 1-3 months (Atkinson et al. 1978; Moore 2007) and our sampling intervals were at least 2 months apart, this method was not applied for this study.

Here, an alternative approach is used to examine how temperature, air-sea gas exchange, biological activity, and mixing control sea surface $p\mathrm{CO_2}$ in the SAB. Instead of comparing $p\mathrm{CO_2}$ results from one survey to another, we focus on $p\mathrm{CO_2}$ of a specific survey. We first try to remove the $p\mathrm{CO_2}$ variations due to the annual temperature cycle and air-sea gas exchange from the measured in-situ $p\mathrm{CO_2}$. The remaining $p\mathrm{CO_2}$ is then assumed to be mainly controlled by biological activity and mixing. For simplicity, we initially treat the $p\mathrm{CO_2}$ changes due to biological activity and mixing together (their separation will be discussed later).

Residual $p\mathrm{CO_2}$ is defined as the $p\mathrm{CO_2}$ after correcting for the impact of the annual temperature cycle and air-sea gas exchange and is calculated as:

$$p\mathrm{CO_2}(\mathrm{residual}) = p\mathrm{CO_2}(\mathrm{in\ situ}) - [\Delta p\mathrm{CO_2}(\mathrm{temp}) + \Delta p\mathrm{CO_2}(\mathrm{air\text{ - }sea})] \quad (4.2)$$

in μatm, where $p\mathrm{CO_2}$(residual) is the residual $p\mathrm{CO_2}$, $p\mathrm{CO_2}$ (in situ) is the observed sea surface $p\mathrm{CO_2}$, $\Delta p\mathrm{CO_2}$(temp) is the $p\mathrm{CO_2}$ change caused by temperature deviation from the annual mean temperature, and $\Delta p\mathrm{CO_2}$(air-sea) is the $p\mathrm{CO_2}$ change due to air-sea gas exchange prior to the survey (normalized to the annual mean sea surface temperature, SST).

Water temperature changes $p\mathrm{CO_2}$ both by shifting the inorganic carbon equilibrium and by altering solubility. $p\mathrm{CO_2}$ in water increases with increasing water temperature, when other parameters are kept constant. The in situ $p\mathrm{CO_2}$ can be normalized to a constant temperature using the equation of Takahashi et al. (1993; 2002):

$$p\mathrm{CO_2}(\overline{\mathrm{SST}}) = p\mathrm{CO_2}\ (\text{in situ}) \times \exp[0.0423 \times (\overline{\mathrm{SST}} - \mathrm{SST})] \tag{4.3}$$

where $\overline{\mathrm{SST}}$ is the annual mean SST, and $p\mathrm{CO_2}(\overline{\mathrm{SST}})$ is the $p\mathrm{CO_2}$ normalized to the annual mean SST. $\overline{\mathrm{SST}}$ used for the calculation is 23.11 $^{\circ}$C, which was determined to be the mean value of the area-averaged SST over the entire shelf in all sampling months. Once $p\mathrm{CO_2}(\overline{\mathrm{SST}})$ is calculated, $p\mathrm{CO_2}$ change due to temperature deviation from the annual mean SST is then calculated as:

$$\Delta p\mathrm{CO_2}(\text{temp}) = p\mathrm{CO_2}(\text{in situ}) - p\mathrm{CO_2}(\overline{\mathrm{SST}}) \tag{4.4}$$

$p\mathrm{CO_2}$ change due to air-sea gas exchange prior to each survey can be calculated using the concept of the Revelle factor. Revelle factor is defined as the ratio of the fractional changes in $\mathrm{CO_2}$ and DIC in the ocean. (Revelle and Suess 1957; Sabine et al. 2004). Assuming that the surface mixed layer on the SAB extends to the seafloor in all sampling months (this is the case for most of our cruises), $p\mathrm{CO_2}$ change due to air-sea gas exchange at the start of each survey can be calculated as:

$$\Delta p\mathrm{CO_2}(\text{air-sea}) = -p\mathrm{CO_2}(\overline{\mathrm{SST}}) \times \frac{\Delta\mathrm{DIC}(\text{air-sea})}{\mathrm{DIC}(\text{per area})} \times \mathrm{Re} \tag{4.5}$$

in μatm, where $\Delta p\mathrm{CO_2}$(air-sea) is the $p\mathrm{CO_2}$ change due to air-sea gas exchange (at the annual mean SST), ΔDIC(air-sea) is the DIC inventory change caused by in situ air-sea gas exchange (units: mmol $\mathrm{m^{-2}}$), DIC(per area) is DIC inventory per unit area (units: mmol $\mathrm{m^{-2}}$), and Re is Revelle factor calculated at the annual mean temperature. Positive $\Delta p\mathrm{CO_2}$(air-sea) means addition of $\mathrm{CO_2}$ to the water through air-sea gas exchange. As a first-order approximation, a 30-day (mean residence time of the entire SAB was 30-90 days, Atkinson et al. 1978; Moore 2007) air-sea gas exchange time was used to calculate the ΔDIC(air-sea). Additional information about how the air-sea $\mathrm{CO_2}$ fluxes were calculated can be found in Jiang et al. (2008a).

Once $\Delta p\mathrm{CO_2}$(temp) and $\Delta p\mathrm{CO_2}$(air-sea) have been estimated, residual $p\mathrm{CO_2}$ can be calculated from Equation (4.2). We can also see that if $\Delta p\mathrm{CO_2}$(temp) in Equation (4.2) is substituted with the right-hand side of Equation (4.4), the following is derived:

$$p\mathrm{CO_2}(\mathrm{residual}) = p\mathrm{CO_2}(\overline{\mathrm{SST}}) - \Delta p\mathrm{CO_2}(\mathrm{air-sea}) \qquad (4.6)$$

Thus, residual $p\mathrm{CO_2}$ can also be expressed as temperature-normalized $p\mathrm{CO_2}$ corrected by the $p\mathrm{CO_2}$ change due to air-sea gas exchange.

After removing $p\mathrm{CO_2}$ variations caused by temperature and air-sea gas exchange, residual $p\mathrm{CO_2}$ is assumed to be mainly controlled by mixing and biological activity. Theoretically, we should be able to divide residual $p\mathrm{CO_2}$ into two parts: $p\mathrm{CO_2}$ that is due to mixing [$p\mathrm{CO_2}$(mixing)] and $p\mathrm{CO_2}$ change that is due to biological activity [$\Delta p\mathrm{CO_2}$(biology)]. $p\mathrm{CO_2}$(mixing) may be derived from its end member data. First, assuming that only mixing occurs, the DIC concentration and total alkalinity (TA) at station i can be estimated based on its end member information (Jiang et al. 2008b). $p\mathrm{CO_2}$(mixing) at station i can then be estimated from the calculated DIC and TA values. Once $p\mathrm{CO_2}$(mixing) is estimated, $\Delta p\mathrm{CO_2}$(biology) can be calculated as the difference between $p\mathrm{CO_2}$(residual) and $p\mathrm{CO_2}$(mixing).

Although this method has been demonstrated to work well in estuaries (Chapter 2), it may not apply to the SAB. First, the nearshore end members are not temporally stable relative to the residence time of the shelf (Loder and Reichard 1981). The nearshore end members are located on the inner shelf, where primary production and respiration are highest and show the largest seasonal variation of the entire shelf (Griffith et al. 1990; Verity et al. 1993; W.-J. Cai, unpublished data 2008). Second, unlike estuaries, where mixing occurs between two end members in a narrow passage, the mixing processes on the SAB shelf are far more complicated (Menzel 1993). Mixing occurs in both cross-shelf and along-shelf directions, and is complicated by the presence of the CFZ, which generally acts as a dynamic barrier to cross-shelf exchange along the shelf at about 10-30 km offshore. The complicated mixing processes make it challenging to choose which specific nearshore end members to use for a given station, as the nearshore end members show large spatial variations. For the above reasons, the partitioning of residual pCO_2 into pCO_2(mixing) and ΔpCO_2(biology) was not applied for this study.

3. Results

3.1. Sea Surface Salinity

Sea surface salinity on the SAB was lowest nearshore (27–33) and increased sharply seaward, approaching open ocean salinity (~36.5) at about 10-30 km offshore in all sampling months (Figure 3.3). The low-salinity zone on the inner shelf extended both northward and southward during January, March, October, and December 2005. In contrast, the low-salinity region only extended northward during May 2006 and July 2005. Overall, this salinity distribution is consistent with 1) most freshwater discharge to the SAB occurring in the central and northern regions of the SAB (Blanton and Atkinson 1983), and 2) the mean alongshore circulation close to the coast being northward during winter, spring, and summer, and southward during fall in most years (Lee et al. 1991; Menzel 1993). The only exceptions occurred in January and March 2005, when the freshwater plume extended southward to St. Augustine, Florida due to strong discharge rates in these two months (United States Geological Survey). In July 2005, a body of low-salinity water was found just south of E-transect on the middle and outer shelf (Figure 3.3) where it is most likely deflected from the inner shelf by the Charleston Bump (centered near 32^{o}N beyond the shelf break, see Figure 4.1 in Bane and Dewar 1988). The occurrence of low salinity water around "the doming region off Long Bay between late June and early August" was also recorded by Singer et al. (1983).

3.2. Surface Water DIC

Surface water DIC concentrations on the SAB ranged from 1900 to 2100 µmol kg^{-1} (Figure 4.2). In all sampling months, DIC concentrations were lowest shoreward of the CFZ compared to those seaward, suggesting dilution of oceanic DIC by riverine freshwater discharge. Overall, DIC showed similar spatial distributions as sea surface salinity on the SAB (Figure 3.3) except when DIC concentrations were unusually low on the middle and outer shelf during July and October 2005 (Figure 4.2).

3.3. Surface Water DOC

In contrast to the DIC distribution, surface water DOC on the SAB was always higher shoreward of the CFZ compared to those seaward (Figure 4.3). Spatially, the highest DOC concentrations occurred in the central part of the inner shelf (160-170 µmol L^{-1} in March 2005 and May 2006, and 230-240 µmol L^{-1} in July and October 2005). The high inner shelf DOC extended northward as well as southward in March and October 2005. Relatively low DOC in the southern part of the inner shelf in May 2006 and July 2005 may be discerned (Figure 4.3), even though DOC was not measured shelf-wide in all sampling months (Figure 4.3). Surface water DOC beyond the CFZ was much lower at 70-100 μmol L^{-1}. Unusually high DOC concentrations were observed on the middle and outer shelf (134 μmol L^{-1}) for D-transect during July 2005 (Figure 4.3).

3.4. Sea Surface pCO_2

Sea surface pCO_2 on the SAB showed large seasonal and spatial variations (Figure 3.4). Relative to the atmosphere (dry atmospheric xCO_2 was about 387-396 ppm), undersaturation (260-400 μatm) occurred in cold months (January, March and December 2005) while supersaturation (370-800 μatm) was observed in warm months (July and October 2005). Spatially, sea surface pCO_2 exhibited strong onshore-offshore gradients in all sampling months. pCO_2 on the inner shelf was lower than that on the middle and outer shelf in cold months, and this pattern was reversed in warm months (Figure 3.4). Additional details about the sea surface pCO_2 distributions in the SAB can be found in Jiang et al. (2008a).

3.5. Impact of Temperature on Sea Surface pCO_2

Temperature-normalized pCO_2 showed spatial distributions distinct from those of in situ pCO_2. The normalized pCO_2 on the inner shelf was higher than that on the middle and outer shelf in all sampling months (Figure 4.4). This is in contrast to in situ sea surface pCO_2, which was lower on the inner shelf than on the middle and outer shelf during winter (Figure 3.4) due to the large onshore-offshore temperature gradient at this time of the year (surface water temperature in winter was about 10-14 ^{o}C on the inner shelf and increased to 20-25 ^{o}C at the shelf break, Jiang et al. 2008a).

The results of ΔpCO_2(temp) (Equation 4.4) show that pCO_2 decreased with lower temperature in winter and increased with higher temperature in summer on all parts (inner, middle, and outer shelf) of the SAB (Figure 4.5). The magnitude of $\Delta p\mathrm{CO}_2$(temp) on the inner shelf was larger than that on the middle and outer shelf partially due to the greater seasonal span of SST on the inner shelf (10-30 ^{o}C) compared to that on the middle and outer shelf (20-30 ^{o}C) (Jiang et al. 2008a).

3.6. Impact of Air-sea Gas Exchange on Sea Surface $p\mathrm{CO}_2$

Air-sea gas exchange had the net effect of modulating the seasonal changes of $p\mathrm{CO}_2$ in the SAB. It increased $p\mathrm{CO}_2$ in winter when sea surface $p\mathrm{CO}_2$ was under-saturated and decreased it in summer when $p\mathrm{CO}_2$ was supersaturated (Figure 4.5). However, although air-sea gas exchange played an important role in controlling $p\mathrm{CO}_2$ of the inner shelf, greater water depths and consequently greater mixed layer DIC inventory on the middle and outer shelf make air-sea gas exchange insignificant in changing the $p\mathrm{CO}_2$ there (Figure 4.5). Here one needs to keep in mind that the calculation of pCO_2 variation that is due to air-sea gas exchange assumed that the mixed layer extended to the bottom in all seasons. As a result, this would lead to underestimation in summer when stratification occurs on the shelf.

3.7. Surface Water Residual $p\mathrm{CO}_2$

The calculated residual $p\mathrm{CO}_2$ showed similar spatial distributions as temperature-normalized $p\mathrm{CO}_2$. It was also higher on the inner shelf than on the middle and outer shelf in all sampling months (Figure 4.6). The largest differences between residual $p\mathrm{CO}_2$ and temperature-normalized $p\mathrm{CO}_2$ (Figure 4.4) were seen on the inner shelf where residual $p\mathrm{CO}_2$ was slightly lower than the corresponding temperature-normalized $p\mathrm{CO}_2$ during January, March 2005 and May 2006, and slightly higher during July and October 2005.

Seasonally, residual $p\mathrm{CO}_2$ shared similar trends on the middle and outer shelf while that on the inner shelf was notably different. On the middle and outer shelf, the area-averaged residual

$p\text{CO}_2$ increased from January to March, leveled off through May, decreased in July and October, and then increased again in December (Figure 4.5). Residual $p\text{CO}_2$ on the inner shelf was always higher than that on the middle and outer shelf. It was lowest in January, and showed the largest increase in March and October (Figure 4.5), when the shelf experienced the greatest riverine freshwater inputs (Jiang et al., in preparation).

4. Discussion

4.1. Impact of Terrestrial Sources on Nearshore $p\text{CO}_2$

DIC on continental shelves is predominantly from oceanic waters, and largely conservative during mixing. The observed DIC on the SAB showed great onshore-offshore gradients due to dilution by riverine freshwater (Figure 4.2). For purposes of this discussion, we define "terrestrial sources" of DIC as all DIC sources landward of the land-ocean boundary. This includes rivers, estuaries, salt marsh, groundwater, and other land sources. To examine how inorganic carbon transported from terrestrial sources contribute to the high nearshore residual $p\text{CO}_2$, excess DIC ($\text{DIC}_{\text{excess}}$) is defined as the DIC concentration in excess of marine DIC values, and was calculated according to Jiang et al. (2008b):

$$\text{DIC}_{\text{excess}} = \text{DIC}_{\text{i}} - \frac{\text{S}_{\text{i}}}{\text{S}_{\text{ocean}}} \times \text{DIC}_{\text{ocean}} \tag{4.7}$$

in μmol kg^{-1}, where DIC_{i} and $\text{DIC}_{\text{ocean}}$ are DIC concentrations of station i and the ocean end member, respectively, and S_{i} and S_{ocean} are the salinities of station i and the ocean end member, respectively. The second term on the right-hand side of Equation (4.7) ($\frac{\text{S}_{\text{i}}}{\text{S}_{\text{ocean}}} \times \text{DIC}_{\text{ocean}}$) represents the DIC concentration if the ocean end member is diluted with a zero-DIC freshwater end member. Thus, excess DIC defined here represents all DIC sources or sinks (e.g., terrestrial input and net ecosystem metabolism on the shelf) except those from the open ocean.

Results show that sea surface excess DIC was highest in the central part of the inner shelf (140-200 μmol L^{-1}) at all sampling times (Figure 4.7). Excess DIC seaward of the CFZ was much lower compared to that shoreward and showed much less seasonal variation (-10 to 50 μmol L^{-1}). In the following, the excess DIC results, along with DOC and salinity data are used to evaluate how terrestrial sources contribute to $p\text{CO}_2$ on the SAB.

Sea surface residual $p\text{CO}_2$ (Figure 4.6) showed similar spatial distributions as both excess DIC (Figure 4.7) and DOC (Figure 4.3). All of these concentrations were greater shoreward of the CFZ compared to those seaward, and they were always highest in the central part of the inner shelf closest to the rivers and extensive marshes of the SAB. In addition, the high values for the central inner shelf all extended both northward and southward during January, March, and October 2005, but only northward during May 2006 and July 2005. Overall, residual $p\text{CO}_2$, excess DIC, and DOC seemed to follow closely the river plume circulation on the SAB, as illustrated by the salinity distribution (Figure 3.3). This is the case even for the parcel of unusually low-salinity water south of E-transect on the middle and outer shelf (due to Charleston Bump) during July 2005 (Figure 3.3). The water also features unusually high residual $p\text{CO}_2$ (Figure 4.6), excess DIC (Figure 4.7) and DOC (Figure 4.3).

Residual $p\text{CO}_2$ showed negative correlations with salinity (Figure 4.8a and b) and positive correlations with both excess DIC (Figure 4.8c and d) and DOC (Figure 4.8e and f) during all sampling periods. Since the high excess DIC and DOC in the nearshore SAB are most likely to be contributed by terrestrial sources (Moran et al. 1991; Wang et al. 2005; DeAlteris et al., in preparation), we suggest that terrestrial sources play an important role in enhancing $p\text{CO}_2$ in the nearshore SAB. Terrestrial sources increase the nearshore $p\text{CO}_2$ by direct inputs of CO_2 from rivers (Cai and Wang 1998; Cai et al. 1999; Jiang et al. 2008b) and salt marshes (Wang and Cai 2004), and indirectly by inputs of organic carbon (Moran et al. 1991; Alberts and Takács 1999; DeAlteris 2007; DeAlteris et al., in preparation) that is later remineralized on the SAB.

Rivers discharging to the SAB enhance $p\text{CO}_2$ on the shelf by delivering water with high CO_2 concentrations that is the result of microbial decomposition of organic matter in soils, river waters, and sediments (Jones and Mulholland 1998; Neal et al. 1998; Cole and Caraco 2001). Studies of the Altamaha and Satilla River estuaries have shown that rivers of this region are highly supersaturated with respect to atmospheric CO_2. Surface water $p\text{CO}_2$ in these river-dominated estuaries is as high as 4000 μatm during summer compared to only about 400-600 μatm on the shelf (Cai and Wang 1998; Jiang et al. 2008b). Even though these riverine waters contribute little in terms of DIC during the mixing with oceanic water, their low pH and considerably greater proportion of DIC in the form of dissolved carbon dioxide enable them to elevate nearshore $p\text{CO}_2$ on the SAB substantially (Jiang et al. 2008b).

Salt marshes contribute to $p\text{CO}_2$ in the SAB by direct release of CO_2 from marsh to the continental shelf. Another important feature of this region is the extensive areas of inter-tidal salt marshes (Pomeroy and Wiegert 1981), where the dominant primary producer is *Spartina alterniflora*. The SAB salt marsh has among the highest rates of primary productivity of any ecosystem (~1100 to 2250 gC m^{-2} yr^{-1}, Dai and Wiegert 1996). CO_2 that is released to the intertidal marsh sediments and waters by bacterial remineralization of *Spartina*-derived organic matter can be exported to coastal waters (Cai et al. 1999; Wang and Cai 2004; Jiang et al. 2008b) via tidal flushing (Neubauer and Anderson 2003) and drainage of sediment interstitial waters (Jahnke et al. 2003).

Rivers and salt marshes also transport significant amounts of reactive organic carbon to the SAB (Moran et al. 1991; Moran and Hodson 1994; Alberts and Takács 1999; DeAlteris 2007), the remineralization of which by microbes (Pomeroy et al. 2000; Jahnke et al. 2005) and photochemistry (Miller and Moran 1997) in shelf waters and sediments will further increase the nearshore $p\mathrm{CO}_2$. Earlier studies have shown that most of the nutrients entering the SAB shelf occur in dissolved or particulate organic form that must be remineralized before they can be taken up by phytoplankton (Dunstan and Atkinson 1976; Hanson et al. 1990; DeAlteris 2007). The potential importance of this pathway in enhancing $p\mathrm{CO}_2$ of the inner shelf is supported by the positive correlation between residual $p\mathrm{CO}_2$ and DOC (Figure 4.8e and f).

4.2. Seasonal Changes of $p\mathrm{CO}_2$ on the Inner Shelf

From the above, we can see that CO_2 on the inner shelf is strongly impacted by inorganic and organic carbon inputs from rivers and salt marshes. In addition, CO_2 may be contributed by net ecosystem metabolism on the inner shelf (Hopkinson 1985). Seasonally, CO_2 exported from SAB rivers is largely related to river discharge rates, and greater amounts of CO_2 will be transported to the shelf when river discharge rates are highest (Borges et al. 2006; Jiang et al. 2008b). The seasonal changes in CO_2 released from salt marshes and the inner shelf, however, are strongly dependent on temporal variability in organic matter remineralization.

Respiration rates in both SAB salt marshes and the inner shelf have been shown to be nearly an order of magnitude higher in summer and fall than in winter and spring (Hopkinson 1985; Griffith et al. 1990; W.-J. Cai, unpublished data 2008). One implication of the large seasonal variability in marsh remineralization is that more CO_2 is released from the salt marsh during summer and fall than during other seasons (Neubauer and Anderson 2003; Wang and Cai 2004). The CO_2 released from net ecosystem metabolism on the inner shelf is, however, more complicated due to differences in carbon fixation processes. Instead of taking up CO_2 from the atmosphere during photosynthesis (as saltmarsh grasses do), primary production by phytoplankton on the inner shelf takes up CO_2 from seawater. Therefore, the additional CO_2 released from heterotrophic processes during summer could be counterbalanced by greater aquatic primary production at this time of the year (Verity et al. 2002). However, inner shelf δ^{13}C-DIC (δ^{13}C of dissolved inorganic carbon) becomes significantly more depleted from spring to fall (DeAlteris 2007; DeAlteris et al., in preparation), suggesting that the inner shelf is more likely to be heterotrophic during summer and fall, and relatively more autotrophic during winter and spring. This is also supported by previously observed seasonal changes in chlorophyll a, where concentrations on the inner shelf in colder months are typically about two or more times great than in warmer months (McClain et al. 1988; Barnard et al. 1997; Signorini and McClain 2006).

Based on the above, we suggest that during summer and early fall, greater release of CO_2 from salt marshes (Wang and Cai 2004) and the inner shelf (Hopkinson 1985) contributes to the higher observed residual pCO_2 on the inner shelf at these times of the year. The unusually high residual pCO_2 in March and October 2005 is most likely due to greater freshwater input, which brings water with high CO_2 concentrations from land (Jiang et al. 2008b). In addition, the extension of high residual pCO_2 to the southern extreme of the inner shelf, coincident with the freshwater plume, also contributes to the high inner shelf residual pCO_2 during March and October 2005 (Figure 4.6).

4.3. Seasonal Changes of pCO_2 on the Middle and Outer Shelf

One of the most important features of residual pCO_2 on the middle and outer shelf is the clear drawdown during July and October 2005 (Figure 4.5). This is most likely caused by phytoplankton blooms at this time of the year (Yoder et al. 1983; Lee et al. 1991). The seasonal SST minimum on the middle and outer shelf was as high as 20 ^{o}C compared to only 10 ^{o}C on the inner shelf. Due to the higher SST throughout the year, respiration rates on the middle and outer shelf showed much smaller seasonal variation compared to those on the inner shelf (W.-J. Cai, unpublished data 2008). Relative to this quasi-stable respiration, variability in primary production would appear to play a larger role in regulating seasonal changes of $p\mathrm{CO}_2$ on the middle and outer shelf.

Primary production on the middle and outer shelf is strongly dependent on intrusions induced by Gulf Stream frontal eddies (Yoder et al. 1983; Yoder 1985; Lee et al. 1991). Shelf break intrusions occur on weekly intervals throughout the SAB (Menzel 1993). As a result, blooms may occur at any time of the year. However, these blooms are usually confined to the shelf break by a density front, and if the upwelled water is resident on the shelf for only a short time, some of the upwelled nutrients may be exported back to the ocean unutilized (Lee et al. 1981; Atkinson et al. 1984).

From May to October, when SAB shelf water warms and density is low, the intruded water may penetrate all the way to the middle and even the inner shelf in the form of subsurface intrusions, particularly under upwelling favorable winds (Atkinson et al. 1984). The presence of nutrients from subsurface intrusions, together with the shallow water depth of the SAB (the euphotic zone extends all the way to the seafloor) and long residence time of the subsurface intrusions (>~10 days), could therefore bring about strong subsurface blooms (Yoder et al. 1983; Yoder 1985), which will lower the residual $p\mathrm{CO}_2$ on the shelf at this time of the year (July and October 2005, Figure 4.5). Such blooms were captured on the middle and outer shelf during the

July and October 2005 cruises, as deduced from DIC, DO, and δ^{13}C-DIC data (Jiang et al., in preparation).

The strong phytoplankton production and clear CO_2 drawdown on the middle and outer shelf during July and October 2005 (Figure 4.5) suggests that the middle and outer shelf may trend toward being autotrophic at these times of the year. This is also supported by a number of findings from earlier biogeochemical studies in the SAB. First, the middle and outer shelf lack significant inputs of allochthonous organic carbon. Most terrestrial organic carbon, except lignin, is remineralized shoreward of the CFZ, and the majority of DOC that manages to cross the CFZ is usually older and relatively less reactive to bacterial utilization before it is exported from the SAB to the open ocean (Moran et al. 1991; DeAlteris 2007; DeAlteris et al., in preparation; L. R. Pomeroy, personal communication). Second, the bloom-produced organic carbon on the middle and outer shelf following injection of upwelled nutrients is usually exported back to the Gulf Stream by the same pattern of eddy circulation that brings new nitrogen onto the shelf (Yoder and Ishimaru 1989; Lee et al. 1991; Menzel 1993).

Prior continental shelf CO_2 studies to date have had limited or no coverage of the inner shelf (e.g., Tsuongai et al. 1999; DeGrandpre et al. 2002). High-resolution $p$$CO_2$ surveys on the SAB have shown that while the middle and outer shelf are sinks of -1.23±0.19 and -1.37±0.21 mol m^{-2} a^{-1}, respectively, the inner shelf is a source of +1.20±0.24 mol m^{-2} a^{-1} (Jiang et al. 2008a). The current study further illustrates differences in CO_2 dynamics between the inner shelf and the middle and outer shelf. Therefore, the inclusion of the nearshore continental shelf is critical for avoiding large errors in the assessment of the “Continental Shelf Pump” (Tsunogai et al. 1999) and the potential role of continental shelves as a net sink for atmospheric CO_2 (currently estimated at ~0.2-1.0 Gt C a^{-1}, Tsunogai et al. 1999; Borges et al. 2005; Cai et al. 2006).

5. Conclusions

Analysis of the potential mechanisms controlling sea surface pCO_2 in the SAB demonstrates that the inner shelf and the middle and outer shelf are different in their CO_2 dynamics. CO_2 on the inner shelf is strongly controlled by inorganic and organic carbon inputs from terrestrial sources (including heterotrophy on the inner shelf). In contrast, the middle and outer shelf are predominantly controlled by primary production that is strongly dependent on Gulf Stream frontal eddy-induced intrusions. This study is consistent with other continental shelf studies that suggest that globally inner continental shelf systems are heterotrophic; while middle and outer continental shelves are overall autotrophic (Rabouille et al. 2001; Chen and Borges 2009).

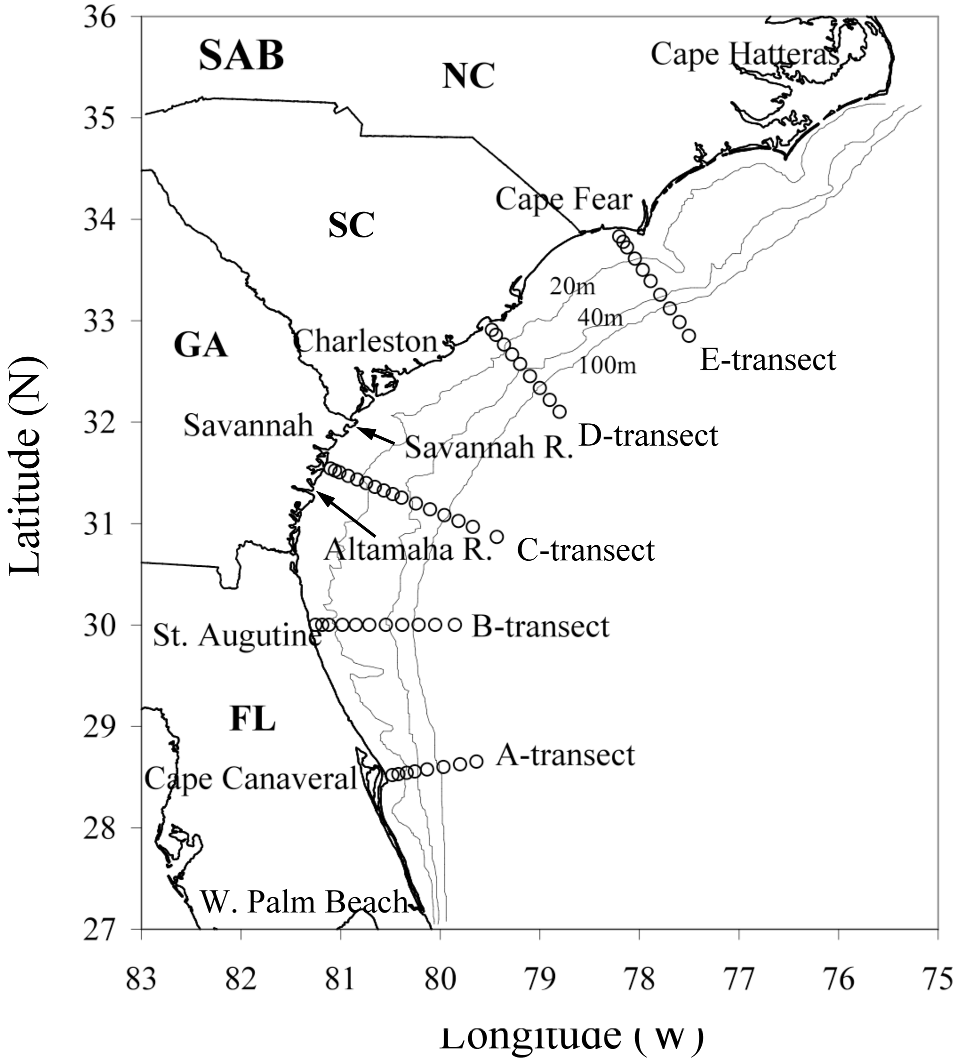

Figure 4.1. Study area is the U.S. South Atlantic Bight from Cape Lookout, North Carolina to Cape Canaveral, Florida. The circles are the sampling stations, which start from the shoreline and extend to about ~500 m water depth.

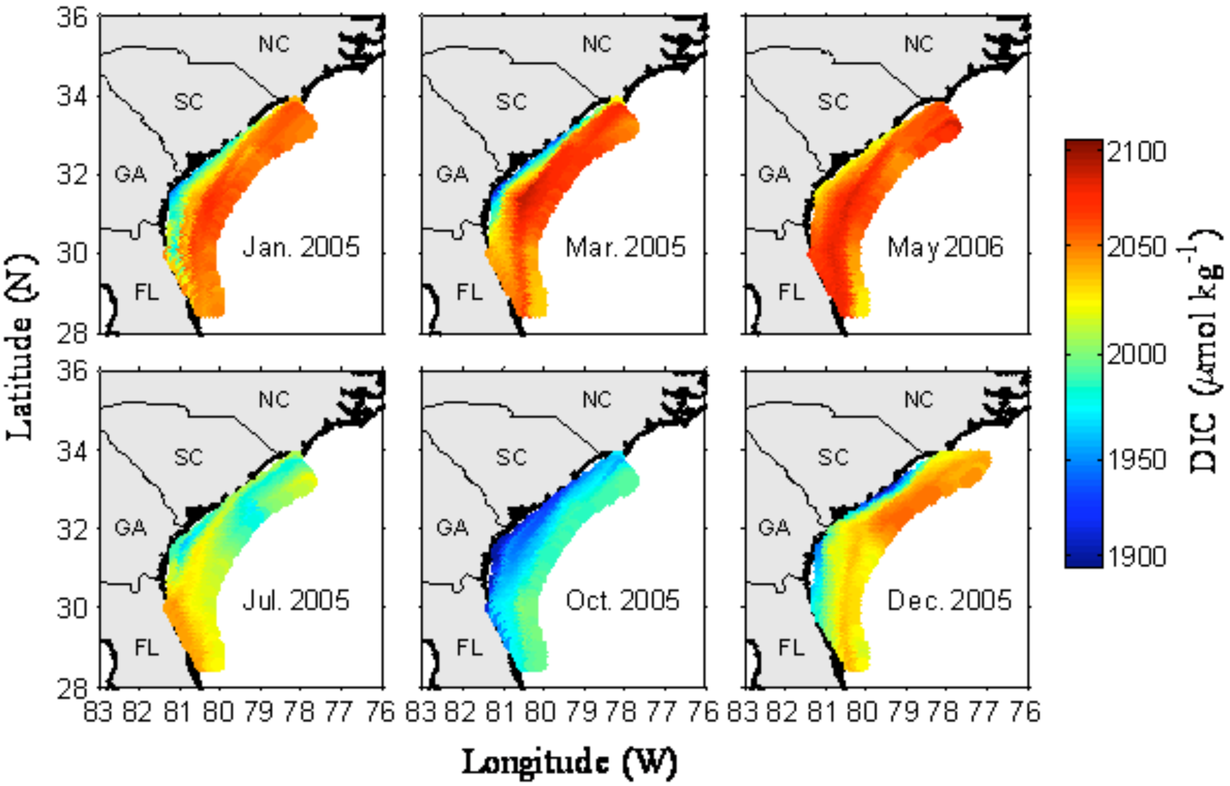

Figure 4.2. Spatial distributions of surface water dissolved inorganic carbon (DIC) on the South Atlantic Bight in all sampling months.

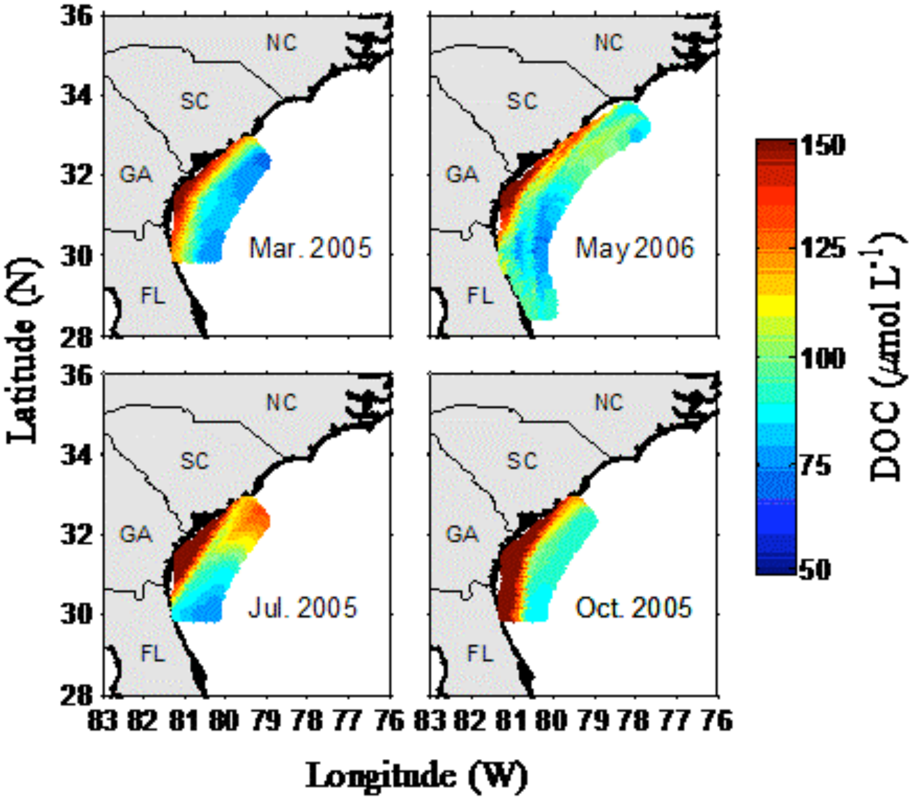

Figure 4.3. Spatial distributions of surface water dissolved organic carbon (DOC) on the South Atlantic Bight in March 2005, May 2006, July 2005, and October 2005.

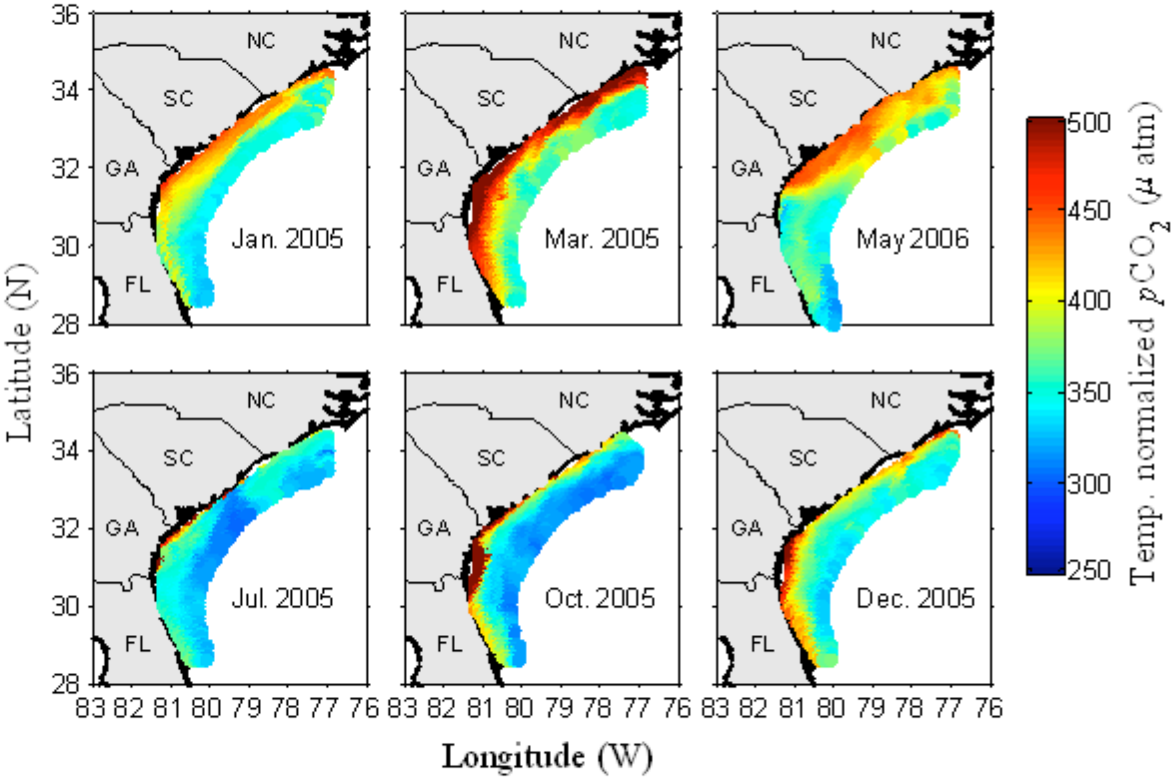

Figure 4.4. Spatial distributions of temperature-normalized (temperature = 23.11 °C) sea surface $p\text{CO}_2$ on the South Atlantic Bight in all sampling months.

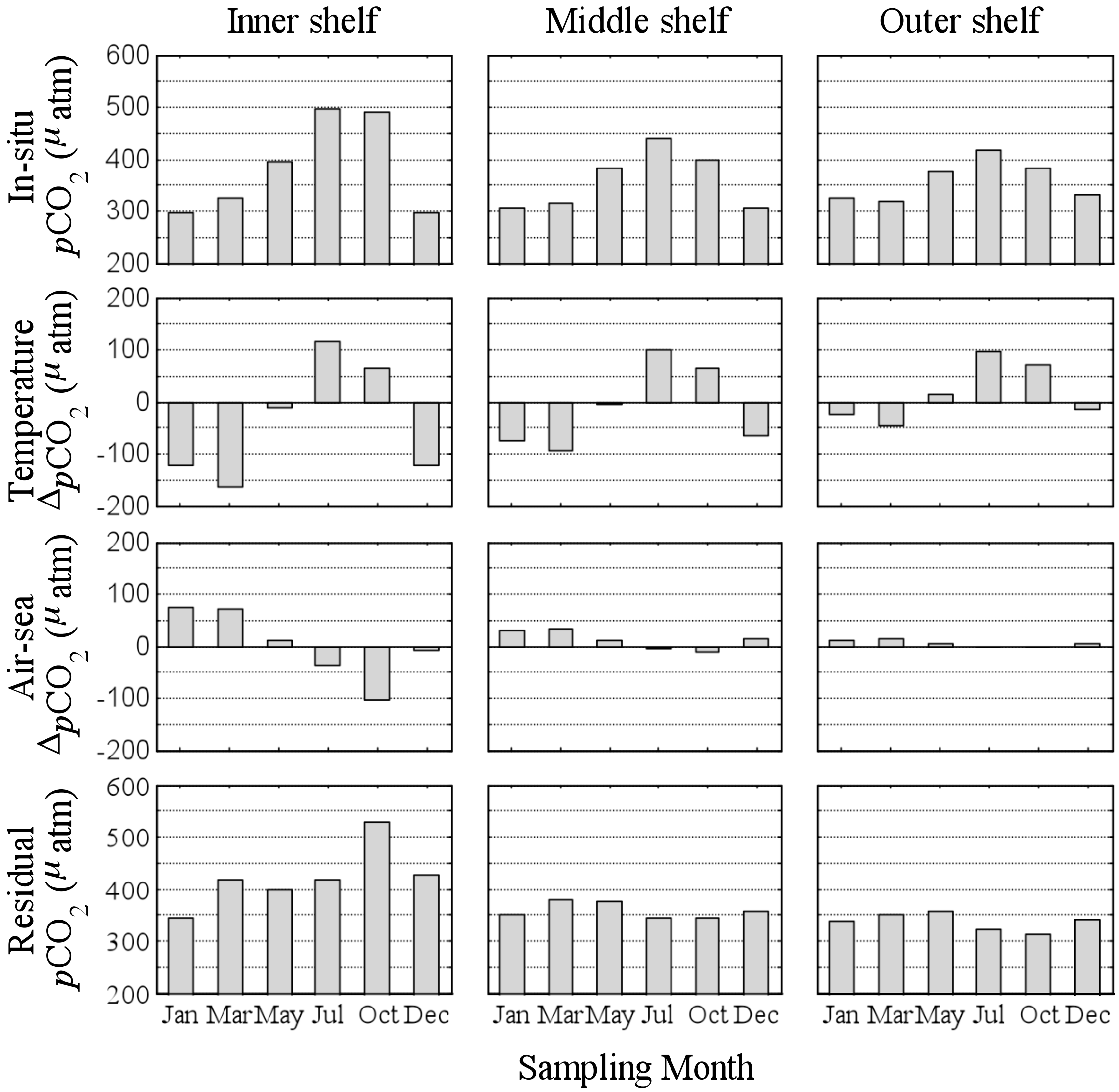

Figure 4.5. Seasonal changes of area-averaged sea surface pCO_2, pCO_2 variations due to temperature deviation from the annual mean temperature (23.11 ^{o}C), pCO_2 variations due to air-sea gas exchange, and residual pCO_2 on the inner, middle, and outer shelf of South Atlantic Bight. The leftmost column is for the inner shelf, the rightmost column is for the outer shelf, and the column in the middle is for the middle shelf. In situ pCO_2 equals the sum of pCO_2 variations due to temperature, pCO_2 variations due to air-sea gas exchange, and residual pCO_2.

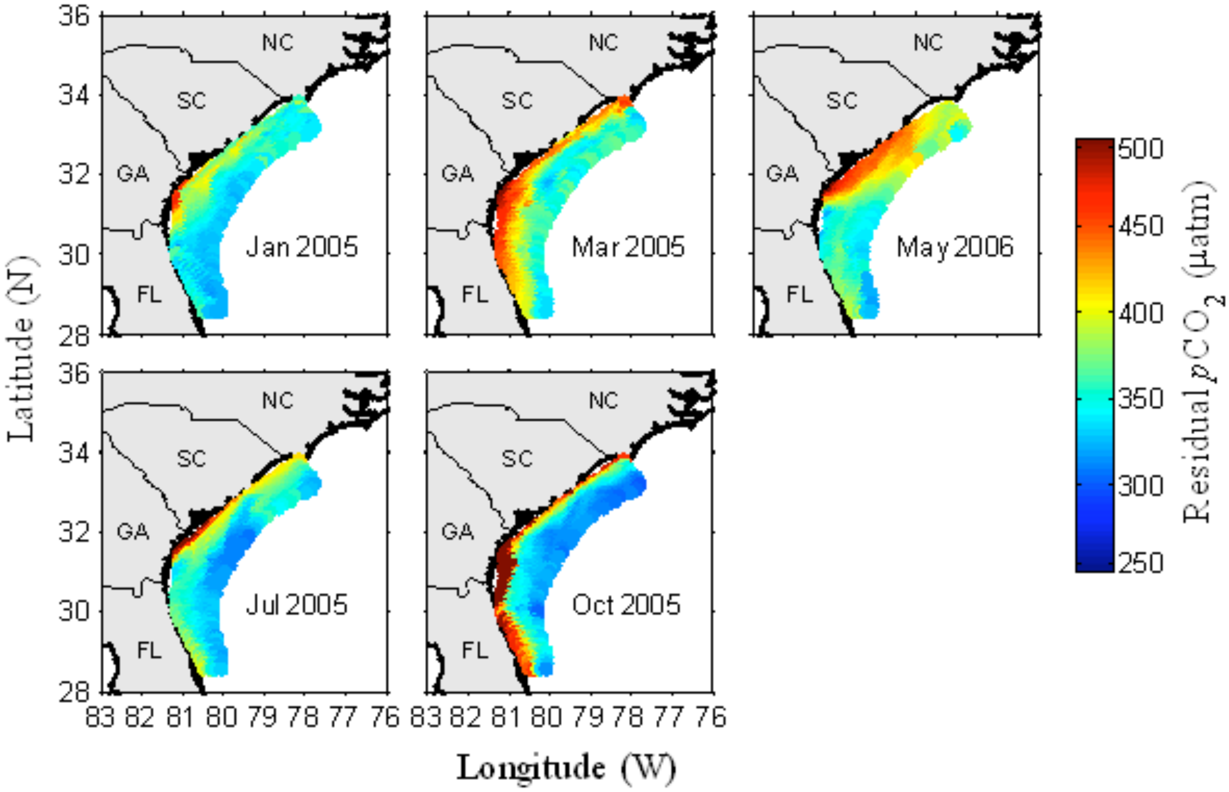

Figure 4.6. Spatial distributions of surface water residual pCO_2 on the South Atlantic Bight in all sampling months except December 2005. Due to lack of DIC data, spatial distribution of residual pCO_2 in December 2005 was not presented, although we still show the average residual pCO_2 in Figure 4.5.

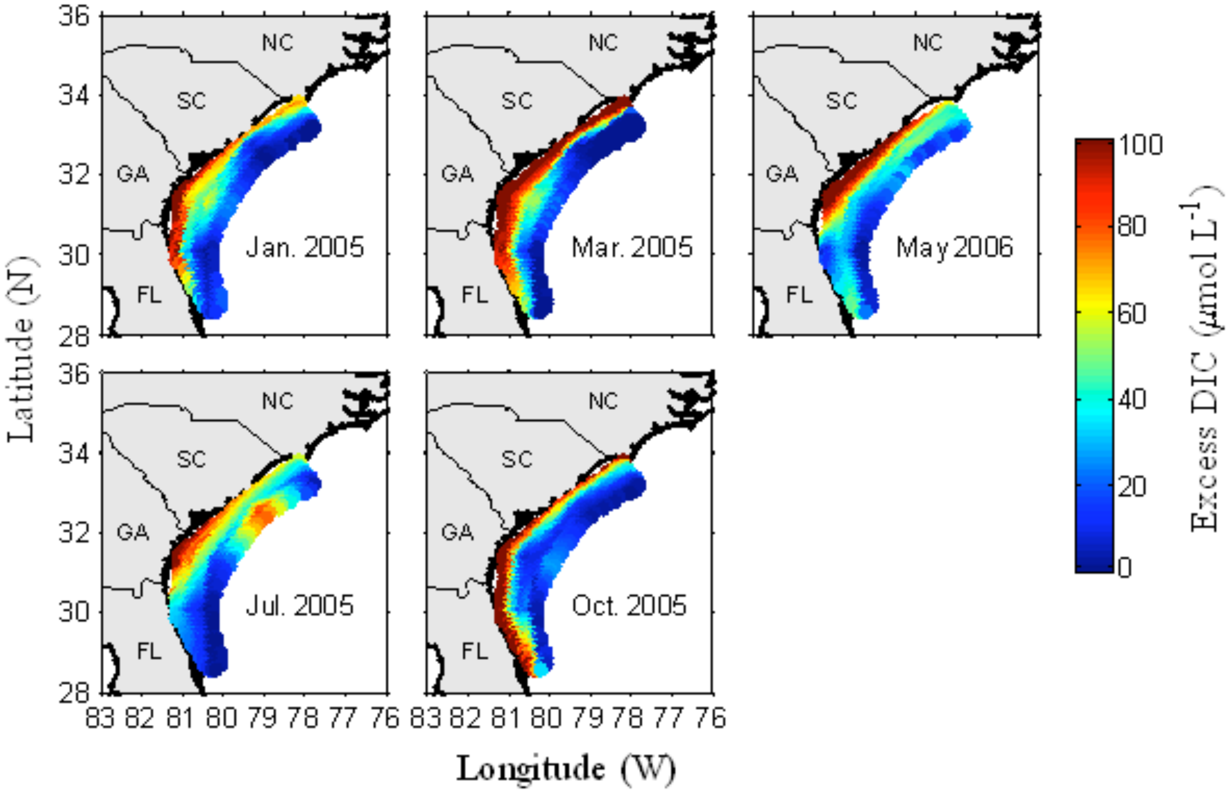

Figure 4.7. Spatial distributions of surface water excess DIC on the South Atlantic Bight in all sampling months except December 2005. Due to lack of data, excess DIC in December 2005 was not calculated.

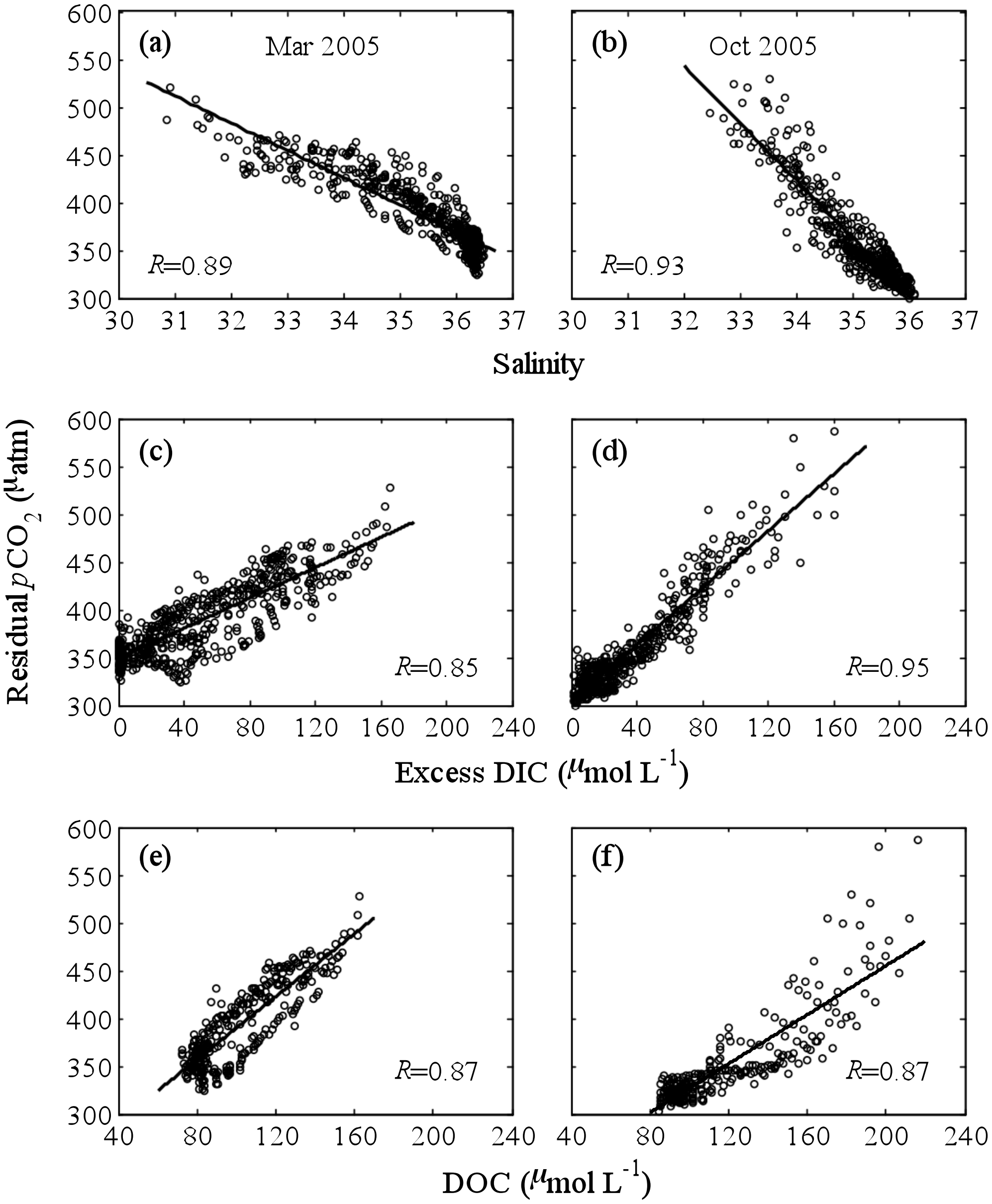

Figure 4.8. Residual pCO$_2$ plotted against salinity (a and b), excess DIC (c and d), and DOC (e and f) in March 2005 (panels on the left) and October 2005 (panels on the right). Data from these two months were chosen as examples, although other months also show similar relationships.

CHAPTER 5

PROCESSES CONTROLLING DISSOLVED INORGANIC CARBON ON THE CONTINENTAL SHELF OF THE SOUTHEASTERN UNITED STATES[1]

---

[1] Jiang, L.-Q., W.-J. Cai, et al. To be submitted to *Marine Chemistry*.

Abstract

This study examines the biological and physical processes controlling dissolved inorganic carbon (DIC) in the US South Atlantic Bight (SAB). Vertical distributions of DIC, dissolved oxygen (DO), total alkalinity (TA), pH were measured on 5 onshore-offshore transects during 6 cruises from January 2005 to May 2006. Nitrate (NO_3^-) plus nitrite (NO_2^-), phosphate (PO_4^{3-}), silicic acid (H_4SiO_4), and $\delta^{13}C$ and $\Delta^{14}C$ of DIC, and δD and $\delta^{18}O$ of H_2O were also measured on selected cruises to help assess DIC sources and cycling. Results show that DIC concentrations in the SAB ranged from 1900 to 2200 μmol kg^{-1}. Concentrations were lowest close to the coast where large amounts of freshwater are introduced. The highest DIC concentration occurred at the deepest stations beyond the shelf break. Findings suggest that DIC in the SAB is mainly controlled landward by inputs and dilution from terrestrial sources and seaward by biological activity on the middle and outer shelf. While freshwater dilutes DIC on the shelf, rivers, marshes, and groundwater concomitantly deliver DIC to the SAB. At the shelf break, upwelling associated with Gulf Stream frontal eddies brings nutrients to the shelf. This process helps to lower continental shelf DIC in summer by enhancing biological activity on the middle and outer shelf. Overall, the SAB exports DIC to the open ocean at a rate of $2.9(\pm1.7)\times10^{12}$ gC yr^{-1}.

1. Introduction

By linking continents, ocean, and atmosphere, continental shelves play a key role in the global carbon cycle (Mackenzie 1991; Smith and Hollibaugh 1993). Despite their limited distribution (~7-8% of the global ocean surface area), continental shelves sustain unusually high primary production, remineralization, and organic carbon burial (Walsh 1988; Wollast 1993; Gattuso et al. 1998; de Hass et al. 2002). Recent studies have shown that continental shelves are globally an important sink of atmospheric carbon dioxide (CO_2). The “continental shelf pump”, which was originally proposed by Tsunogai et al. (1999), takes up CO_2 from the atmosphere at a rate of 0.2-1.0 Gt C each year (Tsunogai et al. 1999; Borges et al. 2005; Cai et al. 2006). Fluxes of this magnitude account for about 15-70% of the current estimate of CO_2 uptake by the open ocean (1.2-1.6 Pg C yr^{-1}) (Takahashi et al., 2009), thus representing a significant portion of the total oceanic uptake of CO_2.

The continental shelf of the southeastern United States, commonly known as the South Atlantic Bight (SAB) is a marsh-dominated western boundary shelf (Cai et al. 2006). A new study revealed that contrary to the earlier conclusions, the SAB is a net sink of atmospheric CO_2 on an annual basis (Jiang et al. 2008a). The CO_2 sink in the SAB is -0.48 ± 0.21 mol m^{-2} yr^{-1}, which is much smaller when compared to the Middle Atlantic Bight (-1.33 mol m^{-2} yr^{-1}, using an atmospheric xCO_2 of 365 ppm, DeGrandpre et al., 2002), the North Sea (-1.38 mol m^{-2} yr^{-1}, Thomas et al., 2004b), and the East China Sea (-2.92 mol m^{-2} yr^{-1}, Tsunogai et al., 1999).

Studies in the East China Sea (ECS) (Tsunogai et al. 1999) and the North Sea (Bozec et al. 2005) all favor the argument that the spatial decoupling of autotrophic processes in the surface layer and the subsequent remineralization and export in the deep layer is the key to the continental shelf pump (Borges et al. 2006). However, the SAB differs from the ECS or the

North Sea in that it is very shallow, only about 50-75 m deep at the shelf break. The shallow depth, together with strong winds and large tidal magnitude, makes the shelf water well-mixed during most time of the year. Thus, mechanisms controlling the continental shelf pump in the SAB may also differ from those in the ECS or the North Sea.

An assessment of inorganic carbon cycling is essential for better understanding the continental shelf pump in the SAB. In addition to the DIC addition from air-sea gas exchange (Jiang et al. 2008a), prior studies have shown that the SAB shelf receives large amounts of inorganic carbon from rivers (0.63×10^{12} gC yr^{-1}, Cai and Wang 1998) and salt marshes (0.71×10^{12} gC yr^{-1}, Wang and Cai 2004). Groundwater might be another important source of DIC from the land (Moore 2007). Since continental shelves have limited capacity to store inorganic carbon, all but a small fraction of the received inorganic carbon from the land and air-sea CO_2 exchange must either be directly exported to the open ocean, or be converted into organic carbon and exported in the form of DOC and POC (Liu 2000).

In this study, we will examine how terrestrial inputs and biological activity impact the DIC distribution on the SAB shelf. We will also try to quantify the DIC imported from groundwater and the DIC exported from the shelf to the open ocean, and reassess the inorganic carbon mass balance of the SAB. To do this, we present a comprehensive data set of DIC, dissolved oxygen (DO), total alkalinity (TA), pH, nutrients, $\delta^{13}C$ and $\Delta^{14}C$ of DIC, and δD and $\delta^{18}O$ of H_2O on the basis of 6 cruises covering the entire SAB with emphasis on their vertical distribution.

2. Study Site and Methods

2.1. Site Description

The South Atlantic Bight extends along the southeastern United States coast from Cape Hatteras, North Carolina to West Palm Beach, Florida (Figure 5.1). The SAB continental shelf is very shallow with a shelf break depth of around ~50-75 meters. The Gulf Stream flows northward along the shelf break. Extensive coastal salt marshes are present between South Carolina and Georgia (Menzel 1993). Tides flood and drain these intertidal marshes twice daily and exchange materials with the adjacent shelf (Hopkinson 1985). From north to south, eleven major rivers (the Cape Fear, Pee Dee, Santee, Cooper, Edisto, Savannah, Ogeechee, Altamaha, Satilla, St Mary's, and St Johns) input freshwater to the SAB (Blanton and Atkinson 1983). Most of the river discharge is located in the central and northern parts of the SAB. River discharge usually peaks in February-April and has minimum flow in September-November with a total annual discharge of about 66 km^3 (~2.7% of the SAB volume) (Menzel 1993). Some evidences have suggested that groundwater discharge, most of which recycled seawater, is also significant (Shaw et al. 1998; Moore 2007). A Coastal Frontal Zone (CFZ) ~10-30 km offshore forms periodically from a cross-shelf pressure gradient induced by freshwater discharge (Blanton 1981). The CFZ presents a dynamic barrier to the seaward transport of both dissolved and particulate materials (Blanton 1981; Blanton and Atkinson 1983).

2.2. Sampling

Surveys were carried out on five onshore-offshore transects, designated A, B, C, D, E from south to north (Figure 5.1) during six cruises: 05-16 January 2005, 19-30 March 2005, 27 July - 05 August 2005, 07-17 October 2005, 16-21 December 2005, and 17-27 May 2006. At each sampling station, a Sea-Bird Electronics, Inc., conductivity-temperature-depth (CTD) instrument was deployed with a 12-Niskin-bottle (10 L) rosette. The vertical spacing of samples was as close as 10 meters near the surface and gradually increased with depth. In December 2005, only the E-, C-, and A-transects were sampled due to limited ship time.

Samples for DIC and TA were preserved with $HgCl_2$ and stored in a refrigerator on the research vessel. DIC was measured using an automated DIC analyzer within a week after each cruise. A 0.5 ml water sample was pumped into a gas-tight reactor, and acidified with 10% H_3PO_4. The extracted CO_2 gas was measured with a LI-COR 6252 infrared CO_2 detector (Wang and Cai 2004). The DIC measurement has a relative precision of 0.1%. TA was measured on the remaining water using 12-ml water samples by Gran Titration to an end point pH of 3.0 (Gran 1952). The relative precision of the TA measurement was 0.1%. Both the DIC and TA analyzers were calibrated with certified reference materials (CRMs) supplied by Scripps Institution of Oceanography.

pH and DO were determined onboard the ship during cruises. pH was measured using a Ross glass electrode connected to an Accumet® model 20 pH meter. The pH samples were kept in a water bath with a constant temperature of $25^{o}C$ for ~30 minutes before measurement. DO concentration was determined using a spectrophotometric Winkler method (Pai et al. 1993). DO samples were collected in 60-ml biological oxygen demand (BOD) bottles. The samples were fixed by addition of 0.5 ml manganese chloride and 0.5 ml alkaline iodide reagents. After being vigorously shaken for about one minute, the BOD bottles were stored in the dark. When most of the precipitate had settled, sample bottles were reopened and 0.5 ml of sulfuric acid solution was added. The mixture was then gently stirred with a magnetic stirrer until all the precipitate had dissolved. Absorbance was measured using a Shimadzu UV-1700 spectrophotometer within three minutes after addition of the sulfuric acid. The spectrophotometric Winkler method has a coefficient of variation of 0.1 % and detection limit of 0.25 mmol m^{-3} for onboard measurement.

Nutrient samples collected during October 2005 were stored frozen onboard and analyzed at the Atlantic Oceanographic and Meteorological Laboratory (AOML). Concentrations of dissolved nitrate (NO_3^-) plus nitrite (NO_2^-), phosphate (PO_4^{3-}) and silicic acid (H_4SiO_4) were determined by gas-segmented continuous flow analysis using a modified Alpkem flow solution Auto-Analyzer. Calibrations were performed prior to each sample run with working standard solutions. Overall analytical precisions were 0.04 μmol L^{-1} for nitrate, 0.01 μmol L^{-1} for phosphate and 0.1 μmol L^{-1} for silicic acid.

Samples for $\delta^{13}C$ and $\Delta^{14}C$ of DIC were collected on D-, C-, and B-transects during the sampling months of March 2005, July 2005, and October 2005. The samples were preserved using $HgCl_2$ until processing back in the lab. Samples were extracted by acidification to pH 2.5 using 85% phosphoric acid, and the CO_2 produced was then stripped from the sample by sparging using ultra-high purity helium gas and collected and purified cryogenically on a vacuum extraction line (DeAlteris 2007). $\delta^{13}C$ was measured on a Thermo-Finnegan Delta Plus isotope ratio mass spectrometer (IRMS) at Ohio State University with an error of ±0.1‰, and $\Delta^{14}C$ was measured by accelerator mass spectrometer (AMS) at the National Science Foundation AMS Facility in the University of Arizona with a relative error of ±5-10‰ (DeAlteris 2007).

Samples for δD and $\delta^{18}O$ of H_2O were collected on C-transect during October 2005 and determined at the Center for Applied Isotope Studies (CAIS) in the University of Georgia. The samples were passed through a 1400^{o}C furnace to dissociate water molecules to elemental H and O with subsequent formation of H_2 and CO gas (H_2 and CO). The H_2 and CO were then chromatographically separated at 200^{o}C on a molecular sieve column and measured for isotopic ratio. The method has a relative error of ±1‰.

3. Results

3.1. SAB Hydrography

Temperature in SAB waters showed large seasonal and spatial variability. Vertically, water temperature was uniform from surface to seafloor during all sampling months except July 2005 when stratifications were observed (Figure 5.2). In January and March 2005, water temperature was very low close to the coast (10-14^{o}C) and increased towards the Gulf Stream where it was as high as 21-25^{o}C (Figure 5.2). Stratifications were seen on all five onshore-offshore transects in July 2005 (Figure 5.2). Beyond the shelf break, water temperature as low as 7^{o}C was observed close to the seafloor. In October 2005, the shelf water was well-mixed again, with a temperature range of 25-29^{o}C.

Most freshwater sources in the SAB are located in the central and northern part of the shelf (E-, D-, and C-transects) and the mean nearshore circulation is to the north during winter, spring and summer, and to the south during fall (Lee et al. 1991; Menzel 1993). As a result, salinity in SAB waters was always lowest (26-33) nearshore and increased offshore (~36) except for A- and B- transects where no clear onshore-offshore gradients were seen in some months (Figure 5.3). Seasonally, little freshwater input occurred on B-transect during May 2006 and July 2005, and noticeable freshwater influences were seen on A-transect only during October 2005 (Figure 5.3). Salinity was exceptionally low in October 2005 perhaps related to Hurricane Katrina (August 2005).

3.2. Dissolved Inorganic Carbon

DIC in SAB waters ranged from 1900 to 2200 μmol kg^{-1}. DIC concentration was lowest near the coast where salinity was low (Figure 5.4). The highest DIC concentration was observed at the deepest stations beyond the shelf break. Seasonally, DIC on the middle and outer shelf showed large variability. On C-transect, where the shelf is widest, DIC on the middle and outer shelf was highest in January 2005, March 2005, and May 2006; and lowest in July and October 2005 (Figure 5.4). For transects where the shelf is narrow (e.g., A-transect), the drawdown of DIC on the outer shelf can be seen throughout the year (Figure 5.4). DIC was unusually low in October 2005 and corresponded to the extremely low salinity at this time.

3.3. Dissolved Oxygen

Dissolved oxygen on the SAB ranged from 140 to 270 μmol L^{-1} (Figure 5.5). Seasonally, DO concentration was highest in winter and lowest in summer. The maximum DO concentrations (260-270 μmol L^{-1}) were found in January and March 2005 close to the coast, where water temperature was lowest. Further offshore, DO dropped quickly in these two months. In May 2006, DO concentration was considerably lower than in winter (Figure 5.5) and reached minimum in October 2005. In July 2005, sub-surface DO maxima were observed on all transects (Figure 5.5), suggesting possible blooms in this month.

Since temperature plays an important role in DO solubility, DO saturation rate was also calculated according to the equation of García and Gordon (1992) to remove temperature effect (Figure 5.6). The results show that the high inner shelf DO concentrations during the cold months of January 2005, March 2005, May 2006, and December 2005 were most likely caused by the low water temperature (Figure 5.2); because even though the inner shelf DO concentrations in these months were high (Figure 5.5), their corresponding DO saturation rates were low (Figure 5.6).

3.4. δ^{13}C and Δ^{14}C of DIC

The δ^{13}C of dissolved inorganic carbon (δ^{13}C-DIC) on D-, C-, B-transects of the SAB ranged from -0.8 to 1.6‰ during the sampling months of March, July, and October 2005 and was lowest on the inner shelf and increased offshore (Figure 5.7, see also DeAlteris 2007; DeAlteris et al. in preparation). δ^{13}C-DIC did not show large vertical gradients. Of the three months when δ^{13}C-DIC was measured, δ^{13}C-DIC in July 2005 and October 2005 were more positive than that in March 2005 (Figure 5.7).

Surface water Δ^{14}C of dissolved inorganic carbon (Δ^{14}C-DIC) showed relatively uniform spatial and seasonal distributions on the shelf, with a narrow range of 55-82‰ (Table 5.1). However, large vertical gradients of Δ^{14}C-DIC were seen beyond the shelf break. In July 2005, Δ^{14}C-DIC at the most offshore stations was about 64-86‰ in the surface and as low as –74% (~500 years old) at a depth of 700m (Table 5.1).

4. Discussion

4.1. Impact of Terrestrial Sources on DIC distribution

DIC concentrations were always lowest close to the coast and increased offshore (Figure 5.4). The onshore-offshore DIC gradients were largely a result of freshwater dilution of oceanic DIC on the shelf. DIC concentrations in rivers of this region are only ~200 to 900 μmol kg^{-1} (Cai, unpublished data), compared to the oceanic DIC concentrations (usually as high as 2100 μmol kg^{-1}). The inputs of low-DIC freshwater lower nearshore DIC concentrations by means of dilution (Figure 5.8).

DIC concentrations on the inner shelf was always higher than predicted from the conservative mixing line up to a salinity of 34 (Figure 5.8), suggesting input of DIC. DIC inputs can also be indicated by salinity-normalized DIC (DIC concentration with dilution effect corrected, Wang et al. 2005) distributions. If DIC distribution is determined only by dilution of ocean end member by a zero-DIC freshwater, salinity-normalized DIC should be the same across the shelf. That is, higher than surrounding salinity-normalized DIC would suggest an input of DIC, or vice versa.

Results show that no DIC inputs to the inner shelf of B-transect were seen during May 2006 and July 2005 (Figure 5.9), and clear DIC inputs to the inner shelf of A-transect were only seen in October 2005 (Figure 5.9), although DIC inputs to the inner shelf on E-, D-, and C -transects occurred in all sampling months. This is consistent with seasonal changes of low salinity water distribution in the SAB (Figure 5.3). That is, most freshwater input from river occurs in the central and northern part of the SAB, and low salinity water was found to the north (transect C-E) during winter, spring, and summer, and also to the south during fall (Lee et al. 1991; Menzel 1993). The close correlation between salinity-normalized DIC and low salinity water suggests the importance of terrestrial sources in contributing to the DIC addition to the nearshore area.

4.2. Nutrient Pumping Processes at the Shelf Break

Instead of showing a linear correlation with salinity like TA, L-shaped DIC vs. salinity relationships were seen at high salinities (Figure 5.8). All data in the “L” were from samplings beyond the shelf break. The low salinity high DIC data above the conservative mixing line were from deep water, and the low salinity low DIC data below were from the surface. The temperature vs. salinity (T-S) plots also showed L-shaped relationships, although with upside-down direction (Figure 5.10). Data above the T-S plots of the shelf water (high temperature, low salinity) were from surface water, and data below the shelf water T-S plots (low temperature low salinity) were from deep water (Figure 5.10). Clearly, the plots of DIC vs. salinity and temperature vs. salinity suggest a multiple-end-member mixing at the shelf break.

Here we use vertical distributions of temperature, salinity, DO, DIC, pH, nutrients, δ^{13}C-DIC, Δ^{14}C-DIC, and δD and δ^{18}O of H_2O on C-transect during October 2005 as an example to examine processes that bring nutrients to the shelf (as data in this month are most complete). The data showed that there were two water masses impinging on the continental slope (Figure 5.11). The water closest to the slope (at the bottom) featured low temperature (Figure 5.11a) and low salinity (Figure 5.11b). It was oldest (about 500 years old at the bottom) (Figure 5.11c) and most remineralized (remineralization process will release ^{13}C-depleted carbon into the water, Figure 5.11j). The water also featured low δD-H_2O (δD of H_2O, Figure 5.11k) and high δ^{18}O-H_2O (δ^{18}O of H_2O, Figure 5.11l). Corresponding to its age, this water had the lowest DO (Figure 5.11d) and the highest DIC (Figure 5.11e). Due to CO_2 addition from remineralization processes, this water showed the lowest pH (Figure 5.11f). This water contains large amounts of nitrate (Figure 5.11g), phosphate (Figure 5.11h) and silicate (Figure 5.11i), which could potentially be upwell onto the shelf and support phytoplankton blooms. Earlier studies showed that this water was most likely Antarctic Intermediate water (AAIW) (Atkinson 1983; Tsuchiya 1989). AAIW, which is characterized by negative salinity anomalies, lowered oxygen concentrations, and elevated nutrient concentrations, have been observed under the Gulf Stream as far north as Onslow Bay, North Carolina (Atkinson 1983 and references therein).

The water right above the AAIW is the Gulf Stream, and contrasting to AAIW, it featured higher temperature (Figure 5.11a) and higher salinity (Figure 5.11b). It was much younger (Figure 5.11c) and less remineralized than AAIW (Figure 5.11j). Consequently, it had relatively higher oxygen concentration (Figure 5.11d), lower DIC concentration (Figure 5.11e), and higher pH (Figure 5.11f) than the AAIW. It does not contain large amounts of nutrients (Figure 5.11g, h, and i).

Early studies have shown that interaction of the Gulf Stream and the deeper AAIW is one of the most important processes controlling biological activity on the continental shelf of this region (Figure 4, Lee et al. 1991). The Gulf Stream frontal meanders and eddies could induce upwelling of the nutrient-loaded deeper AAIW along the southeastern United States continental shelf break (Menzel 1993). Meanders and eddies occur at a frequency of 2-14 days throughout the year (Atkinson et al. 1984). During winter, spring, and fall, the upwelled water is usually restricted to the outer shelf by strong cross-shelf density fronts; during summer when the shelf is stratified and water density is low, the upwelled water could penetrate to the middle shelf or even inner shelf as subsurface intrusions, particularly if aided by upwelling-favorable winds (Atkinson et al. 1984).

4.3. Impact of Biological Activity on DIC distribution

Salinity-normalized DIC indicated a strong removal on the middle and outer shelf of E-, C-, B- and A-transects during July and October 2005 (Figure 5.9). We suggest that the much lower salinity-normalized DIC in these two months compared to other months was most likely caused by phytoplankton blooms. From May to October, when subsurface intrusions occur, large amounts of nutrients can be pumped onto the shelf. This together with the shallow mixed layer depth (the euphotic zone extends all the way to the bottom), makes it possible for subsurface phytoplankton blooms to take place (Yoder et al. 1983; Lee et al. 1991).

Evidence for a phytoplankton bloom in July 2005 is also from the DO data. During July 2005, high DO concentrations (Figure 5.5) were observed where DIC drawdown occurred (Figure 5.9).

In comparison, DO concentration increase was not detected in October 2005 when DIC data also suggested a bloom (Figure 5.9). This might be due to: 1) air-sea exchange rate of oxygen is very fast, and 2) what we captured in October 2005 was a decaying phytoplankton bloom.

The phytoplankton blooms during July and October 2005 can also be detected from the δ^{13}C-DIC data (Figure 5.7). δ^{13}C-DIC is a good indicator of the balance of autotrophic and heterotrophic processes. Autotrophic processes will raise δ^{13}C-DIC in the water by preferential uptake of ^{13}C-depleted inorganic carbon. In contrast, heterotrophic processes will lower δ^{13}C-DIC by release of remineralized ^{13}C-depleted inorganic carbon. The average δ^{13}C-DIC on the middle and outer shelf during March 2005 was 0.73‰; and it increased to 1.43 and 1.21‰ in July 2005 and October 2005, respectively (Figure 5.7). The higher δ^{13}C-DIC during July and October 2005 suggests more autotrophic processes in these two months.

To quantify the impact of primary production on the shelf DIC distribution, we quantified primary productivity from the DIC data. To do that, we assumed: 1) DIC gain and loss via exchange with terrestrial sources and the open ocean can be neglected during the period of the subsurface intrusion; 2) DIC concentrations before the subsurface intrusion of July 2005 can be approximated as those observed in May 2006; 3) the residence time of the bloom is about two weeks (Yoder 1985). First, depth-averaged DIC over the whole shelf was interpolated onto a $0.05\times0.05^{\circ}$ grid. DIC per unit of area at each pixel of the grid within the middle and outer shelf was calculated as the product of interpolated depth-averaged DIC and the real water depth. DIC on the pixel was estimated as the product of area-based DIC at the pixel and the surface area of the pixel. By integrating DIC on all pixels of the middle and outer shelf, volume-averaged DIC in a specific month can be calculated. Primary productivity can then be estimated as the difference between volume-averaged DIC in these two months times the total volume of the middle and outer shelf (2.18×10^{12} m^3, Menzel 1993) and divided by the total surface area of the middle and outer shelf (6.17×10^{10} m^2, Menzel 1993) and duration of the subsurface intrusion (2 weeks).

Results show that primary productivity on the middle and outer shelf of the SAB during the subsurface intrusion of July 2005 was about 390 gC m^{-2} yr^{-1}. It is in the same order as the average primary productivity on the outer shelf of the SAB (360 gC m^{-2} yr^{-1}), as summarized by Menzel (1993). Here the purpose of the calculation is to give a quantitative view of the DIC change caused by the phytoplankton bloom. Due to the many assumptions, there are large uncertainties associated with this estimate. Thus, the results are not appropriate for use in mass balance studies.

4.4. DIC Flux Estimates

4.4.1. DIC Export from the SAB to the Open Ocean

DIC flux from the SAB to the open ocean was estimated using two methods. Method I was based on the concept of “excess DIC”. Excess DIC was defined as the DIC in excess of the marine source and represents all sources or sinks of DIC along the transect except the open ocean end member (Jiang et al. 2008b). DIC flux to the open ocean was then calculated by the excess DIC inventory divided by the shelf flushing time (Wang et al. 2005). Shelf flushing time, which is the average time freshwater stays on the shelf, can be estimated as the total freshwater volume (relative to oceanic water) divided by the total freshwater input from land. As a first order approximation, a 3-month shelf flushing time (Atkinson et al. 1978) was used.

To estimate the excess DIC inventory over the entire SAB shelf, depth-averaged excess DIC at each sampling station was calculated based on vertical distributions of excess DIC. The depth-averaged excess DIC was interpolated onto a 0.05×0.05^{o} grid. Then the interpolated values were multiplied by the water depth at each pixel to get the excess DIC per unit of area. Excess DIC inventory over the entire SAB was then calculated by the cumulative results of the products of excess DIC per unit of area and the surface area of the pixel.

Method II assumed that net water export from the SAB to the open ocean leaves the shelf with a DIC concentration equal to that at the shelf break. Since DIC showed little spatial gradients from the outer shelf to the open ocean, tidal oscillation and diffusion would not contribute much to the net DIC transport to the open ocean unless the flooding and ebbing tides are asymmetrical in terms of water transport. Thus, DIC export to the open ocean can be calculated as the product of net water export from the shelf to the open ocean and the average DIC concentration at the shelf break (2060±42 μmol kg^{-1}).

Net water export from the shelf to the open ocean can be approximated to be the sum of freshwater and net submarine groundwater discharge (SGD), if we assume a steady state for the water reservoir in the SAB and an approximate balance between evaporation and precipitation. An average freshwater riverine discharge of 1.8×10^8 m^3 d^{-1} was used for the calculation (Menzel 1993).

Because a large fraction of the SGD is recycled seawater, net SGD input was calculated as the product of total SGD discharge and the relative proportion of freshwater within the SGD. The total SGD water flux to the SAB was estimated as radium fluxes divided by the average radium concentration in SGD (Moore, 2007; W. S. Moore, personal communication). For ^{228}Ra, we divided ^{228}Ra flux (1.5×10^{12} dpm d^{-1}) by the average ^{228}Ra concentration of 2.50 dpm L^{-1} to get a water flux of 6.0×10^8 m^3 d^{-1} (Table 7a, Moore, 2007). For ^{226}Ra, we divided ^{226}Ra flux (8.2×10^{11} dpm d^{-1}) by the average ^{226}Ra concentration of 1.58 dpm L^{-1} to get a water flux of 5.2×10^8 m^3 d^{-1} (Table 7b, Moore, 2007). The two estimates for SGD water flux agreed very well, and we therefore chose to use the average of 5.6×10^8 m^3 d^{-1} for the calculation. The ratio of freshwater within SGD was calculated from the SGD salinity according to the method of Atkinson et al. (1978). The calculated net SGD input was $1.5(\pm0.7)\times10^7$ m^3 d^{-1}. Here an average SGD salinity of 35.5±0.5 (based on samplings around Oaktree River, South Carolina in July 2003) was used for the calculation, while the SGD salinity of this region could vary from 20 to 38 (Moore, personal communication). Thus, large uncertainties are expected for the estimated net SGD discharge.

The calculated DIC fluxes from the SAB to the open ocean are $4.0(\pm1.5)\times10^{12}$ gC yr^{-1} and $1.8(\pm0.8)\times10^{12}$ gC yr^{-1} based on Methods I and II, respectively (Table 5.2). They are of the same order as the earlier estimate of 2.62×10^{12} gC yr^{-1} by Wang et al. (2005), which was based on one transect and limited seasonal surveys. We can see that the estimated DIC export from the SAB to the open ocean is 3-8 times higher than the air-water CO_2 sink in the SAB [$-0.52(\pm0.23)\times10^{12}$ gC yr^{-1}, Jiang et al., 2008a], suggesting a possible important role for DIC export from the shelf to the open ocean in the "continental shelf pump" (Tsunogai et al., 1999).

4.4.2. DIC Input to the SAB from Land

DIC sources from land include rivers, salt marshes, and groundwater. DIC inputs from salt marshes to the SAB have been previously estimated by Wang and Cai (2004) as 0.71×10^{12} gC yr^{-1}. Here, we focused on DIC inputs from rivers and groundwater. DIC inputs from rivers to the SAB were estimated based on weekly DIC measurements in the Altamaha River (JayCee Landing in Jesup, Georgia, Latitude: N31.67, Longitude: W81.85, about 60 km upstream from the mouth of the Altamaha river) from 11 November 2000 to 9 September 2006 (W.-J. Cai, unpublished data). Discharge-averaged DIC concentration in the Altamaha River was estimated to be 549 μmol L^{-1}. Then DIC inputs from rivers to the SAB were calculated as the product of freshwater discharge to the SAB (1.8×10^8 m^3 d^{-1}, Menzel 1993) and the discharge-averaged DIC concentrations in the Altamaha River. Prior studies have shown that DIC concentrations in some other rivers of the SAB, e.g. the Satilla River, were similar to those in the Altamaha River (Cai and Wang 1998).

DIC fluxes from groundwater to the SAB were calculated as the product of total SGD water flux (5.6×10^{8} m^{3} d^{-1}) and the average SGD excess DIC concentrations. Since a large proportion of the SGD discharge is from recycled seawater, excess DIC (DIC in excess of marine sources, Jiang et al. 2008b) instead of DIC of the SGD was used to exclude the DIC originally derived from seawater and travelled back to the shelf via SGD. Average excess DIC concentrations from wells around the Oaktree River, South Carolina in July 2003 (840±700 μmol L^{-1}, W.-J. Cai, unpublished data) were used for the calculation.

DIC flux from groundwater to the shelf is estimated to be $2.1(\pm1.7)\times10^{12}$ gC yr^{-1} (Table 5.2). Since this estimate is based on groundwater samplings around Oaktree River, South Carolina in July 2003 only, there is expected to be a large uncertainty in the value. However, if the DIC flux from groundwater is representative, it is one of the most important pathways to transport DIC from land to the continental shelf. Adding DIC inputs from rivers (0.44×10^{12} gC yr^{-1}), salt marshes (0.71×10^{12} gC yr^{-1}, Wang and Cai, 2004), and air-sea gas exchange (0.52×10^{12} gC yr^{-1}, Jiang et al., 2008a), the total DIC inputs from abiotic processes in the SAB are estimated to be $3.8(\pm1.8)\times10^{12}$ gC yr^{-1}, which is slightly larger than the average DIC export from the SAB shelf to the open ocean [$2.9(\pm1.7)\times10^{12}$ gC yr^{-1}] estimated in this study (Table 5.2).

5. Conclusions

Through surveys of vertical distributions of DIC, DO, TA, pH, nutrients, δ^{13}C-DIC, Δ^{14}C-DIC, δD-H_2O, and δ^{18}O-H_2O; processes controlling DIC in the South Atlantic Bight are discussed. DIC in the SAB is mainly controlled landside by terrestrial inputs and dilution, and seaside by biological activity. Terrestrial sources lower DIC on the shelf by means of dilution, while concomitantly input DIC to the shelf. Interaction of Gulf Stream and AAIW brings nutrients to the shelf, and causes phytoplankton blooms to occur. This process could lower DIC on the middle and outer shelf substantially during summer. Calculation shows that the SAB exported DIC to the open ocean at a rate of $2.9(\pm1.7)\times10^{12}$ gC yr^{-1}. This study suggests that both DIC export to the open ocean and biological activity on the shelf could play important roles in contributing to the continental shelf pump in the SAB.

Table 5.1. $\Delta^{14}C$ of DIC (‰) on B-, C-, and D-transects of the SAB during March, July, and October 2005.

Mar 2005			**Jul 2005**			**Oct 2005**		
Station	Depth (m)	$\Delta^{14}C$ (‰)	Station	Depth (m)	$\Delta^{14}C$ (‰)	Station	Depth (m)	$\Delta^{14}C$ (‰)
B01	2	54	C01	2	56	B01	2	74
B01	15	54	C01	2	55	B01	14	56
B07	2	64	C05	2	67	B01	14	55
B07	2	66	C09	2	85	B07	1	67
B07	38	70	C09	2	74	B07	36	70
C01	2	60	C09	34	76	C01	2	67
C01	2	57	C09	34	80	C01	2	61
C05	2	56	C15	1	86	C05	2	64
C05	19	60	C15	1	79	C09	1	69
C09	2	64	C15	50	70	C09	1	70
C09	2	73	C15	50	79	C09	27	73
C09	25	68	C15	151	21	C09	27	66
C14	2	85	C15	151	32	C13	6	83
C14	2	48	C15	300	-47	C13	43	66
C14	50	66	C15	300	-40	C15	2	66
C14	50	94	C15	454	-66	C15	2	70
C14	150	78	C16	2	64	C15	51	70
C14	150	63	C16	52	58	C15	51	68
C14	249	63	C16	150	87	C16	2	70
C14	249	73	C16	301	82	C16	51	73
C15	2	70	C16	497	-33	D02	1	65
C15	51	69	C16	761	-74	D02	8	54
C15	150	74				D07	2	68
C15	459	-52				D07	39	67
C16	2	67				D07	39	68
C16	50	69						
C16	150	81						
C16	500	22						
C16	765	-58						
D02	2	62						
D02	9	62						
D02	9	59						
D07	2	68						
D07	31	70						

Table 5.2. Inorganic carbon fluxes in the SAB (Units: 10^{12} gC yr^{-1}).

Processes	**Carbon fluxes**	**Reference**
DIC inputs from rivers	0.44	This study
DIC inputs from salt marshes	0.71	Wang and Cai (2004)
DIC inputs from SGD	2.1 ±1.7	This study
Air-sea CO_2 exchange	0.52±0.23	Jiang et al. (2008a)
Sum of all abiotic sources	3.8±1.8[a]	—
DIC export to the open ocean	-4.0±1.5[b]	This study (Method I)
DIC export to the open ocean	-1.8±0.8	This study (Method II)
DIC export to the open ocean	-2.9±1.7	Average of Method I and II

[a] The errors of DIC inputs from rivers and salt marshes are unknown and assumed to be zero during the calculation. As a result the real standard deviation should be larger.

[b] Assuming a residence time of 3 months in the SAB, as found to be representative by Atkinson et al. (1978).

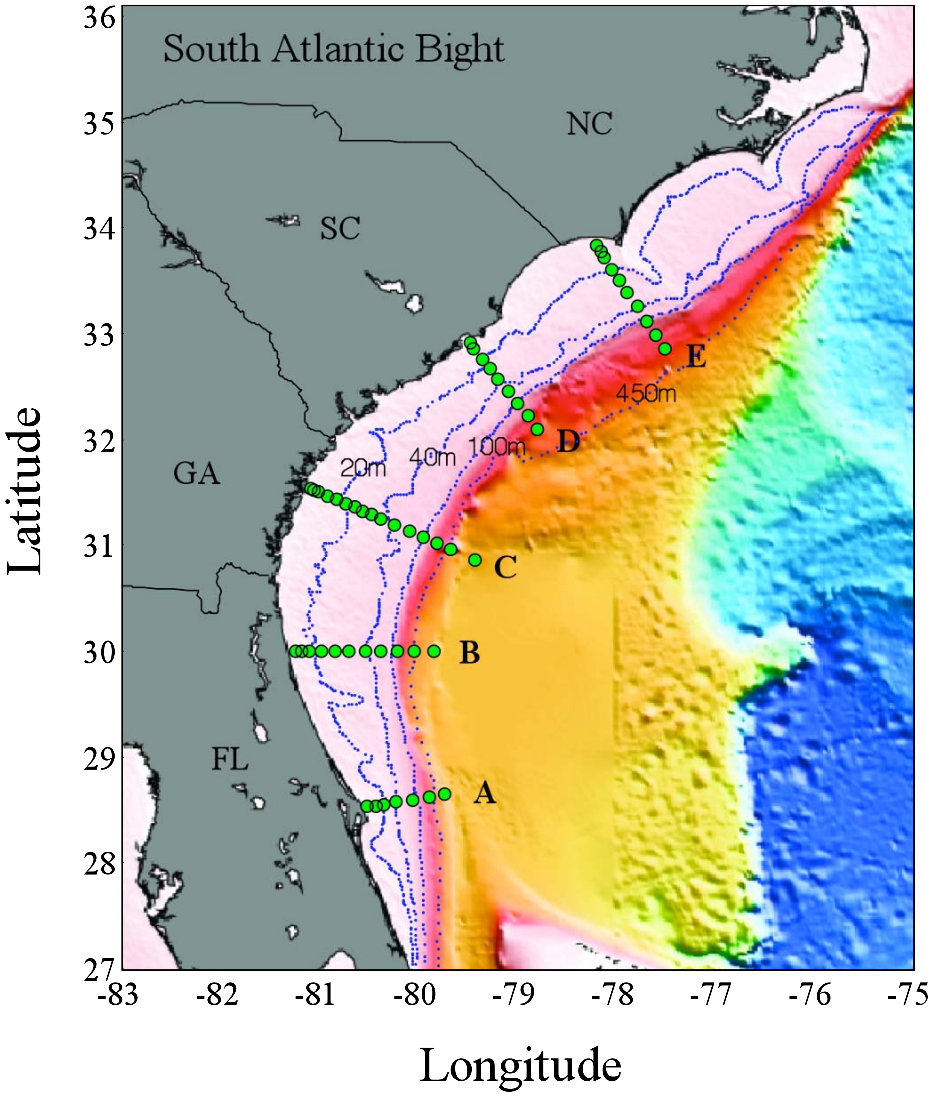

Figure 5.1. Sampling locations in the United States South Atlantic Bight. Green circles are the sampling stations, which originate inshore and extend beyond the shelf break. Blue dotted lines on the continental shelf are 20, 40, 100, and 450m isobaths.

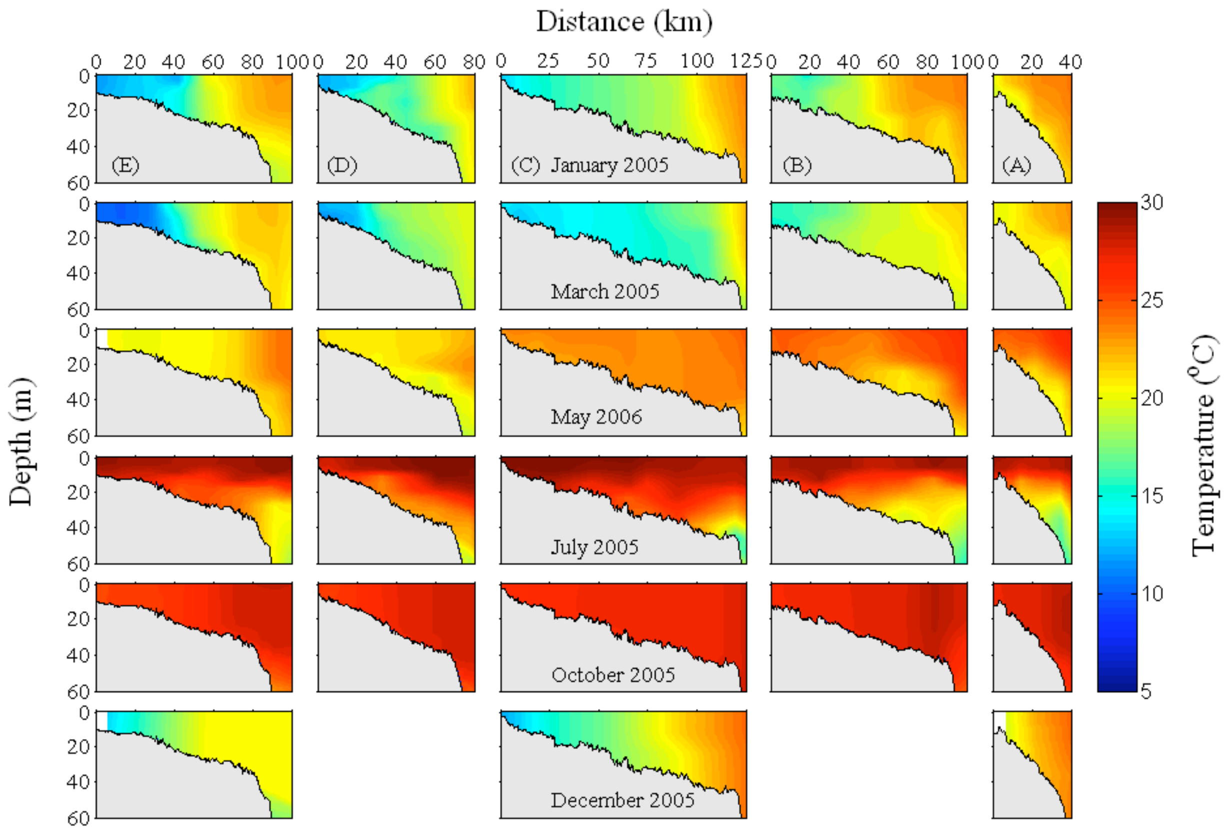

Figure 5.2. Vertical temperature distributions on the five onshore-offshore transects (E-, D-, C-, B-, and A-transects from left to right). D- and B-transects were not surveyed during the December 2005 cruise.

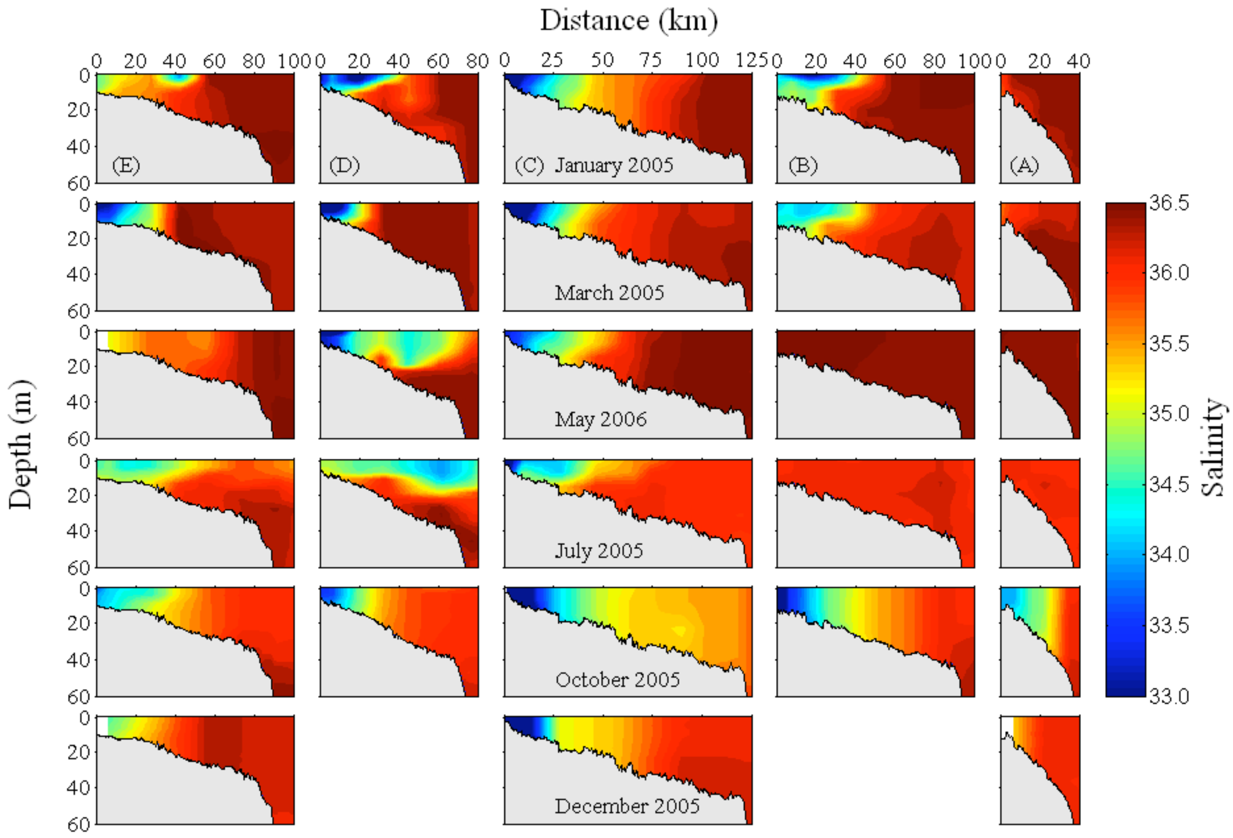

Figure 5.3. Vertical distributions of seawater salinity on the five onshore-offshore transects (E-, D-, C-, B-, and A-transects from left to right). D- and B-transects were not surveyed during the December 2005 cruise.

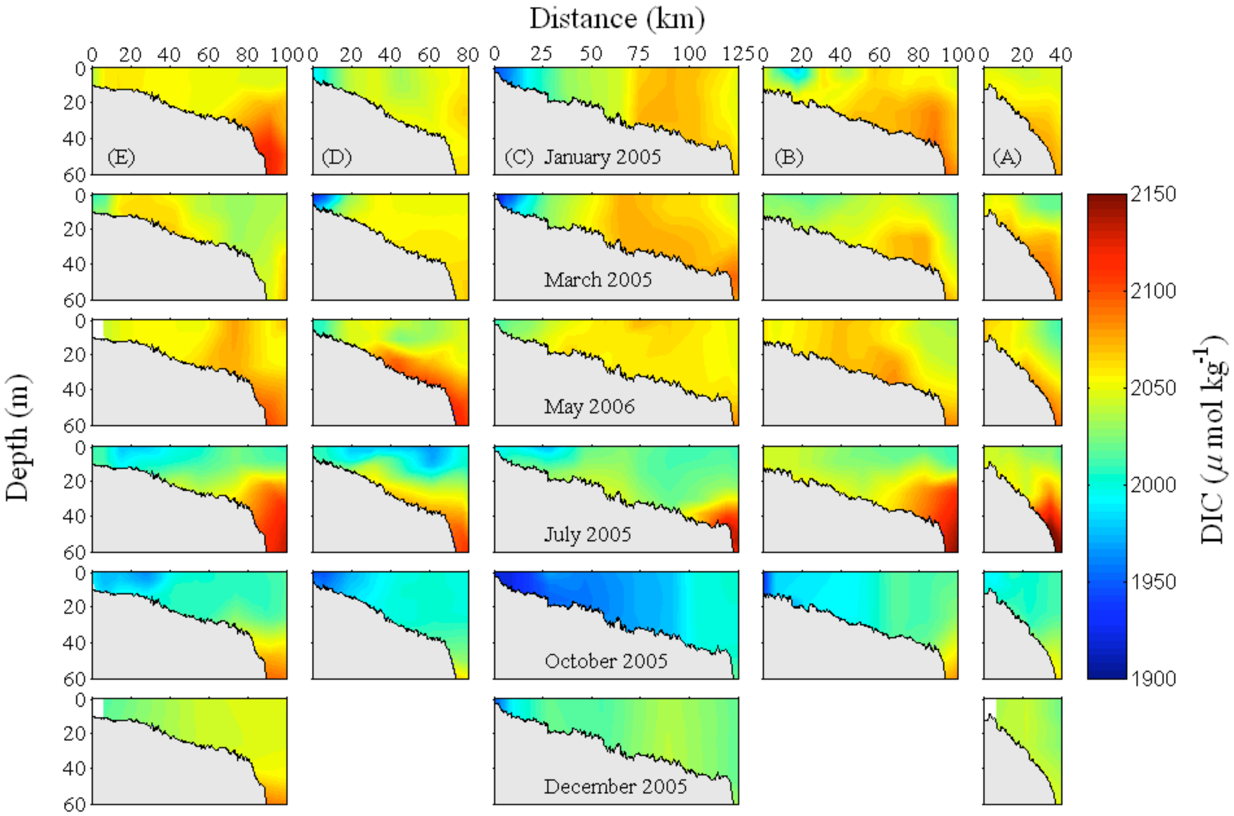

Figure 5.4. Vertical distributions of dissolved inorganic carbon (DIC) concentration on the five onshore-offshore transects (E-, D-, C-, B-, and A-transects from left to right). D- and B-transects were not surveyed during the December 2005 cruise.

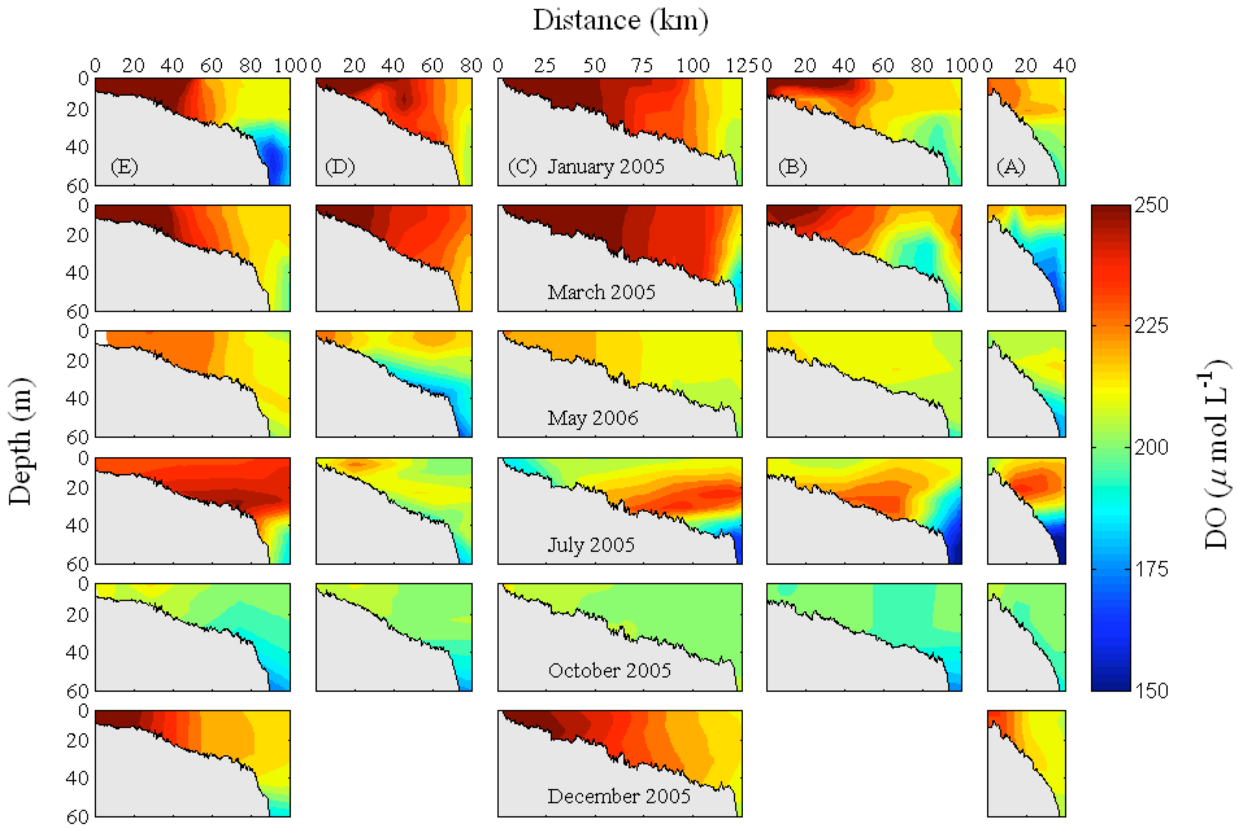

Figure 5.5. Vertical distributions of seawater dissolved oxygen (DO) concentration on the five onshore-offshore transects (E-, D-, C-, B-, and A-transects from left to right). D- and B-transects were not surveyed during the December 2005 cruise.

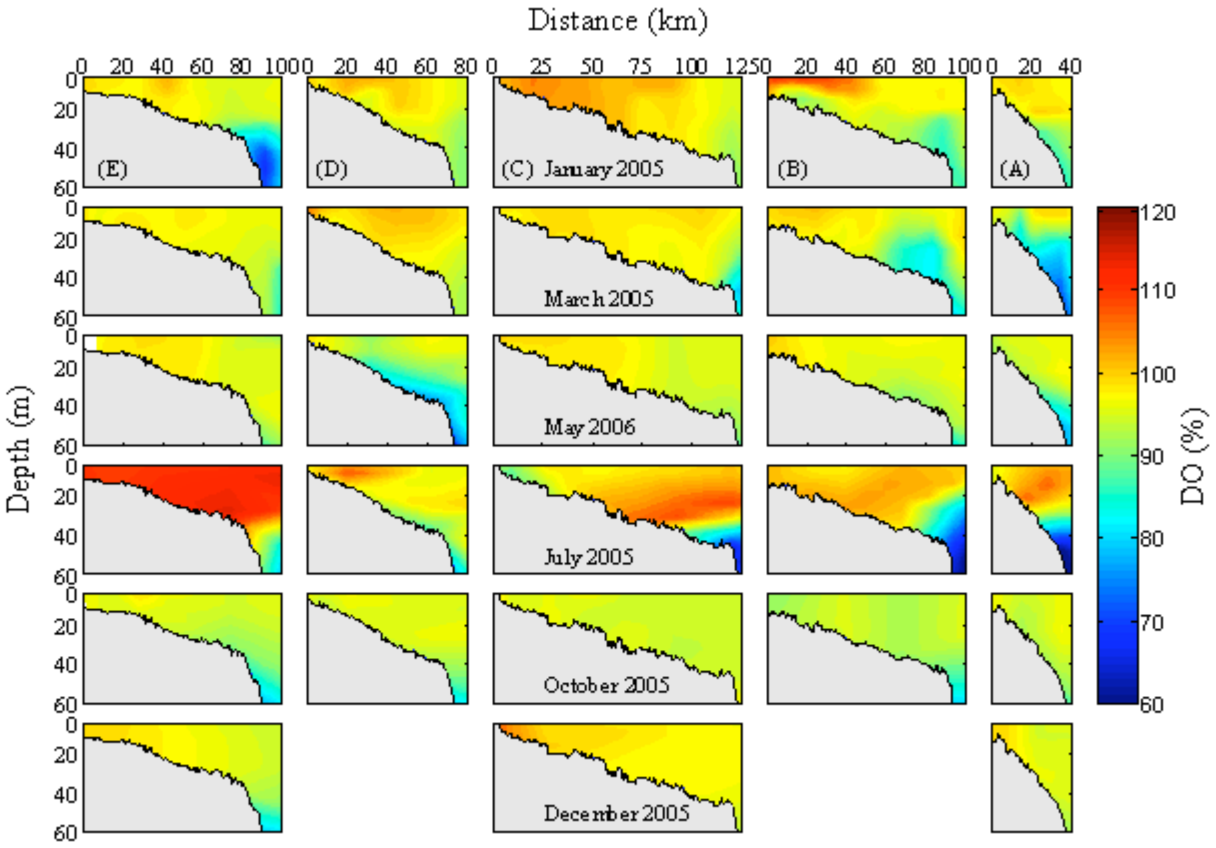

Figure 5.6. Vertical distributions of dissolved oxygen (DO) saturation rate on the 5 onshore-offshore transects (E-, D-, C-, B-, and A-transect from left to right) in the SAB. D- and B-transects were not surveyed during the December 2005 cruise.

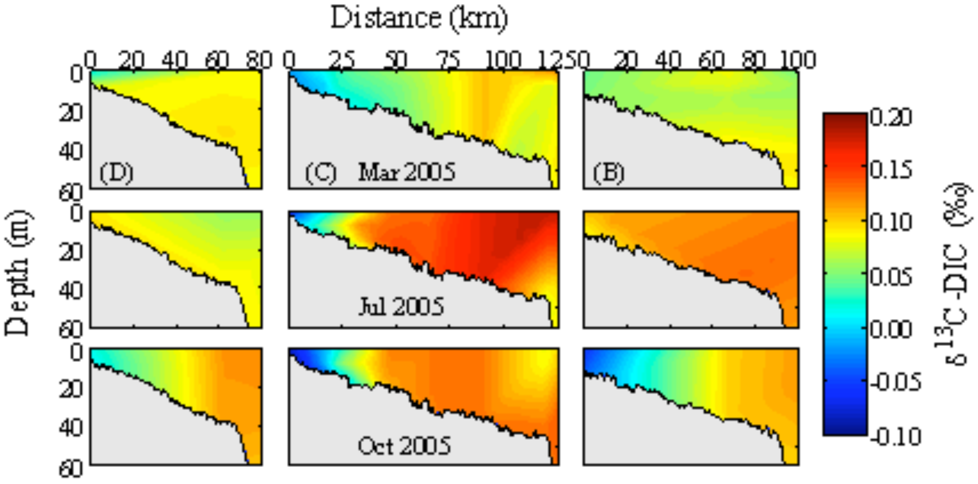

Figure 5.7. Vertical distributions of δ^{13}C-DIC on D-, C-, and B-transects in March, July, and October 2005.

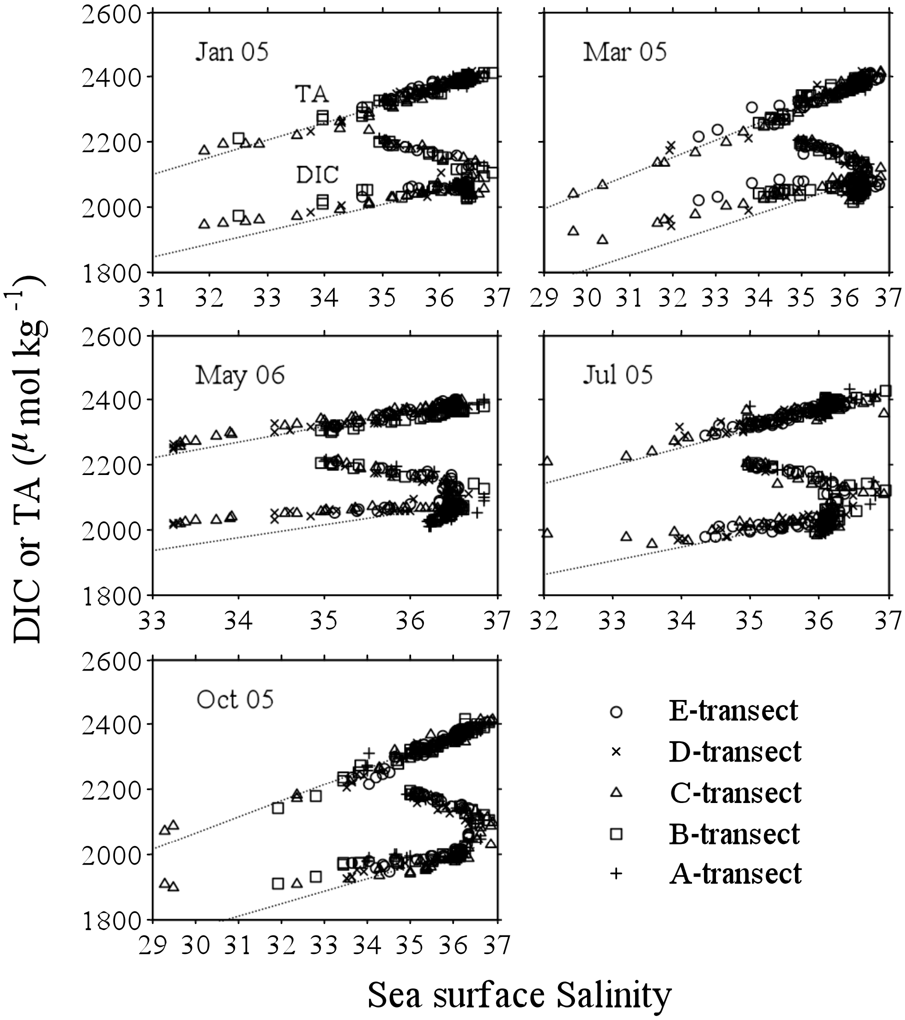

Figure 5.8. Plots of dissolved inorganic carbon (DIC) and total alkalinity (TA) vs. salinity in the SAB. Each panel shows the data from one sampling month. The dotted lines are the conservative mixing line estimated using the river and ocean end members.

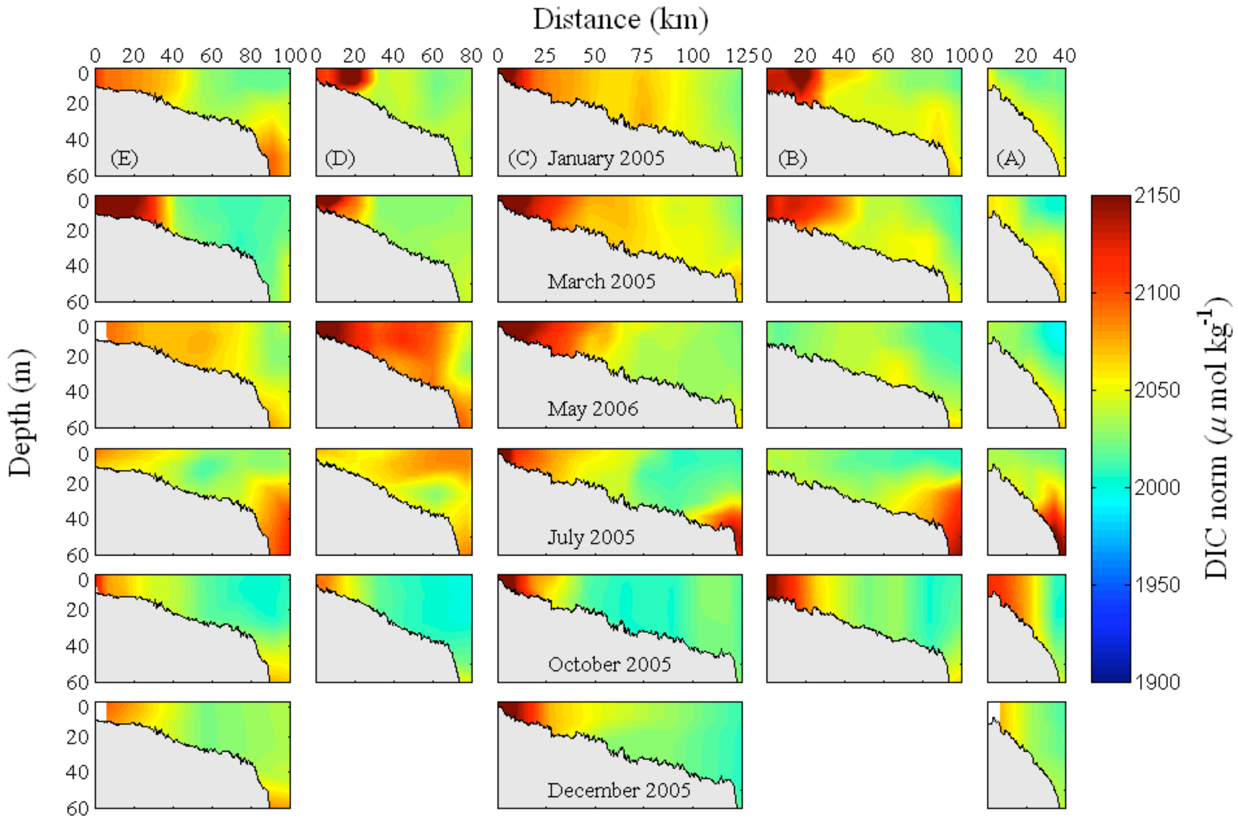

Figure 5.9. Vertical distributions of salinity-normalized DIC on the five onshore-offshore transects (E-, D-, C-, B-, and A-transects from left to right). D- and B-transects were not surveyed during the December 2005 cruise.

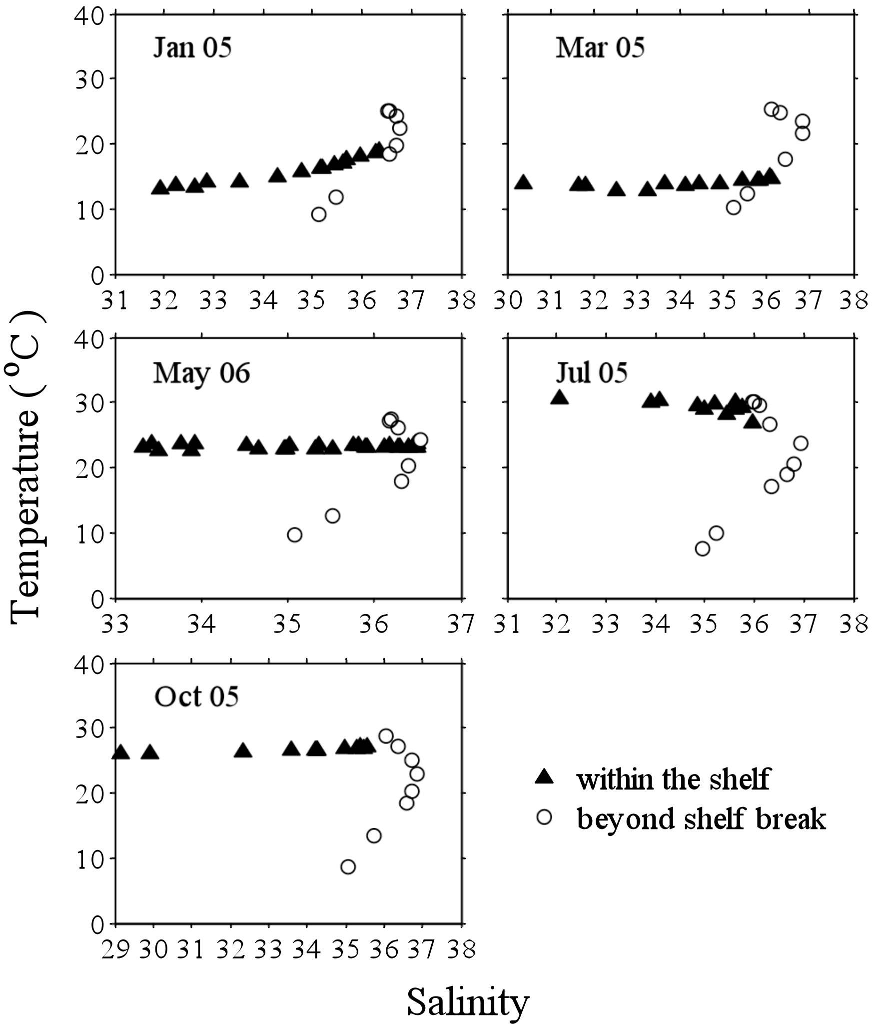

Figure 5.10. Temperature vs. salinity plots on C-transect of the SAB. Filled triangles are data from the shelf, and open circles are data from beyond the shelf break.

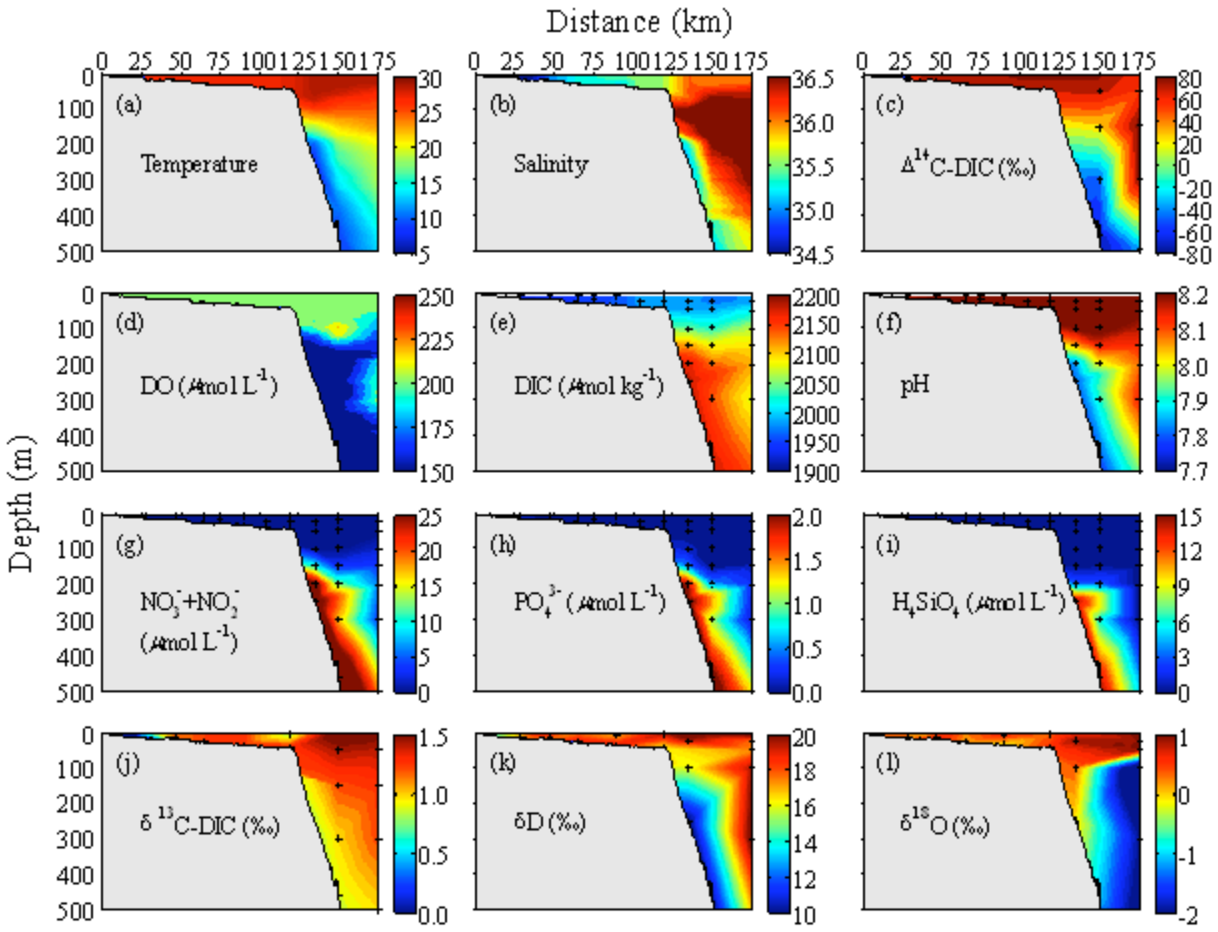

Figure 5.11. Vertical distributions of temperature, salinity, Δ^{14}C-DIC, DO, DIC, pH, NO_3^- +NO_2^-, PO_4^{3-}, H_4SiO_4, δ^{13}C-DIC, δD-H_2O, and δ^{18}O-H_2O on C-transect during October 2005. Pluses show the sampling depths, panels without pluses are from CTD data.

CHAPTER 6

CONCLUSIONS

Part I (CO_2 in estuaries):

During all sampling months, the three estuaries (Sapelo and Doboy are two marine-dominated estuaries and Altimaha is a river-dominated estuaries) were supersaturated in CO_2 (390 - 3380 μatm) with respect to the atmosphere due to CO_2 inputs from the estuarine zone (mainly intertidal marshes) and the river. Some shared characteristics of the CO_2 in the three estuaries include: surface water pCO$_2$ was lowest at the ocean end and increased towards the innermost area of the estuaries; and, surface water pCO$_2$ at low tide was always higher than at high tide for any given point, although the difference is barely noticeable for a given salinity value.

Overall, surface water pCO$_2$ in the river-dominated estuary was much higher than that in the two marine-dominated estuaries. The calculated annual air-water CO_2 flux in Altamaha Sound (69.3 mmol m^{-2} d^{-1}) was 2.4 times that of Sapelo and Doboy Sounds (28.7-29.4 mmol m^{-2} d^{-1}). This study suggests that CO_2 inputs from the river are likely to be responsible for the extra higher CO_2 degassing in the river-dominated estuary relative to the two marine-dominated estuaries. River water entering estuaries is usually supersaturated with CO_2. Sources of CO_2 in the river include microbial decomposition of organic matter in soils, river waters, and sediments. High concentrations of humic substances also contribute to the high pCO$_2$ in river water by increasing acidity of source waters.

Higher CO_2 degassing in estuaries that are more influenced by freshwater was also found in other regions of the world, e.g. the three estuaries in the Cantabrian Sea (north of Spain), and the estuaries in Kaneohe Bay, Oahu, Hawaii. If the conclusions from the present study can be applied globally, one implication is that the current estimates of global air-water CO_2 fluxes from estuaries could be overestimated. The global air-water CO_2 fluxes in estuaries based on the synthesis of Borges (2005) and Borges et al. (2005) is about +0.40 Pg C yr^{-1}. There might be problems associated with these pioneering global estimates. First, the air-water CO_2 fluxes used for the synthesis were mainly from river-dominated estuaries (of small and intermediate sized rivers) (Borges 2005; Borges et al. 2005). Second, the surface area of global estuaries used included both river- and marine-dominated estuaries (Woodwell et al. 1973). Since air-water CO_2 fluxes in marine-dominated estuaries could be considerably lower than those in river-dominated estuaries, the estimates of global CO_2 fluxes from estuaries by Borges (2005) and Borges et al. (2005) might be an overestimation.

Globally, estuaries are far more complicated than being simply classified as either river- or marine-dominated estuaries. Abril and Borges (2004) and Borges (2005) also demonstrated large CO_2 differences between macro-tidal and micro-tidal estuaries. In addition, there are estuaries that are dominated by large rivers, such as those of the Amazon River (Cooley et al. 2007), Mississippi River (Cai 2003; W.-J. Cai unpublished data, 2008), and Yangtze River (Zhai et al. 2007), where the estuaries are usually weaker CO_2 sources compared to most small and intermediate river-dominated estuaries that have been studied. There are also large estuarine systems such as Chesapeake Bay, Long Island Sound, Pamlico Sound and Puget Sound whose surface area covers a large proportion of the total surface area of global estuaries but have generally been under-studied in terms of CO_2. More work is clearly needed to better constrain the global air-water CO_2 fluxes from estuaries.

Part II (CO_2 on the continental shelf):

Intense sea surface $p$$CO_2$ surveys allow us to create the first maps of the sea surface $p$$CO_2$ over the SAB for all seasons. Contrary to the earlier studies that were based on limited spatial and seasonal coverage, this study shows that the SAB is a net sink of atmospheric CO_2 on an annual and whole shelf basis (-0.48 ± 0.21 mol m^{-2} yr^{-1}). The CO_2 sink in the SAB is smaller than the Middle Atlantic Bight (-1.33 mol m^{-2} yr^{-1}, using an atmospheric xCO_2 of 365 ppm, DeGrandpre et al. 2002), the North Sea (-1.38 mol m^{-2} yr^{-1}, Thomas et al. 2004b), and the East China Sea (-2.92 mol m^{-2} yr^{-1}, Tsunogai et al. 1999). The inner shelf of the SAB is a source of +1.20±0.24 mol m^{-2} yr^{-1}, while the middle and outer shelves are sinks of -1.23±0.19 and -1.37±0.21 mol m^{-2} yr^{-1}, respectively. Seasonally, the SAB shifts from a sink for atmospheric CO_2 in winter to a source in summer. The annual cycle of sea surface temperature plays a dominant role in controlling the seasonal variations of $p$$CO_2$. Wind speeds are highest when the shelf is taking up atmospheric CO_2, and lowest when the shelf is releasing CO_2 to the atmosphere. This seasonal anti-correlated of wind speeds with the direction of air-sea gas exchange is an important factor in contributing to the atmospheric CO_2 sink in the SAB.

Examination of mechanisms controlling sea surface $p$$CO_2$ suggests that temperature played a key role in the seasonal variation of $p$$CO_2$ over the entire SAB. $p$$CO_2$ was lowest in winter and highest in summer on all parts (inner, middle, and outer shelf) of the SAB. The magnitude of ΔpCO_2(temp) on the inner shelf was larger than that on the middle and outer shelf partially due to the greater seasonal span of SST on the inner shelf (10-30 ^{o}C) compared to that on the middle and outer shelf (20-30 ^{o}C) (Jiang et al. 2008a).

Air-sea gas exchange helped to modulate pCO_2 on the inner shelf due to the shallow water depth. It raised pCO_2 in winter when sea surface pCO_2 was under-saturated and lowered it in summer when pCO_2 was supersaturated. However, although air-sea gas exchange played an important role in controlling pCO_2 of the inner shelf, greater water depths and the consequently greater mixed layer DIC inventory on the middle and outer shelf make air-sea gas exchange insignificant in changing the pCO_2 there (Figure 4.7).

In addition to temperature and air-sea gas exchange, CO_2 shoreward of the Coastal Frontal Zone (a dynamic barrier along the shelf at about 10-30 km offshore) is controlled by terrestrial inputs of inorganic and organic carbon from rivers and salt marshes, as well as net heterotrophy on the inner shelf. Rivers discharging to the SAB enhance pCO_2 on the shelf by delivering water with high CO_2 concentrations that is the result of microbial decomposition of organic matter in soils, river waters, and sediments (Jones and Mulholland 1998; Neal et al. 1998; Cole and Caraco 2001). Salt marshes contribute to pCO_2 in the SAB by direct release of CO_2 from marsh to the continental shelf. Rivers and salt marshes also transport significant amounts of reactive organic carbon to the SAB (Moran et al. 1991; Moran and Hodson 1994; Alberts and Takács 1999; DeAlteris 2007), the remineralization of which by microbes (Pomeroy et al. 2000; Jahnke et al. 2005) and photochemistry (Miller and Moran 1997) in shelf waters and sediments will further increase the nearshore pCO_2.

In contrast, CO_2 seaward of the Coastal Frontal Zone is mainly controlled by primary production that is itself strongly dependent on Gulf Stream-induced nutrient intrusions. Shelf break intrusions occur on weekly intervals throughout the SAB (Menzel 1993). As a result, blooms may occur at any time of the year. However, these blooms are usually confined to the shelf break by a density front, and if the upwelled water is resident on the shelf for only a short time, some of the upwelled nutrients may be exported back to the ocean unutilized (Lee et al. 1981; Atkinson et al. 1984). From May to October, when SAB shelf water is warm and water density is low, the intruded water may penetrate all the way to the middle and even the inner shelf in the form of subsurface intrusions, particularly under upwelling favorable winds (Atkinson et al. 1984). The presence of nutrients from subsurface intrusions, together with the shallow water depth of the SAB (the euphotic zone extends all the way to the seafloor) and long residence time of the subsurface intrusions (>~10 days), could therefore bring about strong subsurface blooms (Yoder et al. 1983; Yoder 1985), which will lower the $p\mathrm{CO}_2$ on the shelf at this time of the year (July and October 2005).

The study of DIC cycling in the SAB suggests that DIC in this region is mainly controlled by inputs from terrestrial sources, as well as freshwater dilution on the landside, and biological activity on the middle and outer shelves. While diluting DIC on the shelf by input of freshwater, terrestrial sources concomitantly delivered DIC to the SAB. This study shows from a DIC point of view how interaction of the Gulf Stream and the Antarctic Intermediate Water (AAIW) help bring nutrients to the shelf and enhance biological activity, which plays an important role in lowering DIC on the middle and outer shelves during summer.

DIC flux from groundwater to the shelf is estimated to be $2.1(\pm 1.7)\times 10^{12}$ gC yr^{-1}. If the DIC flux from groundwater is representative, it is one of the most important pathways to transport DIC from land to the continental shelf. Adding DIC inputs from rivers (0.44×10^{12} gC yr^{-1}), salt marshes (0.71×10^{12} gC yr^{-1}, Wang and Cai, 2004), and air-sea gas exchange (0.52×10^{12} gC yr^{-1}, Jiang et al., 2008a), the total DIC inputs from abiotic processes in the SAB are estimated to be

3.8(±1.8)$\times10^{12}$ gC yr^{-1}, which is slightly larger than the average DIC export from the SAB shelf to the open ocean [2.9(±1.7)$\times10^{12}$ gC yr^{-1}] estimated in this study.

One of the largest problems of this dissertation has been the lack of groundwater sampling. All the calculations were based on data from stations around Oaktree River, South Carolina in July 2003 only. Therefore, there are large uncertainties in the derived values. Further study of the groundwater is needed in order to verify the conclusions related to groundwater. Another problem is related to the estimation of air-sea CO_2 flux on the inner shelf of the SAB. Due to the limited spatial coverage but large spatial variation, large uncertainties are expected from the spatial interpolation of surface water pCO_2 on the inner shelf.

REFERENCES

Abril, G., and A. V. Borges (2004), Carbon dioxide and methane emissions from estuaries, in *Greenhouse gases emissions from natural environments and hydroelectric reservoirs: fluxes and processes*, edited by A. Tremblay, et al., pp. 187-207, Springer, New York, New York.

Abril, G., H. Etcheber, A. V. Borges, and M. Frankignoulle (2000), Excess atmospheric carbon dioxide transported by rivers into the Scheldt estuary, *Earth Planet. Sci., 330*, 761-768.

Alberts, J. J., and M. Takács (1999), Importance of humic substances for carbon and nitrogen transport into southeastern United States estuaries, *Organic Geochem., 30*, 385-395.

Alexander, C. E., et al. (1986), *An Inventory of Coastal Wetlands of the USA*, NOAA, U.S. Department of Commerce, Washington, DC.

Atkinson, L. P. (1983), Distribution of Antarctic Intermediate Water over the Blake Plateau, *J. Geophys. Res., 88*, 4699-4704.

Atkinson, L. P., J. A. Yoder, and T. N. Lee (1984), Review of upwelling off the southeastern United States and its effect on continental-shelf nutrient concentrations and primary productivity, *Rapp. P.-v. Cons. Int. Explor. Mer, 183*, 70-78.

Atkinson, L. P., J. O. Blanton, and E. Haines (1978), Shelf flushing rates based on the distribution of salinity and freshwater in the Georgia Bight, *Est. Coast. Shelf Sci., 7*, 465-472.

Atkinson, L. P., P. G. O'Malley, J. A. Yoder, and G.-A. Paffenhöffer (1984), The effect of summertime shelf break upwelling on nutrient flux in southestern United States continental shelf waters, *J. Mar. Res., 42*, 969-993.

Bane, J. M., and J. K. Dewar (1988), Gulf Stream bimodality and variability downstream of the Charleston Bump, *J. Geophys. Res., 93*, 6695-6710.

Barnard, A. H., P. M. Stegmann, and J. A. Yoder (1997), Seasonal surface ocean variability in the South Atlantic Bight derived from CZCS and AVHRR imagery, *Cont. Shelf Res.*, *17*(10), 1181-1206.

Blanton, J. O. (1981), Ocean currents along a nearshore frontal zone on the continental shelf of the southeastern United States, *J. Phys. Oceanogr., 11*, 1627-1637.

Blanton, J. O., and L. P. Atkinson (1983), Transport and fate of river discharge on the continental shelf of the southeastern United States, *J. Geophys. Res., 88*, 4730-4738.

Boehme, S. E., C. L. Sabine, and C. E. Reimers (1998), CO_2 fluxes from a coastal transect: a time-series approach, *Mar. Chem., 63*, 49-67.

Borges, A. V. (2005), Do we have enough pieces of the jigsaw to integrate CO_2 fluxes in the coastal ocean? *Estuaries, 28*(1), 3-27.

Borges, A. V., and M. Frankignoulle (2002), Distribution of surface carbon dioxide and air-sea exchange in the upwelling system off the Galician coast, *Global Biogeochem. Cycles, 16*(2), 1020, doi:10.1029/2000GB001385.

Borges, A. V., B. Delille, and M. Frankignoulle (2005), Budgeting sinks and sources of CO_2 in the coastal ocean: Diversity of ecosystems counts, *Geophys. Res. Lett., 32*, L14601, doi:10.1029/2005GL023053.

Borges, A. V., B. Delille, L. S. Schiettecatte, F. Gazeau, G. Abril, and M. Frankignoulle (2004a), Gas transfer velocities of CO_2 in three European estuaries (Randers Fjord, Scheldt and Thames), *Limnol. Oceanogr., 49*(5), 1630-1641.

Borges, A. V., J.-P. Vanderborght, L.-S. Schiettecatte, F. Gazeau, S. Ferrón-Smith, B. Delille, and M. Frankignoulle (2004b), Variability of the gas transfer velocity of CO_2 in a macrotidal estuary (the Scheldt), *Estuaries, 27*(4), 593-603.

Borges, A. V., L.-S. Schiettecatte, G. Abril, B. Delille, and F. Gazeau (2006), Carbon dioxide in European coastal waters, *Est. Coast. Shelf Sci., 70*, 375-387.

Borges, A. V., S. Djenidi, G. Lacrois, J.-M. Théate, B. Delille, and M. Frankignoulle (2003), Atmospheric CO_2 flux from mangrove surrounding waters, *Geophysical Research Letters*, *30*(11), 1558, doi: 10.1029/2003GL017143.

Bozec, Y., H. Thomas, K. Elkalay, and H. J. W. de Baar (2005), The continental shelf pump for CO_2 in the North Sea—evidence from summer observation, *Mar. Chem., 93*, 131-147.

Cai, W.-J. (2003), Riverine inorganic carbon flux and rate of biological uptake in the Mississippi River plume, *Geophys. Res. Lett., 30*, 1032, doi:10.1029/2002GL016312.

Cai, W.-J., and M. Dai (2004), Comment on "enhanced open ocean storage of CO_2 from shelf sea pumping", *Science, 306*, 1477c.

Cai, W.-J., and Y. Wang (1998), The chemistry, fluxes, and sources of carbon dioxide in the estuarine waters of the Satilla and Altamaha Rivers, Georgia, *Limnol. Oceanogr., 43*(4), 657-668.

Cai, W.-J., L. R. Pomeroy, M. A. Moran, and Y. Wang (1999), Oxygen and carbon dioxide mass balance for the estuarine-intertidal marshe complex of five rivers in the southeastern U.S., *Limnol. Oceanogr., 44*(3), 639-649.

Cai, W.-J., M. Dai, and Y. Wang (2006), Air-sea exchange of carbon dioxide in ocean margins: A province-based synthesis, *Geophys. Res. Lett., 33*, L12603, doi:10.1029/2006GL026219.

Cai, W.-J., Z. A. Wang, and Y. Wang (2003), The role of marsh-dominated heterotrophic continental margins in transport of CO_2 between the atmosphere, the land-sea interface and the ocean, *Geophys. Res. Lett., 30*, doi:10.1029/2003GL017633.

Cameron, W. M., and D. W. Pritchard (1963), Estuaries, in *The Sea*, edited by M. N. Hill, pp. 306-324, Volume 2. John Wiley & Sons, New York.

Carini, S., N. Wetson, C. S. Hopkins, J. Tucker, A. Giblin, and J. Vallino (1996), Gas exchange in the Parker Estuary, Massachusetts, *Biol. Bull., 191*, 333-334.

Chen, C. T. A., K.-K. Liu, and R. Macdonald (2003), Continental margin exchanges, in *Ocean Biogeochemistry: the Role of the Ocean Carbon Cycle in Global Change*, edited by M. J. R. Fasham, pp. 53-98, Springer, New York.

Chen, C.-T. A., and A. V. Borges (2009), Reconciling opposing views on carbon cycling in the coastal ocean: Continental shelves as sinks and near-shore ecosystems as sources of atmospheric CO_2, *Deep-Sea Res. II*, doi:10.1016/j.dsr2.2009.01.001.

Clark, J. F., R. Wanninkhof, P. Schlosser, and H. J. Simpson (1994), Gas exchange rates in the tidal Hudson river using a dual tracer technique, *Tellus, 46B*, 274-285.

Cole, J. J., and N. F. Caraco (2001), Carbon in catchments: connecting terrestrial carbon losses with aquatic metabolism, *Mar. Freshwater Res., 52,* 101-110.

Cooley, S. R., V. J. Coles, A. Subramaniam, and P. L. Yager (2007), Seasonal variations in the Amazon plume-related amtospheric carbon sink, *Global Biogeochem. Cycles, 21*, GB3014, doi:10.1029/2006GB002831.

Dai, T., and R. G. Wiegert (1996), Estimation of the primary productivity of Spartina alterniflora using a canopy model, *Ecography, 19*, 410-423.

de Hass, H., T. C. E. van Weering, and H. de Stigter (2002), Organic carbon in shelf seas: sinks or sources, processes and products, *Cont. Shelf Res., 22*, 691-717.

DeAlteris, J. A. (2007), Elemental and isotopic characterization of organic matter and carbon in the South Atlantic Bight, M.S. thesis, 196 pp, College of William & Mary, Williamsburg, Virginia, 18 April.

DeAlteris, J.A., J.E. Bauer and W.-J. Cai (in preparation), Sources and cycling of dissolved and particulate organic matter in a marsh-dominated ocean margin, *Global Biogeochemical Cycles*.

DeGrandpre, M. D., G. J. Olbu, C. M. Beatty, and T. R. Hammar (2002), Air-sea CO_2 fluxes on the US Middle Atlantic Bight, *Deep-Sea Res. II, 49,* 4355-4367.

Ducklow, H. W., and S. L. McCallister (2004), The biogeochemistry of carbon dioxide in the coastal oceans, in *The Sea, Volume 13. The global Coastal Ocean- Multi-scale Interdisciplinary Processes*, edited by A. R. Robinson and K. Brink, pp. 269-315, John wiley & Sons, New York.

Dunstan, W. M., and L. P. Atkinson (1976), Sources of new nitrogen for the South Atlantic Bight, in *Estuarine Processes, Volume I, Uses, Stresses, and Adaptation to the Estuary*, edited by M. Wiley, pp. 69-78, Academic Press, New York.

Elliott, M., and D. S. McLusky (2002), The need for definitions in understanding estuaries, *Est. Coast. Shelf Sci., 55*, 815-827.

Elsinger, R. J., and W. S. Moore (1983), Gas exchange in the Pee Dee River based on 222Rn evasion, *Geophys. Res. Lett., 10,* 443-446.

Fagan, K. E., and F. T. Mackenzie (2007), Air-sea CO_2 exchange in a subtropical estuarine-coral reef system, Kaneohe Bay, Oahu, Hawaii, *Mar. Chem., 106,* 174-191.

Feely, R. A., et al. (2004), Impact of anthropogenic CO_2 on the $CaCO_3$ system in the oceans, *Science*, *305,* 362-366.

Frankignoulle, M., and A. V. Borges (2001), European continental shelf as a significant sink for atmospheric carbon dioxide, *Global Biogeochem. Cycles, 15*, 569-576.

Frankignoulle, M., G. Abril, A. Borges, I. Bourge, C. Canon, B. Delille, E. Libert, and J.-M. Théate (1998), Carbon dioxide emission from European estuaries, *Science, 282*(5388), 434-436.

Frew, N. M. (1997), The role of organic films in air-sea gas exchange, in *Sea Surface and Global Change,* edited by P. Liss and R. Duce, pp. 121-172, Cambridge Univ. Press, New York.

Friederich, G. E., P. M. Walz, M. G. Burczynski, and F. P. Chavez (2002), Inorganic carbon in the central California upwelling system during the 1997-1999 El Niño-La Niña Event, *Prog. Oceanogr.*, *54*, 185-203.

García, H. E., and L. I. Gordon (1992), Oxygen solubility in seawater: Better fitting equations, *Limnol. Oceanogr.*, *37*(6), 1307-1312.

Gattuso, J.-P., M. Frankignoulle, and R. Wollast (1998), Carbon and carbonate metabolism in coastal aquatic ecosystems, *Annu. Rev. Ecol. Syst.*, *29*, 405-434.

Gran, G. (1952), Determination of the equivalence point in potentiometric titration, *Analyst, 77*, 661-671.

Griffith, P. C., D. J. Douglas, and S. C. Wainright (1990), Metabolic activity of size-fractionated microbial plankton in estuarine, nearshore, and continental shelf waters of Georgia, *Mar. Ecol. Prog. Ser., 59*, 263-270.

Guérin, F., G. Abril, D. Serça, C. Delon, S. Richard, R. Delmas, A. Tremblay, and L. Varfalvy (2007), Gas transfer velocities of CO_2 and CH_4 in a tropical reservoir and its river downstream, *J. Mar. Syst., 66*, 161-172.

Hales, B., T. Takahashi, and L. Bandstra (2005), Atmospheric CO_2 uptake by a coastal upwelling system, *Global Biogeochem. Cycles, 19*, GB1009, doi:10.1029/2004GB002295.

Hanson, R. B., C. Y. Robertson, J. A. Yoder, P. G. Verity, and S. S. Bishop (1990), Nitrogen recycling in coastal waters of southeastern U.S. during summer 1986, *J. Mar. Res., 48*, 641-660.

Hartman, B., and D. H. Hammond (1984), Gas exchange across the sediment-water and air-water interfaces in south San Francisco Bay, *J. Geophys. Res., 89*, 3593-3603.

Ho, D. T., C. S. Law, M. J. Smith, P. Schlosser, M. Harvey, and P. Hill (2006), Measurements of air-sea gas exchange at high wind speeds in the Southern Ocean: Implications for global parameterizations, *Geophys. Res. Lett., 33*, L16611, doi:10.1029/12006GL026817.

Hopkinson, C. S. (1985), Shallow-water benthic and pelagic metabolism: evidence of heterotrophy in the nearshore Georgia Bight, *Mar. Biol., 87*, 19-32.

Jahnke, R. A., C. R. Alexander, and J. E. Kostka (2003), Advective pore water input of nutrients to the Satilla River Estuary, Georgia, USA, *Est. Coast. Shelf Sci., 56*, 641-653.

Jahnke, R., M. Richards, J. Nelson, C. Robertson, A. Rao, and D. Jahnke (2005), Organic matter remineralizaiton and porewater exchange rates in permeable South Atlantic Bight continental shelf sediments, *Cont. Shelf Res., 25*, 1433-1452.

Jiang, L.-Q., W.-J. Cai, R. Wanninkhof, Y. Wang, and H. Lüger (2008a), Air-sea CO_2 fluxes on the U.S. South Atlantic Bight: spatial and seasonal variability, *J. Geophys. Res., 113*, C07019, doi:10.1029/2007JC004366.

Jiang, L.-Q., W.-J. Cai, and Y. Wang (2008b), A comparative study of carbon dioxide degassing in river- and marine-dominated estuaries, *Limnol. Oceanogr., 53*(6), 2603-2615.

Jiang, L.-Q., and W.-J. Cai (in review), Controlling mechanisms of carbon dioxide on the U.S. South Atlantic Bight, *J. Geophys. Res.*

Jiang, L.-Q., W.-J. Cai, Y. Wang, J. E. Bauer, L. Zhang, F. Chen, J. Hartmann, and X. Guo (in preparation), Processes controlling dissolved inorganic carbon on the Continental Shelf of Southeastern United States. .

Jones, J. B., and P. J. Mulholland (1998), Carbon dioxide variation in a hardwood forest stream: an integrative measure of whole catchment soil respiration, *Ecosystems*, *1*, 183-196.

Kremer, J. N., A. Peischauer, and C. D'Avanzo (2003), Estuary-specific variation in the air-water gas exchange coefficient for oxygen, *Estuaries, 26*(4A), 829-836.

Lee, T. N., J. A. Yoder, and L. P. Atkinson (1991), Gulf Stream frontal eddy influence on productivity of the southeast U.S. continental shelf, *J. Geophys. Res., 96*(C12), 22191-22205.

Lee, T. N., L. P. Atkinson, and R. Legeckis (1981), Observations of a Gulf Stream Frontal Eddy on the Georgia Continental Shelf, April 1977, *Deep-Sea Res. I*, *28*, 347-378.

Loder, T. C., and R. P. Reichard (1981), The dynamics of conservative mixing in estuaries, *Estuaries*, *4*(1), 64-69.

Mackenzie, F. T. (1991), What is the importance of ocean margin processes in Global Change? in *Ocean Margin Processes in Global Change*, edited by R. F. C. Mantoura et al., pp. 433-454, John Wiley and Sons, N.Y.

Marino, R., and R. W. Howarth (1993), Atmospheric oxygen exchange in the Hudson river: Dome measurements and comparison with other natural waters, *Estuaries, 16*, 433-445.

McClain, C. R., J. A. Yoder, L. P. Atkinson, J. O. Blanton, T. N. Lee, J. J. Singer, and F. Muller-Karger (1988), Variability of surface pigment concentrations in the South Atlantic Bight, *J. Geophys. Res.*, *93*(C9), 10675-10697.

McGillis, W. R., and R. Wanninkhof (2006), Aqueous CO_2 gradients for air-sea flux estimates, *Mar. Chem.*, *98*, 100-108.

McGillis, W. R., J. B. Edson, C. J. Zappa, J. D. Ware, S. P. McKenna, E. A. Terrary, J. E. Hare, C. W. Fairall, W. Drennan, M. Donelan, M. D. DeGrandpre, R. Wanninkhof, and R. A. Feely (2004), Air-sea CO_2 exchange in the equatorial Pacific, *J. Geophys. Res.*, *109*, C08S02, doi:10.1029/2003JC002256.

McGillis, W. R., J. B. Edson, J. D. Ware, J. W. H. Dacey, J. E. Hare, C. W. Fairall, and R. Wanninkhof (2001), Carbon dioxide flux techniques performed during GasEx-98, *Mar. Chem.*, *75*, 267-280.

Menzel, D. W. (1993), Ocean Processes: U. S. Southeast Continental Shelf, 112 pp., U.S. Department of Energy.

Middelburg, J. J., G. Klaver, J. Nieuwenhuize, A. Wielemaker, W. de Hass, T. Vlug, and F. W. A. van der Nat (1996), Organic matter mineralization in intertidal sediments along an estuarine gradient, *Mar. Ecol. Prog. Ser.*, *132*, 157-168.

Miller, W. L., and M. A. Moran (1997), Interaction of photochemical and microbial processes in the degradation of refractory dissolved organic matter from a coastal marine environment, *Limnol. Oceanogr.*, *42*(6), 1317-1324.

Millero, F. J., and A. Poisson (1981), International one-atmosphere equation of state for sea water, *Deep-Sea Res.*, *28*, 625-629.

Moore, W. S. (2007), Seasonal distribution and flux of radium isotopes on the Southeastern U.S. Continental Shelf, *J. Geophys. Res., 112*, C10013, doi:10.1029/2007JC004199.

Moran, M. A., and R. E. Hodson (1994), Dissolved humic substances of vascular plant origin in a coastal marine environment, *Limnol. Oceanogr., 39*(4), 762-771.

Moran, M. A., L. R. Pomeroy, E. S. Sheppard, L. P. Atkinson, and R. E. Hodson (1991), Distribution of terrestrial derived dissolved organic matter on the southeastern U.S. continental shelf, *Limnol. Oceanogr., 36*(6), 1134-1149.

National Ocean Service (1985), National Estuarine Inventory Data Atlas, Volume 1: Physical and Hydrologic Characteristics, U.S. Department of Commerce, National Oceanic and Atmospheric Administration, National Ocean Service.

Neal, C., W. A. House, H. P. Jarvie, and A. Eartherall (1998), The significance of dissolved carbon dioxide in major lowland rivers entering the North Sea, *Sci. Total Environ., 210/211*, 187-203.

Nelson, J. R., J. E. Eckman, C. Y. Robertson, R. L. Marinelli, and R. A. Jahnke (1999), Benthic microalgal biomass and irradiance at the sea floor on the continental shelf of the South Atlantic Bight: spatial and temperal variability and storm effects, *Cont. Shelf Res., 19*, 477-505.

Neubauer, S., and I. C. Anderson (2003), Transport of dissolved inorganic carbon from a tidal freshwater marsh to the York River estuary, *Limnol. Oceanogr., 48*(1), 299-307.

Nightingale, P. D., G. Malin, C. S. Law, A. J. Watson, P. S. Liss, M. I. Liddicoat, J. Boutin, and R. C. Upstill-Goddard (2000), In situ evaluation of air-sea gas exchange parameterizations using novel conservative and volatile tracers, *Global Biogeochem. Cycles, 14*, 373-387.

Ortega, T., R. P. J. Forja, and Gómez-Parra (2005), Fluxes of dissolved inorganic carbon in three estuarine systems of the Cantabrian Sea (north of Spain), *J. Mar. Syst.*, *53*, 125-142.

Pai, S.-C., G.-C. Gong, and K.-K. Liu (1993), Determination of dissolved oxygen in seawater by direct spectrophotometry of total iodine, *Mar. Chem.*, *41*, 343-351.

Perillo, G. M. E. (1995), Definitions and geomorphologic classifications of estuaries, in *Geomorphology and Sedimentology of Estuaries*, edited by G. M. E. Perillo, pp. 17-47, Elsevier, New York.

Pierrot, D., C. Neil, A. Olsen, K. Sullivan, R. Wanninkhof, and T. Johannson (2007), Recommendations for autonomous pCO_2 measuring systems and data reduction routines, *Deep-Sea Res.*, in preparation.

Pomeroy, L. R., and R. G. Wiegert (1981), The Ecology of a Salt Marsh, Springer-Verlag, New York.

Pomeroy, L. R., J. E. Sheldon, W. M. Sheldon, J. O. Blanton, J. Amft, and F. Peters (2000), Seasonal changes in microbial processes in estuarine and continental shelf waters of the south-eastern U. S. A., *Est. Coast. Shelf Sci.*, *51*, 415-428.

Prentice, I. C., G. D. Farquhar, M. J. R. Fasham, M. L. Goulden, M. Heimann, V. J. Jaramillo, H. S. Kheshgi, C. Le Quéré, R. J. Scholes, and D. W. R. Wallace (2001), The carbon cycle and atmospheric carbon dioxide, in *Climate Change 2001: The Scientific Basis*, edited by J. T. Houghton et al., pp. 183-237, Cambridge University Press.

Rabouille, C., F. T. Mackenzie, and L. M. Ver (2001), Influence of the human perturbation on carbon, nitrogen, and oxygen biogeochemical cycles in the global coastal ocean, *Geochim. Cosmochim. Acta*, *65*(21), 3615-3641.

Raymond, P. A., and J. J. Cole (2001), Gas exchange in rivers and estuaries: Choosing a gas transfer velocity, *Estuaries*, *24*, 312-317.

Raymond, P. A., J. E. Bauer, and J. J. Cole (2000), Atmospheric CO_2 evasion, dissolved inorganic carbon production, and net heterotrophy in the York River estuary, *Limnol. Oceanogr.*, *45*, 1707-1717.

Reimold, R. J. (1977), Mangals and salt marshes of eastern United States, in *Wet coastal ecosystems. Ecosystems of the World: Vol. 1.*, edited by V. J. Chapman, pp. 157-166, Elsevier, Amsterdam.

Revelle, R., and H. E. Suess (1957), Carbon dioxide exchange between atmosphere and ocean and the question of an increase of atmospheric CO_2 during the past decades, *Tellus*, *9*(1), 18-27.

Robertson, J. E., and A. J. Watson (1992), Thermal skin effect of the surface ocean and its implication for CO_2 uptake, *Nature*, *358*, 738-740.

Roques, P. F. (1985), Rate and stoichiometry of nutrient remineralization in an anoxic estuary, the Pettaquamscutt River., Ph.D. Dissertation thesis, Univ. of Rhode Island, Narragansett, Rhode Island.

Sabine, C. L., R. A. Feely, N. Gruber, R. M. Key, K. Lee, J. L. Bullister, R. Wanninkhof, C. S. Wong, D. W. R. Wallace, B. Tilbrook, F. J. Millero, T.-H. Peng, A. Kozyr, T. Ono, and A. F. Rios (2004), The oceanic sink for anthropogenic CO_2, *Science*, *305*, 367-371.

Sarmiento, J. L., and C. Le Quéré (1996), Oceanic carbon dioxide uptake in a model of century-scale global warming, *Science*, *274*, 13461350.

Shaw, T. J., W. S. Moore, J. Kloepfer, and M. A. Sochaski (1998), The flux of barium to the coastal waters of the southeastern United States: The importance of submarine groundwater discharge, *Geochim. Cosmochim. Acta, 62*, 3047-3052.

Shim, J., D. Kim, Y. C. Kang, J. H. Lee, S.-T. Jang, and C.-H. Kim (2007), Seasonal variations in pCO_2 and its controlling factors in surface seawater of the northern East China Sea, *Cont. Shelf Res.*, *27*, 2623-2636.

Signorini, S. R., and C. R. Mcclain. (2006), *Remote versus Local Forcing of Chlorophyll Variability in the South Atlantic Bight*, 34 pp., NASA/TM

Singer, J. J., L. P. Atkinson, J. O. Blanton, and J. A. Yoder. (1983), Cape Romain and the Charleston Bump: Historical and Recent Hydrographic Observations, *Journal of Geophysical Research, 88*(C8), 4685-4697.

Smith, S. V., and J. T. Hollibaugh (1993), Coastal metabolism and the oceanic organic carbon balance, *Rev. Geophys., 31*, 75-89.

Smith, S. V., and F. T. Mackenzie (1987), The ocean as a net heterotrophic system: Implications from the carbon biogeochemical cycle, *Global Biogeoch. Cycles*, *1*, 187-198.

Sverdrup HV (1953) On conditions for the vernal blooming of plankton. J. Cons. 18: 287-295

Takahashi, T., J. Olafsson, J. G. Goddard, D. W. Chipman, and S. C. Sutherland (1993), Seasonal variation of CO_2 and nutrients in the high-latitude surface oceans: A comparative study, *Global Biogeochem. Cycles, 7*, 843-878.

Takahashi, T., S. C. Sutherland, C. Sweeney, A. Poisson, N. Metzl, B. Tilbrook, N. Bates, R. Wanninkhof, R. A. Feely, C. Sabine, J. Olafsson, and Y. Nojiri (2002), Global sea-air CO_2 flux based on climatological surface ocean pCO_2, and seasonal biological and temperature effects, *Deep-Sea Res. II, 49*, 1601-1622.

Takahashi, T., S. C. Sutherland, R. Wanninkhof, C. Sweeney, R. A. Feely, D. W. Chipman, B. Hales, G. Friederich, F. Chavez, C. Sabine, A. J. Watson, D. C. E. Bakker, U. Schuster, N. Metzl, H. Yoshikawa-Inoue, M. Ishii, T. Midorikawa, Y. Nojiri, A. Körtzinger, T. Steinhoff, M. Hoppema, J. Olafsson, T. S. Arnarson, B. Tilbrook, T. Johannessen, A. Olsen, R. Bellerby, C. S. Wong, B. Delille, N. R. Bates, and H. J. W. de Baar (2009), Climatological mean and decadal change in surface ocean pCO_2 and net sea-air CO_2 flux over the global oceans, *Deep-Sea Research, Part II*, doi:10.1016/j.dsr1012.2008.1012.1009.

Tans, P. P., I. Y. Fung, and T. R. Takahashi (1990), Observational constraints on the global atmospheric CO_2 Budget, *Science*, *247*(4949), 1431-1438.

Taylor, J. R. (1997), *An Introduction to Error Analysis: The Study of Uncertainties in Physical Measurements (Second Edition)*, 327 pp., University Science Books.

Thomas, H., Y. Bozec, H. J. W. de Baar, K. Elkalay, M. Frankignoulle, L.-S. Schiettecatte, and A. V. Borges (2004b), The carbon budget of the North Sea, *Biogeosciences Discuss.*, *1*, 367-392.

Thomas, H., Y. Bozec, K. Elkalay, and H. J. W. De Baar (2004), Enhanced open ocean storage of CO_2 from shelf sea pumping, *Science*, *304*, 1005-1008.

Tokoro, T., A. Watanabe, H. Kayanne, K. Nadaoka, H. Tamura, K. Nozaki, K. Kato, and A. Negishi (2007), Measurement of air-water CO_2 transfer at four coastal sites using a chamber method, *J. Mar. Syst.*, *66*, 140-149.

Tsuchiya, M. (1989), Circulation of the Antarctic Intermediate Water in the North Atlantic Ocean, *J. Mar. Res.*, *47*, 747-755.

Tsunogai, S. (2002), The western North Pacific playing a key role in global biogeochemical fluxes, *J. Oceanogr.*, *58*, 245-257.

Tsunogai, S., S. Watanabe, and T. Sato (1999), Is there a "continental shelf pump" for the absorption of atmospheric CO_2? *Tellus, 51B*, 701-712.

Verity, P. G., D. G. Redalje, S. R. Lohrenz, C. Flagg, and R. Hristov (2002), Coupling between primary production and pelagic consumption in temperate ocean margin pelagic ecosystems, *Deep-Sea Res. II*, *49*, 4553-4569.

Verity, P. G., S. S. Bishop, J. R. Nelson, D. B. Craven, J. O. Blanton, C. Y. Robertson, and C. R. Tronzo (1993), Composition, productivity, and nutrient chemistry of a coastal ocean planktonic food web, *Cont. Shelf Res.*, *13*, 741-776.

Walsh, J. J. (1988), On the Nature of Continental Shelves, Academic, San Diego.

Wang, S.-L., C.-T. A. Chen, G.-H. Hong, and C.-S. Chung (2000), Carbon dioxide and related parameters in the East China Sea, *Cont. Shelf Res., 20*, 525-544.

Wang, Z. A., W.-J. Cai, Y. Wang, and H. Ji (2005), The southeastern continental shelf of the United States as an atmospheric CO_2 source and an exporter of inorganic carbon to the ocean, *Cont. Shelf Res., 25*, 1917-1941.

Wang, Z. A., W.-J. Cai, Y. Wang, and H. Ji (2005), The southeastern continental shelf of the United States as an atmospheric CO_2 source and an exporter of inorganic carbon to the ocean, *Cont. Shelf Res., 25*, 1917-1941.

Wang, Z., and W.-J. Cai (2004), Carbon dioxide degassing and inorganic carbon export from a marsh dominated estuary (the Duplin River): A marsh CO_2 pump, *Limnol. Oceanogr., 49*, 341-352.

Wang, Z., and W.-J. Cai (2004), Carbon dioxide degassing and inorganic carbon export from a marsh dominated estuary (the Duplin River): A marsh CO_2 pump, *Limnol. Oceanogr., 49*(2), 341-352.

Wanninkhof, R. (1992), Relationship between gas exchange and wind speed over the ocean, *J. Geophys. Res., 97*, 7373-7381.

Wanninkhof, R., and M. Knox (1996), Chemical enhancement of CO_2 exchange in natural waters, *Limnol. Oceanogr., 41*, 689-698.

Wanninkhof, R., and W. R. McGillis (1999), A cubic relationship between air-sea CO_2 exchange and wind speed, *Geophys. Res. Lett., 26*, 1889-1892.

Wanninkhof, R., S. C. Doney, T. Takahashi, and W. R. McGillis (2002), The effect of using time-averaged winds on regional air-sea CO_2 fluxes, in *Gas Transfer at Water Surfaces*, edited by M. A. Donelan et al., pp. 351-356, American Geophysical Union, Washington, DC.

Watson, D. F., and G. M. Philip (1984), Triangle based interpolation, *Math. Geol., 16*(8), 779-795.

Weiss, R. F. (1974), Carbon dioxide in water and seawater: The solubility of a non-ideal gas, *Mar. Chem., 2*, 203-215.

Weiss, R. F., and B. A. Price (1980), Nitrous oxide solubility in water and seawater, *Mar. Chem., 8*, 347-359.

Wollast, R. (1993), Interactions of carbon and nitrogen cycles in the coastal zone, in *Interactions of C, N, P and S Biogeochemical Cycles and Global Change*, edited by R. Wollast, et al., pp. 195-210, Springer, Berlin.

Woodwell, G. M., P. H. Rich, and C. A. S. Hall (1973), Carbon in estuaries, in *Carbon and the biosphere; Proceedings of the 24th Brokhaven Symposium in Biology, Upton, N.Y., May 16-18, 1972*, edited by G. M. Woodwell and E. V. Pecan, pp. 221-240.

Woolf, D. K. (2005), Parameterization of gas transfer velocities and sea-state-dependent wave breaking, *Tellus B, 57*, 87-94.

Yoder, J. A. (1985), Environmental control of phytoplankton production on the southeastern U.S. Continental Shelf, in *Oceanography of the southeastern U.S. continental shelf*, edited by L. P. Atkinson, et al., pp. 93-103, American Geophysical Union, Washington, D. C.

Yoder, J. A., and T. Ishimaru (1989), Phytoplankton advection off the southeastern United States continental shelf, *Cont. Shelf Res.*, *9*, 547-553.

Yoder, J. A., L. P. Atkinson, S. S. Bishop, E. E. Hofmann, and T. N. Lee (1983), Effects of upwelling on phytoplankton productivity of the outer southeastern United States continental shelf, *Cont. Shelf Res.*, *1*(4), 385-404.

Zappa, C. J., W. R. McGillis, P. A. Raymond, J. B. Edson, E. J. Hintsa, H. J. Zemmelink, J. W. H. Dacey, and D. T. Ho (2007), Environmental turbulent mixing controls on air-water gas exchange in marine and aquatic systems, *Geophys. Res. Lett.*, *34*, L10601, doi:10.1029/2006GL028790.

Zhai, W., M. Dai, and X. Guo (2007), Carbon system and CO_2 degassing fluxes in the inner estuary of Changjiang (Yangtze) River, China, *Mar. Chem.*, *107*(3), 342-356.

Zhang, X., and W.-J. Cai (2007), On some biases of estimating the global distribution of air-sea CO_2 flux by bulk parameterizations, *Geophys. Res. Lett.*, *34*, L01608, doi:10.1029/2006GL027337.

APPENDICES

This data set shows a diagram of the CO_2 equilibrator and the pCO_2 distributions along the ship track during the surface water surveys in the South Atlantic Bight.

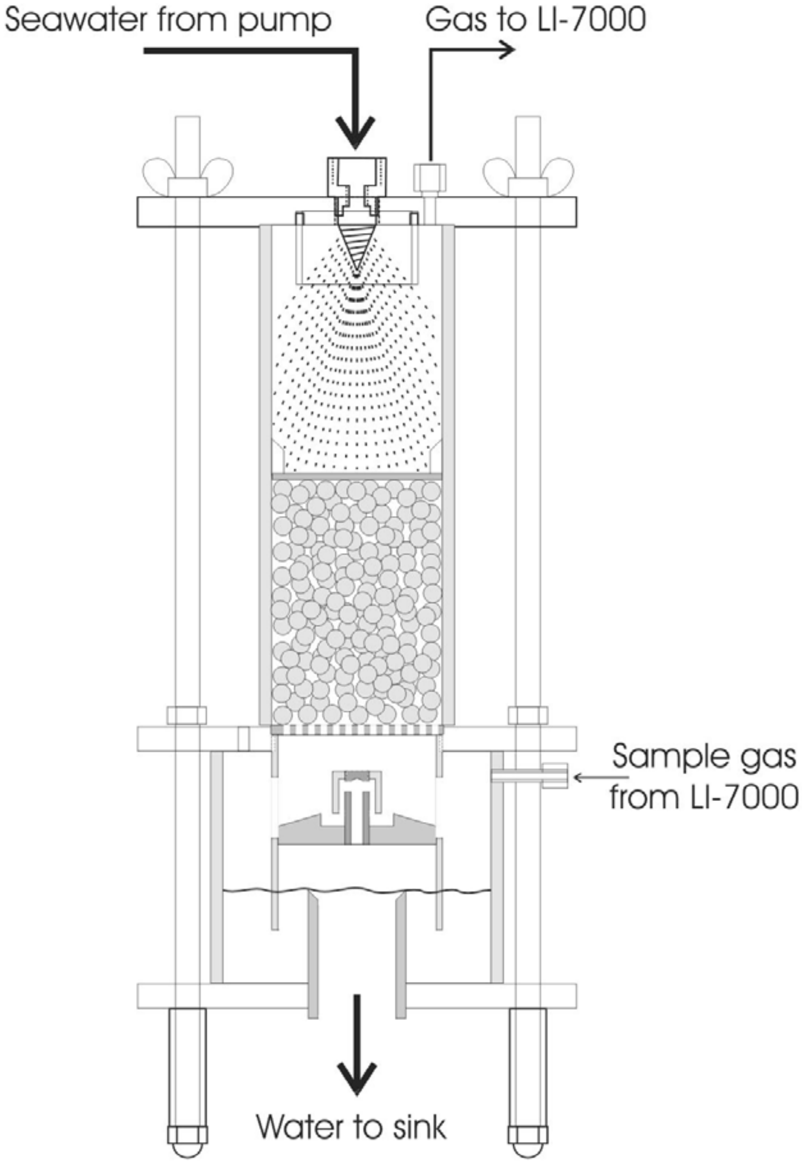

Figure A01. Diagram of the CO_2 equilibrator. The equilibrator is composed of an equilibrium chamber, a shower head at the top, some beads to facilitate the equilibration, and a water drain at the bottom.

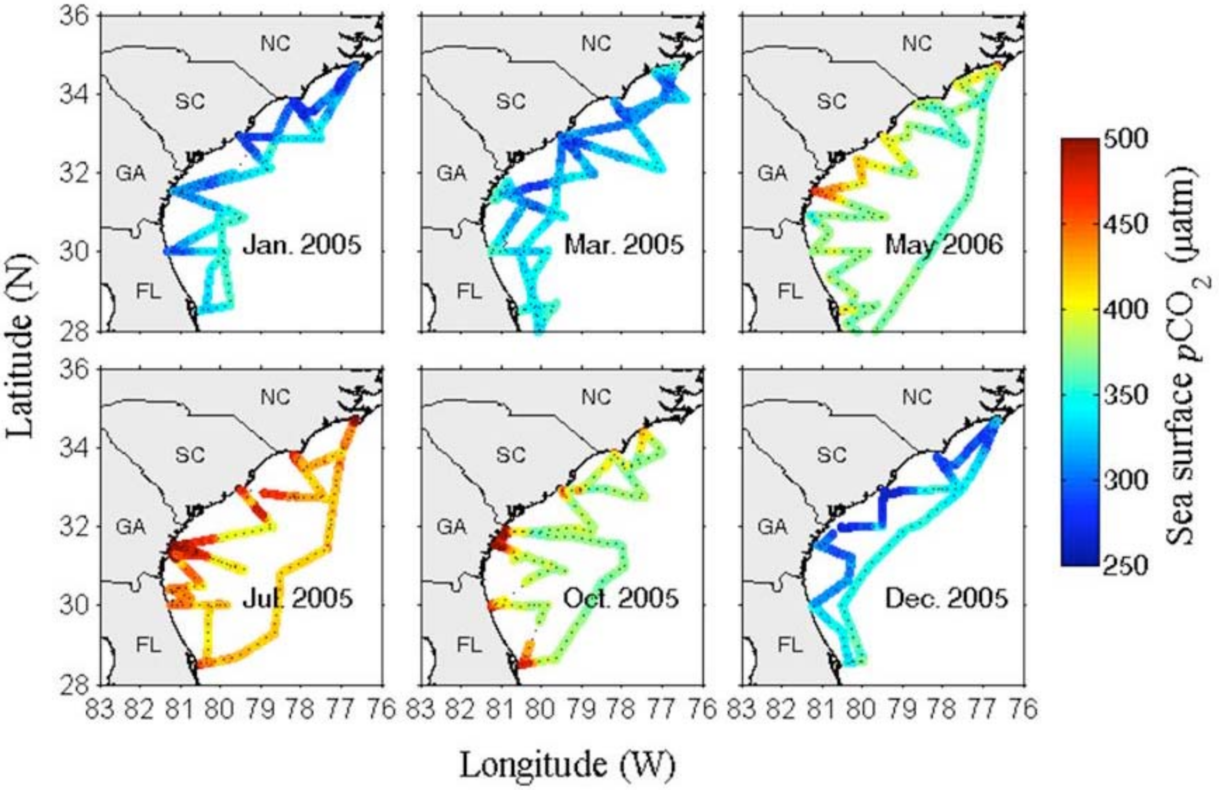

Figure A02. Sea surface $p\text{CO}_2$ along the ship track on the South Atlantic Bight during all of the sampling months. The sampling months are January 2005, March 2005, May 2006, July 2005, October 2005, and December 2005.